

Enabling Distributed Applications with SAGA

João Abecasis, Shantenu Jha, Hartmut Kaiser, Joohyun Kim, André Merzky, and Ole Weidner

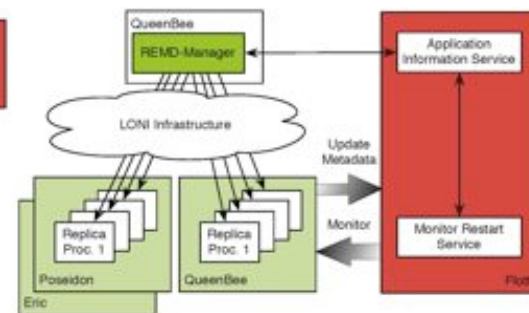
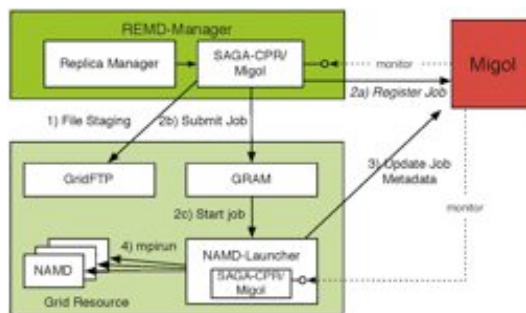
Center for Computation & Technology, Louisiana State University, Baton Rouge, U.S.A.

Abstract

The Simple API for Grid Applications (SAGA), a proposed recommendation of the Open Grid Forum (OGF), defines a high-level programmatic interface for developers of Distributed Applications [1]. The fundamental idea of SAGA is to lower the barrier for applications and application scientists to utilize distributed infrastructure. SAGA provides a simple, uniform, stable interface to the most often required functionality in order to construct general purpose, extensible and scalable applications.

Our group has lead the SAGA effort, starting from the specification effort at the OGF to providing the first C++ implementation [2]. We are also developing several different novel applications, using SAGA to harness the power of distributed infrastructure.

SAGA has already been used to develop different types of distributed applications. Namely, (i) converting legacy applications to utilize distributed resources; (ii) development of applications based upon abstractions and frameworks that are themselves developed using SAGA; (iii) first principles applications, explicitly cognizant of the fact that they will operate in a distributed environment, where the application logic is coupled with the distributed logic. SAGA supports the development of these applications and many others, thus providing a tool to develop a broad and general class of applications.



Simple, Powerful Abstraction Layer

SAGA facilitates the use of distributed infrastructure by providing a simple interface across different middleware distributions and environments. Therefore once an application has been written using SAGA it can be deployed and run on any environment in which SAGA is supported.

We are developing adaptors for the most commonly occurring distributed environments. Additionally SAGA provides the abstractions from which commonly occurring execution patterns and usage modes can be supported. For example for data-intensive applications, we create a framework that supports the common MapReduce pattern. Applications involving basic functionality such as searching, can then be deployed over distributed environments

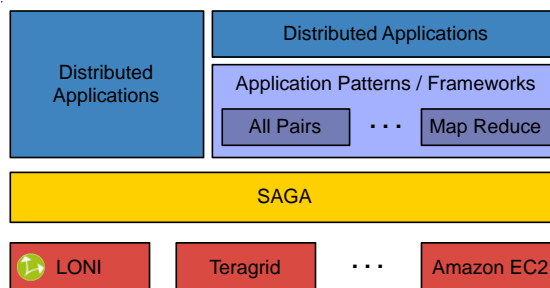
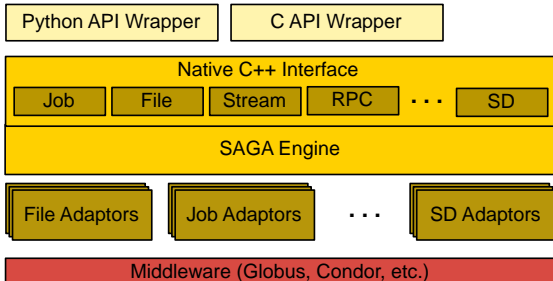
Connections with CyberTools

SAGA is being used within the CyberTools project in several critical ways:

- It is being used to create a general purpose "Application Manager", that will enable many science drivers to utilize remote LONI machines without any changes to the execution environment. In particular it can be used to support specific application usage patterns, for example, it has been used for distributed replica-exchange (RE) simulations using NAMD. The same infrastructure can be used for use with other codes such as LAMMPS, etc. The figure above provides details on how SAGA is used to implement RE.
- SAGA will be interfaced with Cactus applications to use Information Services and other advanced CyberInfrastructure features.
- SAGA will also provide the basic capability for interfacing multi-physics applications (via extension to the API to support messaging)

References

- Goodale, T, Jha, S, Kaiser, H, Kielmann, T, Kleijer, P, Merzky, A, Shalf, J, Smith, C, (2007) GFD-R-P.90 A Simple API for Grid Applications (SAGA), Open Grid Forum
- SAGA C++ Project [Online]. <http://saga.cct.lsu.edu>



Abstract

Visual verification of theories and data from experiments and simulations follow a chain of processes. From formatting data in suitable format to streaming data to the points of interpretation like rendering or analysis; to rendering the data in the rendering farms or in a local cluster; retrieving the rendered data and convert them to the image pixel and streaming those pixels live to the desired destinations local or remote. Our aim is to investigate each of these steps and offer a better tool, algorithm or mechanism to smoothen and optimize each of the aforementioned steps in the visualization pipeline. We have discretely looked into each of these steps with a certain degree of success and further discuss the idea to realize the project and share our experience.

Goal: Optimization of visualization of large data through parallelism and intelligent resource selection

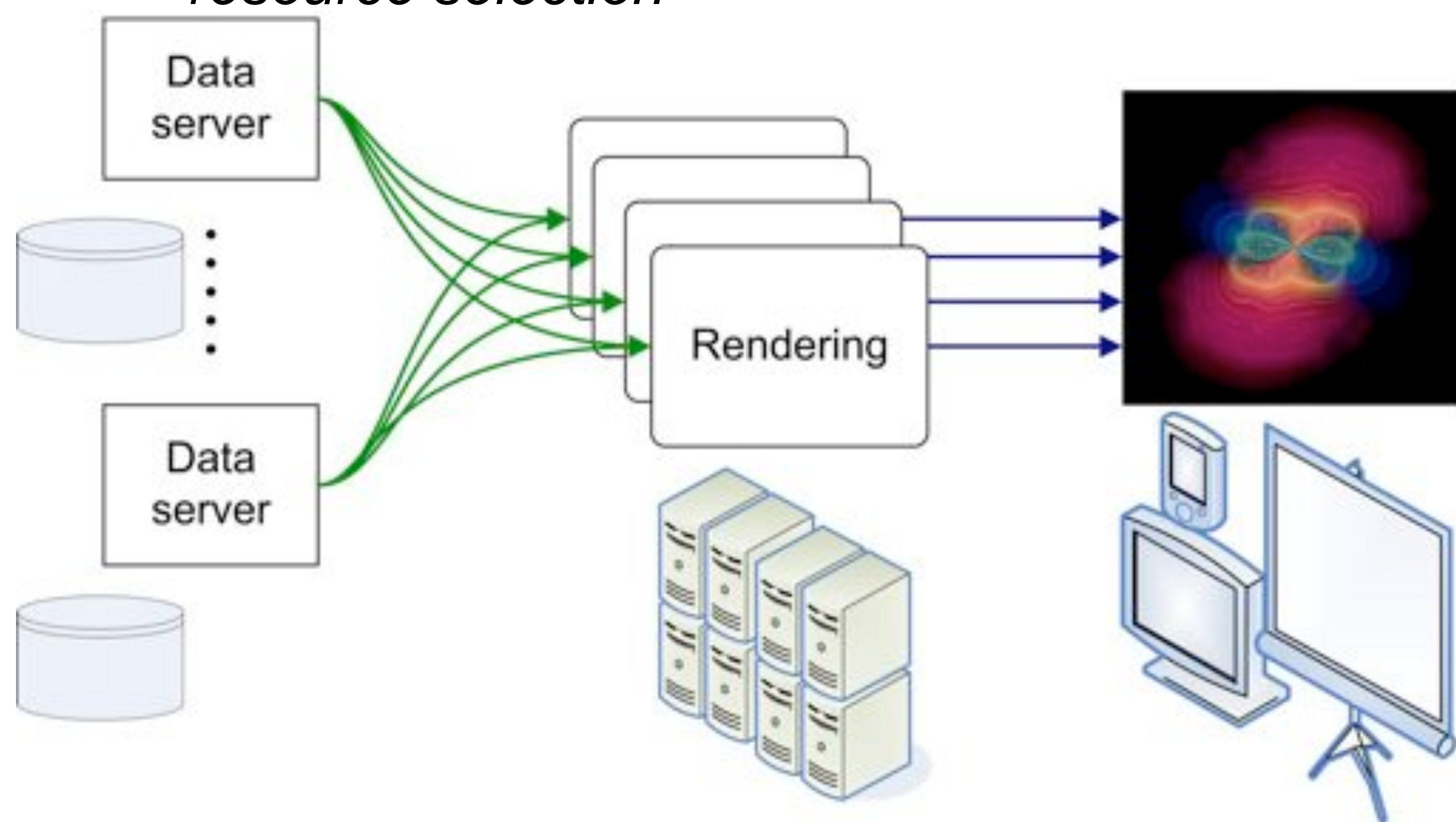


Fig. 1 Distributed Visualization Pipeline

Streaming



Transport resulting images to user
Options: hardware-assisted, software (integrated in the application or external)
Current status:

Successfully used hardware-assisted system based on HD videoconferencing set-up used for HPC classes.

Advantage: can be used with any visualization application,

Disadvantage: poor scalability,

Evaluating software-only rendering options (SAGE, visit built-in streaming)

Advantage: scalable, but needs high bandwidth

Future work: automatic tuning of video streaming parameters



Fig.9 Distributed Visualization

Data

Use distributed data servers
Designed an algorithm to use information about network topology and link capacity to optimize throughput
Flexible, pipelined high-performance data transfer system

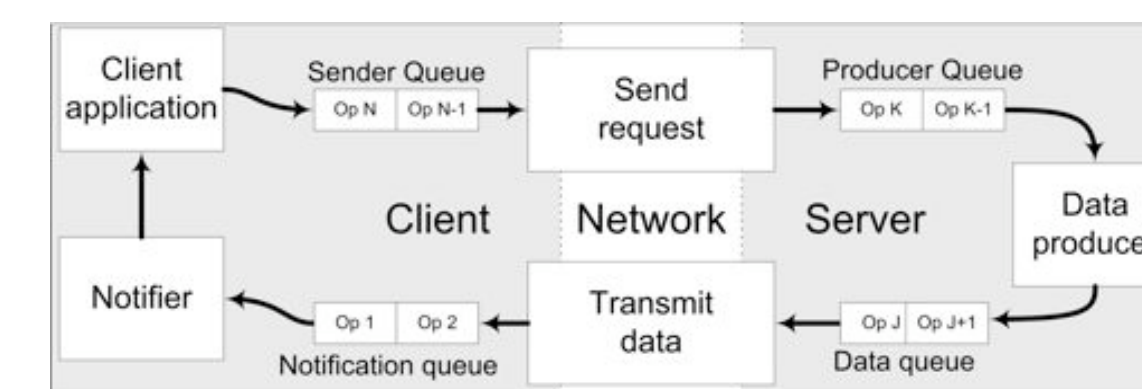
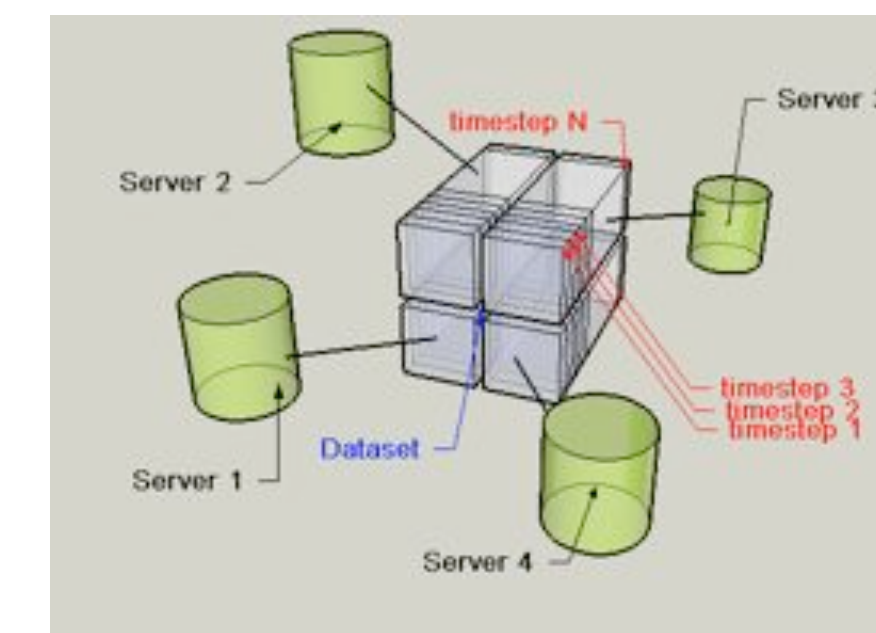


Fig.2 & 3 Overview of distributed data server implementation and actual data transfer process

Rendering

Use HPC and visualization clusters to render large datasets
Choose rendering options (data distribution, image distribution or hybrid) and configuration

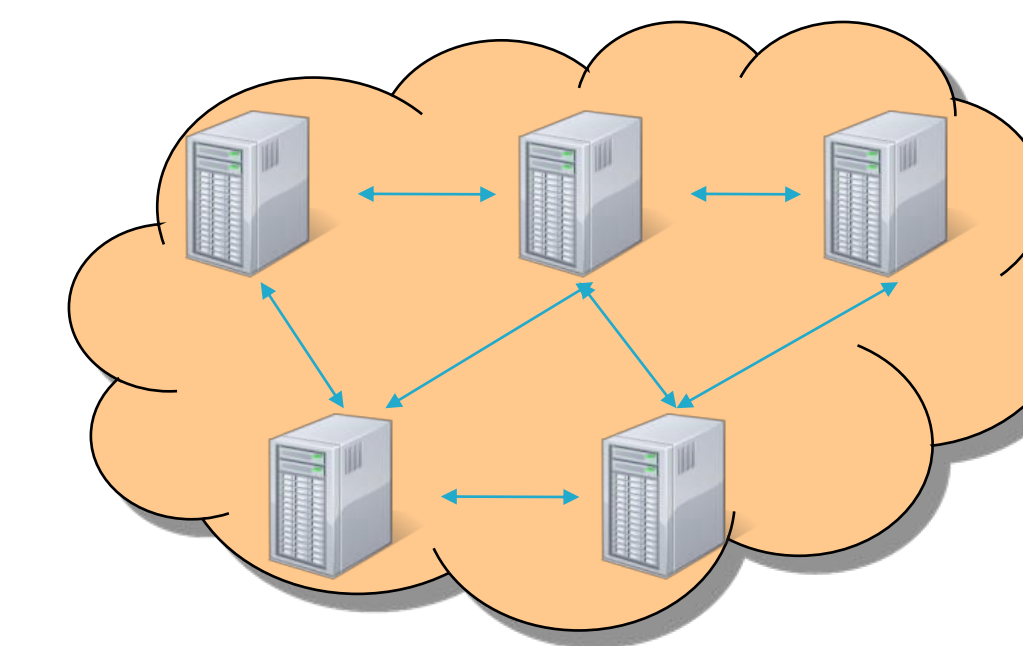


Fig.4 Distributed Rendering

Currently investigating two visualization systems:
Visit and Equalizer, testing with an example dataset

Equalizer

Flexible system designed for parallel rendering
Supports distributed rendering and frame compositing, Multiple Decomposition – Recomposition Modes

Status:
Equalizer has been tested on scientific experimental data

Future steps: benchmark and compare various rendering options, long-term: automatic tuning of configuration parameters; test on display walls, cave displays, scalable rendering

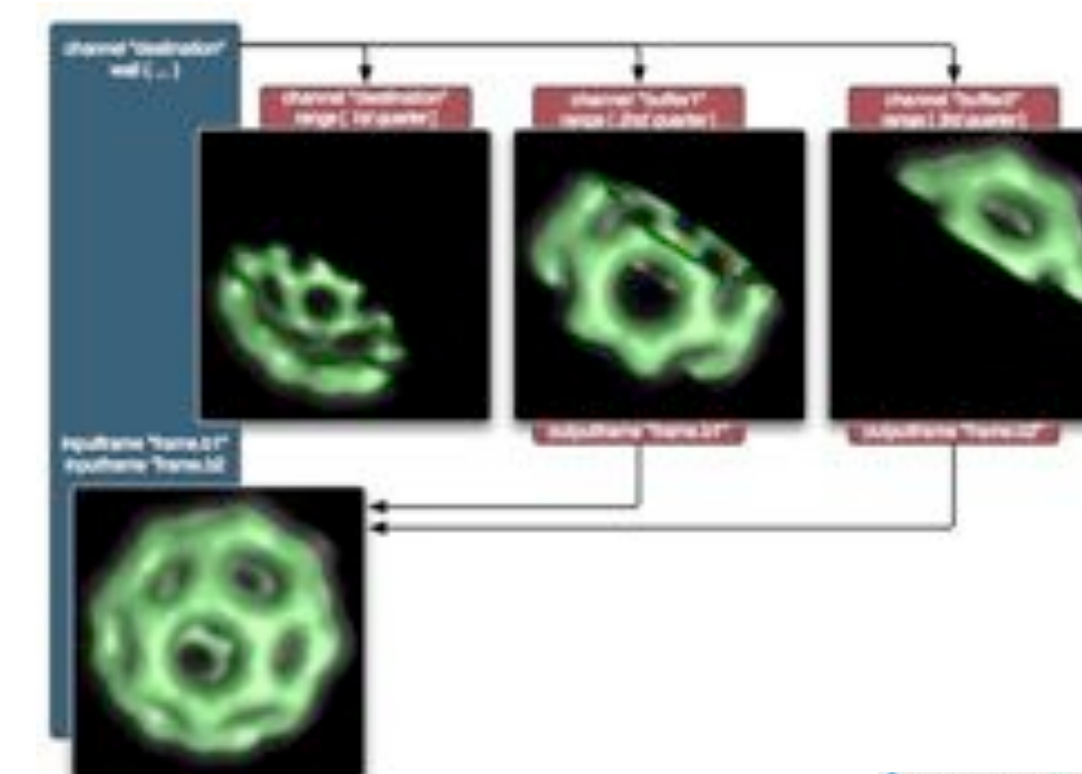


Fig. 7 An example of compound specification for sort-last rendering using 3 channels

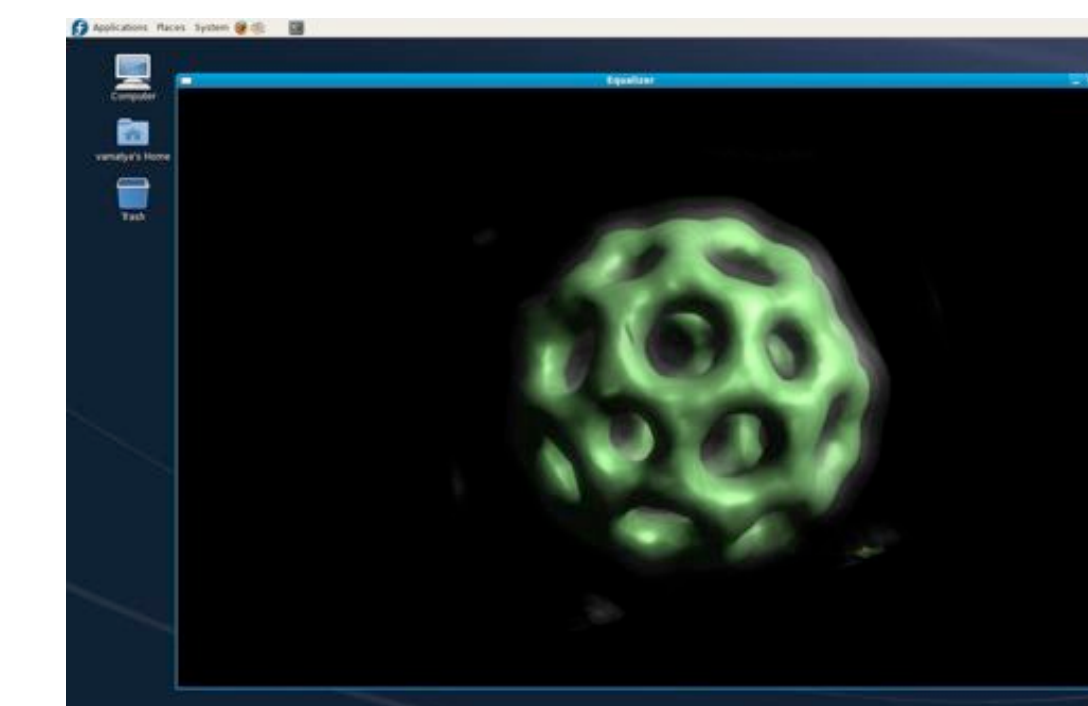


Fig.8 Snapshot of display for Equalizer running on two separate machines graphics cards

Status:

Data transfer system implemented
Optimization algorithm for prefetching and deterministic network links designed

Next steps:

Tuning the data transfer system and integrate in visualization application (currently using Petashare)
Implement optimization algorithm and integrate in data transfer system

Visit

Complete visualization system, does not support hardware – accelerated parallel rendering
Free, Open Source, Platform Independent, distributed, parallel
Distributed architecture allows to take advantage of both compute power of large parallel computer and local graphics hardware
Rendering on remote parallel machine, while display on local machine

Status:

Visit has been tested on scientific experimental data

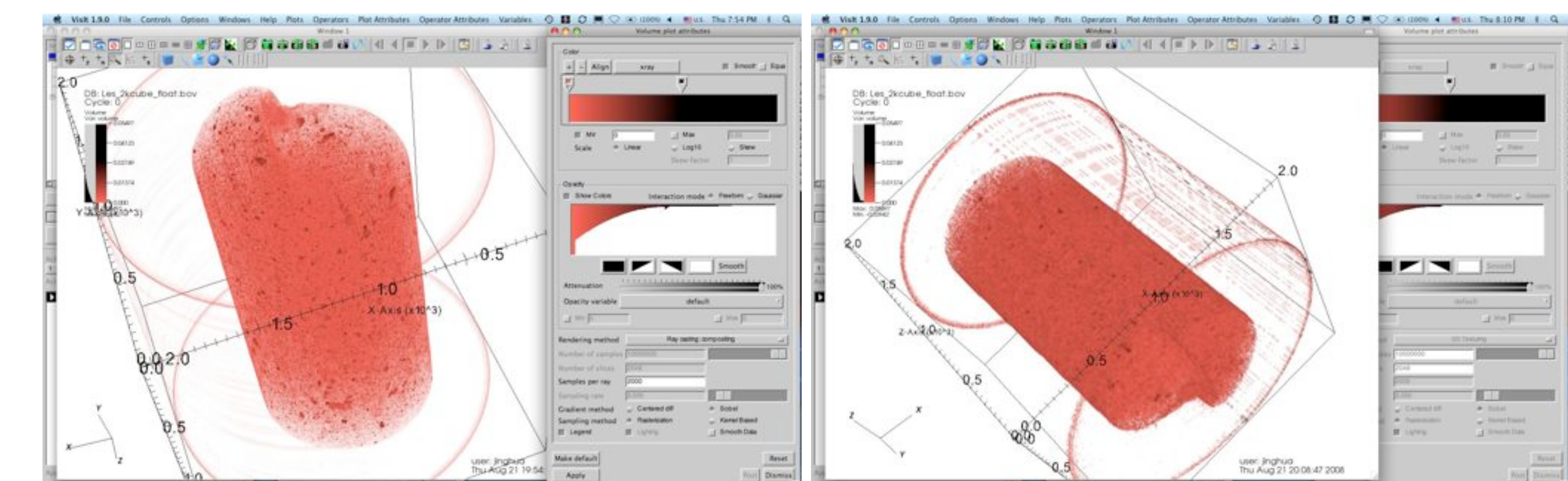


Fig.5 & 6 Visit Snapshotson of Scientific Experimental Data

Connections with CyberTools

Workpackage-3: Visualization Services

Acknowledgements

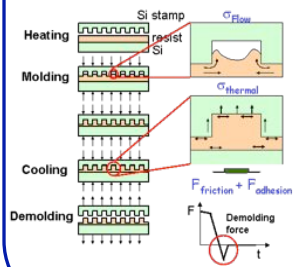
We would, sincerely, extend our gratitude to all the IT persons in LSU for their active assistance. We would like to heartily thank the facility and manpower lent to our cause by LSU and CCT. Last but not the least we offer deepest thanks to the NSF for funding the project.

Abstract

Most of structural failures in nanoimprint lithography occur during demolding, a process to separate the stamp from the molded substrate. In this work, we studied stress and deformation behavior for the molded polymer layer using numerical simulation. Via parametric studies, a general rule to improve the demolding process has been proposed.

Introduction

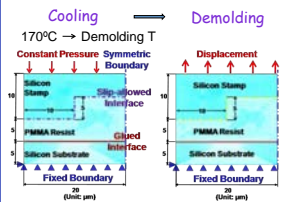
Demolding in nanoimprint lithography



- NIL has potential as a production-type tool to fabricate micro- and nanostructures in polymer via molding.
- Demolding is a process to overcome all the chemical and mechanical interactions between stamp and substrate.
 - Most of imprint failures occur at this process step.
- A systematic study on demolding is needed to develop processes leading to low stress and deformation in the molded substrate.

Simulation Method

2-D model for demolding simulation



- Assumptions
 - Governed by continuum mechanics.
 - PMMA is initially filled into stamp.
 - No initial stress.
 - Sliding is allowed, but not separation between stamp and PMMA.
 - All materials are isotropic
- Simulation was performed using ANSYS 10.0.

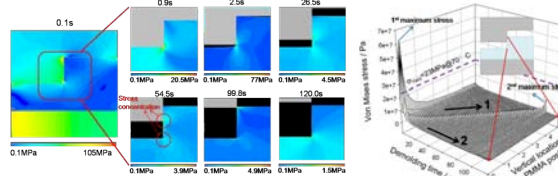
Materials

- PMMA: viscoelastic → 10 element Maxwell model was used.
- Si: linear elastic → $E = 128\text{GPa}$, $\nu = 0.28$, $\alpha = 2.5 \times 10^{-6} / ^\circ\text{C}$

Simulation Results

1. Single symmetric structure

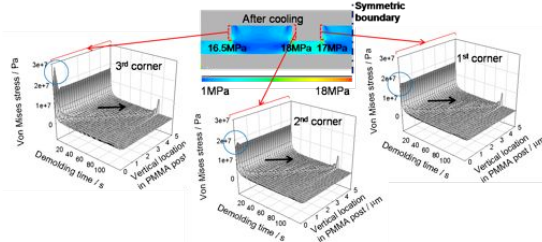
Stress evolution during demolding



- Local stress evolution during demolding shows two maximums: at the beginning and end of demolding.
 - Demolding failure can also occur at the end of demolding.

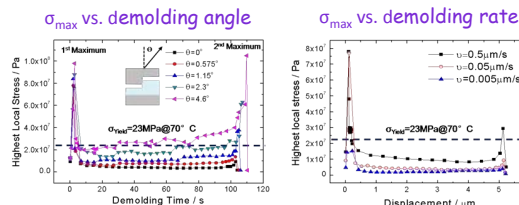
2. Multiple symmetric structure

Stress evolution at different side walls



- Higher stress is shown at the outmost structures.
 - An auxiliary outer structure could protect the inner structures.

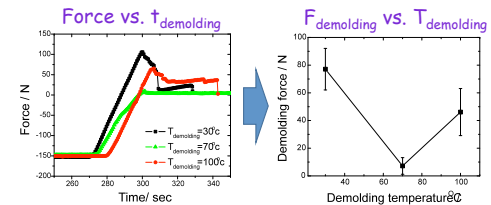
3. Parametric studies



- To have accurate alignment in demolding direction is critical!
- High demolding rate leads to high local stress.

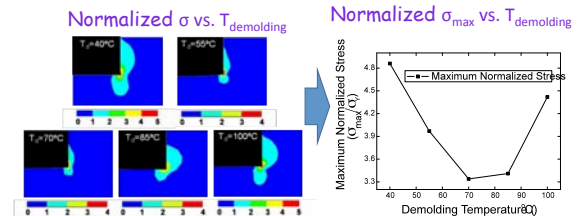
Experimental Verification (Effect on demolding temperature)

1. Demolding force measurements



- A minimum in $F_{\text{demolding}}$ vs. $T_{\text{demolding}}$ curve → 70°C

2. Demolding simulation



- Stress is normalized by σ_{yield} at each $T_{\text{demolding}}$.
- A minimum in normalized σ_{max} vs. $T_{\text{demolding}}$ curve → 70°C

Connections with CyberTools

- The ability of the FEM simulation for complicated yet actual structures will enable prediction of the demolding process as well as determination of a range of process parameters for successful demolding even at the stage of a process design in an economical and reliable way.

- For more accurate simulation, it is also necessary to incorporate nanoscale phenomena such as non-Furrier type heat conduction and nanoscale friction.

→ This requires more powerful computational tools, for which supports from CyberTools are critical.

Acknowledgements

This research was supported by the Center for Nanoscale Mechatronics & Manufacturing (CNMM), one of the 21st Century Frontier Research Programs from the Ministry of Science and Technology, KOREA (Grant No. M102KNO-1000706K1401-00710), and by the Louisiana Board of Regents - RCS (Contract No. LEQSF (2006-09) - RD - A - 09) and NSF-EPSCoR RII.



Workflow Enabling Large Scale Scientific Applications via Pegasus

Emir M Bahsi, Tefvik Kosar

Center for Computation and Technology, Louisiana State University



Abstract

Our first goal is end-to-end automation of two large scale applications: DNA folding and reservoir uncertainty analysis. Our implementation is based on Pegasus workflow tool that uses Condor, Condor-G, DAGMan, and Stork.

Our second goal is to implement a site selector that aims to achieve intelligent resource selection and load balancing among different grid Resources.

DNA Folding

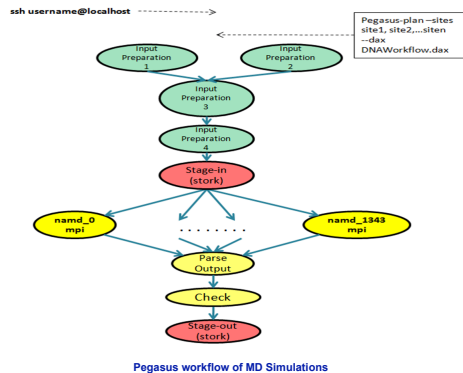
In order to identify how DNA sequence proteins rotate the global structure and dynamics of chromatin, Dr. Bishop and his research team developed suite of scripts and following is the way how scripts run by a scientist manually:



Folded DNA Structure

- **Input preparation 1:** Downloading pdb files.
- **Input preparation 2:** Processing pdb files via 3DNA software.
- **Input preparation 3:** Creating additional files.
- **Input preparation 4:** Creation of proper directories and files for each sims.
- **Stage in:** Transferring input data to clusters via *rsync* command.
- **Connect:** ssh to cluster
- **PBS Submission:** All simulations are executed via submitting a pbs submit file that submits each simulation sequentially.
- **Parse Output:** Energy value 2000 is parsed for each simulation
- **Check:** Checked each output and simulations are decided as passed or failure
- **Stage-out:** Outputs are transferred back to local machine via *rsync* command

We have designed a workflow in Pegasus using those scripts:



Pegasus workflow of MD Simulations

UCoMS

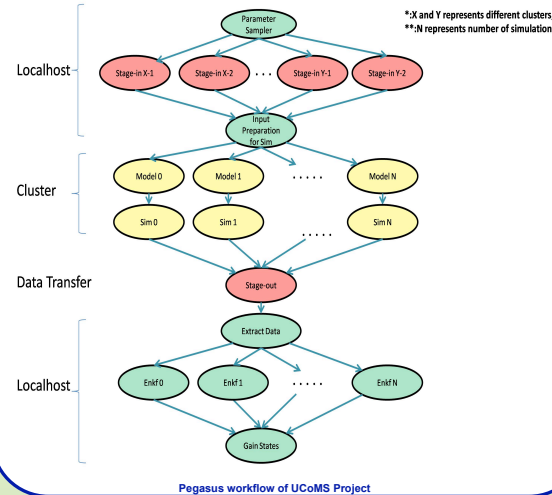


UCoMS (Ubiquitous Computing and Monitoring System), which is an ongoing project with the collaboration of Louisiana universities, aims to discover and manage energy sources.

There are four steps that are commonly performed for uncertainty analysis:

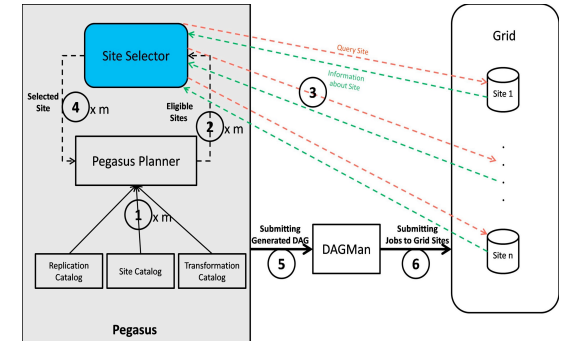
- Seismic inversion
- Reservoir modeling
- Flow simulation
- Post processing

We have designed workflow in Pegasus by using those steps to have end-to-end processing:

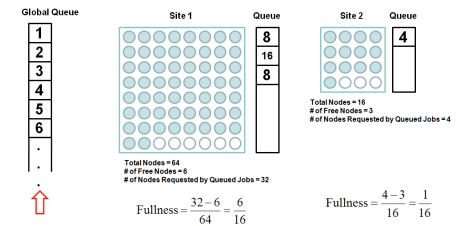


Pegasus workflow of UCoMS Project

Site Selection



$$\text{Fullness} = \frac{\text{\# of Nodes Requested by Queued Jobs} - \text{\# of Free Nodes}}{\text{Total \# of Nodes}}$$



Improvements Achieved by Pegasus

- **Automation of Tasks:** saves time to scientists instead of running programs manually in a sequence.
- **Reliability:** Most of the failures can be corrected via retry mechanism.
- **Separation of Computing and Data Tasks:** Different type of tasks are handled differently. Stork is used for data transfers.
- **Running Jobs on Heterogeneous Batch Systems:** Pegasus uses Condor-G at the bottom level to submit jobs to different batch systems (PBS, Loadleveler, Condor, etc.)
- **Resource Independency:** Since Pegasus generates proper files for each site, scientists do not have to write different scripts for each site.
- **Utilization of Resources to Gain Extra Performance:** Our site selection mechanisms aim to get high throughput by mapping large number of jobs to least loaded sites therefore they give better performance comparing to simple site selection algorithms.

Connections with CyberTools

In our studies we attempted to introduce workflow concepts to science drivers in two large-scale scientific applications: DNA Folding and UCoMS. Both applications are workflow-enabled and have gained reliability and performance improvements.

We are currently in the process of workflow-enabling Coastal Ocean Observing and Prediction projects.

Acknowledgements

This project is in part sponsored by the National Science Foundation under award numbers CNS-0619843 (PetaShare) and EPS-0701491 (CyberTools), and by the Board of Regents, State of Louisiana, under Contract Number NSF/LEQSF (2007-10)-CyberRII-01.



Enhancements in Stork Data Placement Scheduler

Mehmet Balman, Tevfik Kosar

Center for Computation and Technology, Louisiana State University



STORK: A Scheduler for Data Placement Activities

Data management has been a crucial problem in every stage of computer engineering, from micro to macro level systems. We focus on data access and data placement problems in distributed systems for large scale applications. We study aggregation of requests in order to increase the throughput especially for transfers of small data files. We also explore the possibility of an efficient error detection and reporting system for distributed environments. In addition, we are investigating techniques to make use of replicas for multi-source downloads. We also work on several enhancements like file similarity analysis and semantic compression methods to reduce total transfer size.

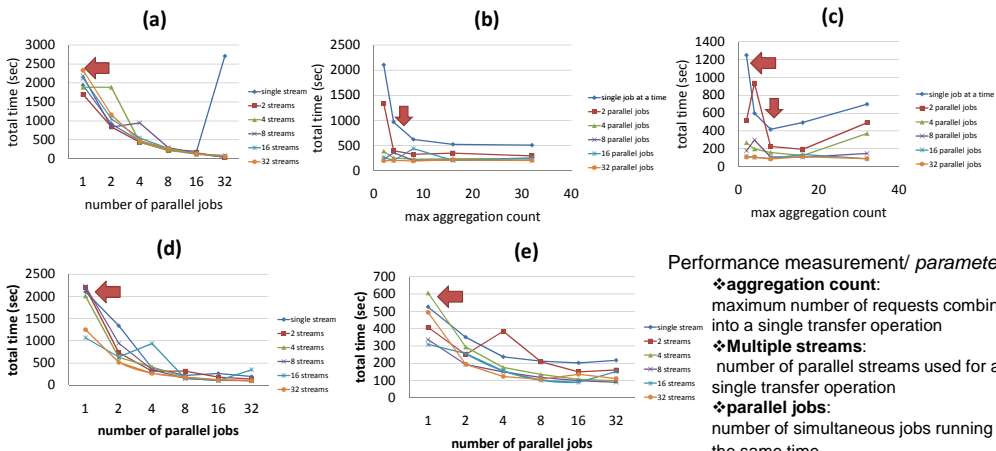
Aggregation of Data Placement Jobs

According to the file size and source/destination pairs, data placement jobs are combined and processed as a single transfer job. Information about the aggregated job is stored in the job queue and it is tied to a main job which is actually performing the transfer operation such that it can be queried and reported separately.

We have seen vast performance improvement, especially with small data files, simply by combining data placement jobs based on their *source* or *destination* addresses. The main performance gain comes from decreasing the amount of protocol usage and reducing the number of independent network connections. Thus, Stork makes better use of underlying infrastructure by coordinating and arranging data placement jobs.

Experiments on LONI (Louisiana Optical Network Initiative)

✓ **Test-set:** 1024 transfer jobs from Ducky to Queenbee (rtt avg 5.129 ms) - 5MB data file per job



Performance measurement/ parameters:

- ✦ **aggregation count:** maximum number of requests combined into a single transfer operation
- ✦ **Multiple streams:** number of parallel streams used for a single transfer operation
- ✦ **parallel jobs:** number of simultaneous jobs running at the same time.

Fig: Effects of parameters over total transfer time of the test-set

- without job aggregation – number of parallel jobs vs number of multiple streams
- transfer over single data stream – aggregation count vs number of parallel jobs
- transfer over 32 streams – aggregation count vs number of parallel jobs
- at most 2 requests are aggregated – number of parallel jobs vs multiple streams
- at most 16 requests are aggregated – number of parallel jobs vs multiple streams

Connection with CyberTools

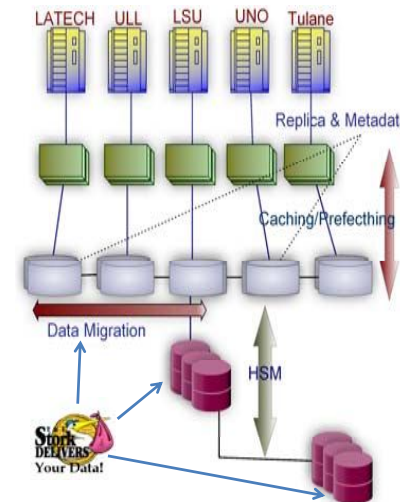
PetaShare Core Architecture

Two types of data movement:

- o First, data needs to be perfected from low level storage layers to the higher levels such that management of data access has to be handled in an efficient manner.
- o Second, data should be migrated between those five contributing institutions; moreover, data should be scheduled and moved between distributed sites and the clients.

Protocols:

- file:// -> local file
- ftp:// -> FTP
- http:// -> HTTP
- gsiftp:// -> GridFTP
- srb:// -> SRB (Storage Resource Broker)
- irods:// -> iRODS



Error Detection and Recovery

Stork, data placement scheduler, checks network connection and availability of data transfer protocol beforehand with the help of new network exploration module. We have implemented error detection and classification as new features inside Stork. Our experiments, in which we are generating artificial errors for testing purpose, shows that current data transfer protocol are not always able to generate adequate log information; therefore we also focus on tracing the transfer job and preparing the infrastructure to explore dynamic instrumentation while transfer is in progress.

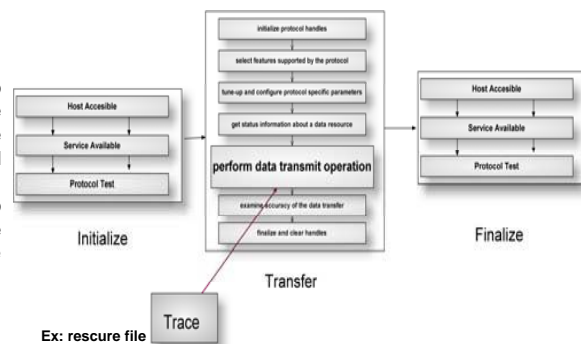
stork.globus-url-copy:

(supports wildcards and recursive copy)

Stork GridFtp data transfer module is able to verify the successful completion of the operation by controlling checksum and file size. Besides, it can recover from a failed operation. In case of a retry from a failure, scheduler informs the transfer module to recover and restart the transfer using the information from a rescue file created by the transfer module.

Stork.globus-url-copy features

```
-ckp | -checkpoint -
    use a rescue file for checkpointing
-ckpdebug | -checkpoint-debug
-ckpfile <filename> | -checkpoint-file <filename>
    checkpoint filename. Default is "<pid>.rescue"
-cksm | -checksum >
    checksum control after each transfer
-pchck | -port-check
    check network connectivity and availability of the protocol
```



Ex: rescue file

```
#failed_list (1):
gsiftp://dsl-turtle06.csc.lsu.edu/tmp/test/x_ttest2.tar file://tmp/x_ttest2.tar
#expanded_url_list (7):
gsiftp://dsl-turtle06.csc.lsu.edu/tmp/test/out file://tmp/out
gsiftp://dsl-turtle06.csc.lsu.edu/tmp/test/test2/test22/ file://tmp/test2/test22/
#transferred_list (2):
# gsiftp://dsl-turtle06.csc.lsu.edu/tmp/test/test1/ file://tmp/test1/
# gsiftp://dsl-turtle06.csc.lsu.edu/tmp/test/test2/ file://tmp/test2/
```

Acknowledgement

DSL Distributed System Laboratory
www.dsl.csc.lsu.edu



www.storkproject.org

This project is in part sponsored by the National Science Foundation under award numbers CNS-0619843 (PetaShare) and EPS-0701491 (CyberTools), and by the Board of Regents, State of Louisiana, under Contract Number NSF/LEQSF (2007-10)-CyberRII-01.



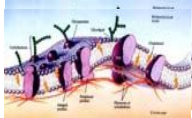
Abstract

We present low cost fabrication of a large area, free-standing SU-8 membranes with perforated micropores up to 4 inch diameter. For the fabrication, a combination of imprint lithography and a sacrificial layer technique was employed in order to obtain a clean, fully released, and mechanically stable membrane. The fabricated membrane was used to selectively immobilize lipid vesicles at the micropores in the membrane. This result indicates that the perforated polymer membranes with micro- and nanoscale pores have potential as a platform for fundamental study of biological systems. We also show integration of the polymer membrane into microfluidic devices made of polydimethylsiloxan (PDMS), which allows for in-situ study of lipid adsorption.

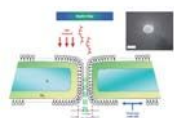
Objective

- To study an adsorption behavior of lipid at the micro pores in the polymer membrane made by a combination of imprint lithography and a sacrificial layer technique.
- Immense **research potential in biological systems** [1], protein lipid studies, DNA sequencing [2], polymer photonics and component for BioMEMS.
- Need to **develop a low cost, parallel process allowing for controlled pores size, location and mechanical stability** for fabrication of the perforated membranes.

Lipid bilayer in cell membrane [1]

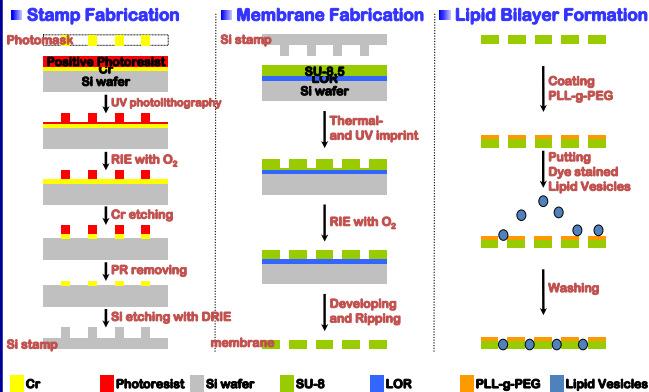


Nanopores for DNA sequencing [2]



Experiments

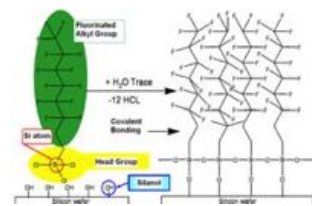
1. Fabrication Process



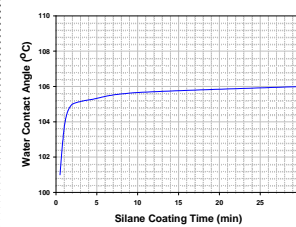
2. Surface Treatment on Si Stamp

A vapor phase deposition process was employed in a home-made chemical vapor deposition chamber to coat stamp surface with fluorinated silane to reduce adhesion of stamp surface. [3]

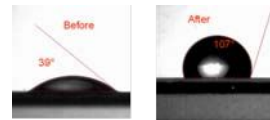
Chemistry of Silane Adsorption



Optimization of Deposition Time



Water Contact Angle Measurement

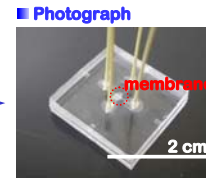
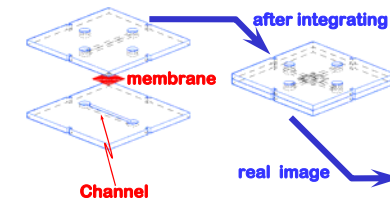


- The silane coating increased hydrophobicity of Si stamp surfaces.
- The optimum value of silane deposition time was 10 minutes.

3. Integration of the Membrane into Microchips

The membrane with perforated micropores was sandwiched by two PDMS microfluidic devices. The microchannels in the two PDMS devices were so aligned to be perpendicular to each other.

Schematic Images



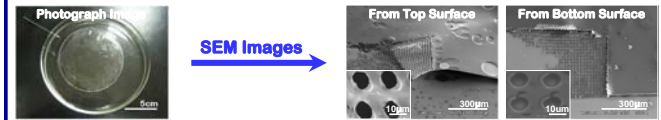
Results

1. Stamp Fabrication



- DRIE results in almost vertical sidewalls and a scallop-like features on the sidewalls.
- The smallest feature obtained by photolithography and Si DRIE is pillars of 2 μm diameter.

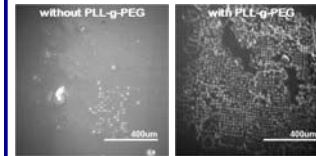
2. Free Standing SU-8 Membrane



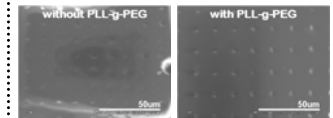
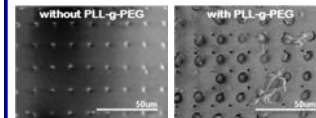
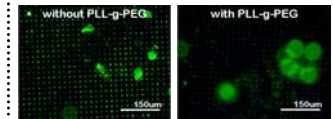
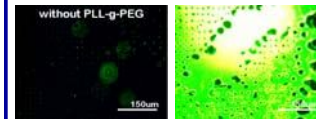
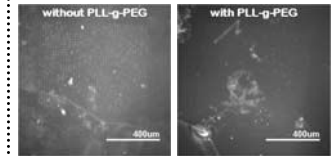
- Clean and fully released polymer membrane, 4 inch size, was achieved.

3. Microscope, Fluorescence and SEM Images after Staining with Dye

lipid : chloroform = 1 : 10



lipid : chloroform = 1 : 100



- Lipid vesicles adsorb at the micropore sites in the SU-8 membrane.
- Lipid adsorption behavior was affected by quality of imprinted patterns and dilution of lipid solution.
- When the membrane surface was treated with PLL-g-PEG prior to the lipid adsorption, the fluorescence signal becomes weaker. This indicates a possible formation of lipid bilayers at the pore sites.

Conclusions

- Technology to produce free-standing perforated membranes in SU-8 layers using all parallel processes were successfully developed using a novel combination of imprinting lithography and sacrificial layer techniques.
- Lipid vesicles were selectively immobilized at the fabricated pores in the membranes. Lipid adsorption behavior depend on the concentration of the lipid solution, surface treatment as well as the fouling of the membrane surface due to imprint failure.
- The number of active pores can be controlled simply by using microchannels of different widths. This will also alleviate the requirement of high accuracy in aligning two PDMS devices for bonding.

References

- <http://med.tn.tudelft.nl/~hadley/nanoscience/week4/4.html>
- S. M. Lqbal et al, *Nature Nanotechnology* 2007, 2, 243-248
- H. Schiff et al, *PSI scientific reports* 2004

Development and Application of Material Point Method for Structure Calculations in Biological Systems

Timur Gilmanov¹, Anvar Gilmanov², Sumanta Acharya^{1,2}

¹LSU, Mechanical Engineering
²LSU, Center for Computation and Technology

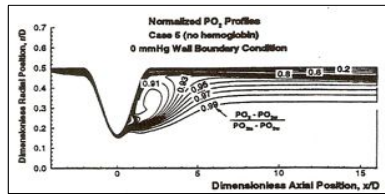
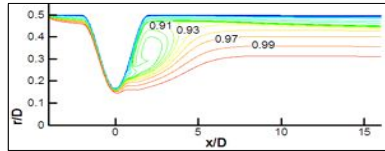


Abstract

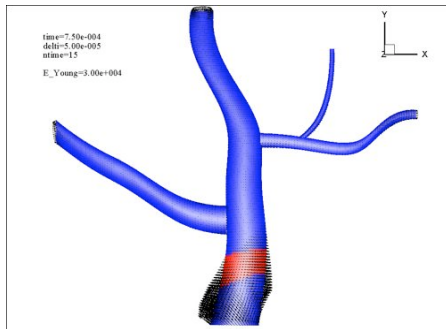
For many problems in biological systems it is essential to take into account the deformation of tissue under the action of fluid/blood flow and conversely, the influence of the tissue deformation on the fluid flow.

Fluid-Structure interaction (FSI) problems are considered as a solution of a coupled system of equations describing the behavior of fluid and structure which act on each other across the common boundaries.

An improved FSI technique is being developed that will efficiently handle problems with large structural deflections.



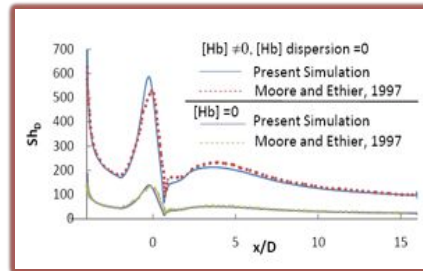
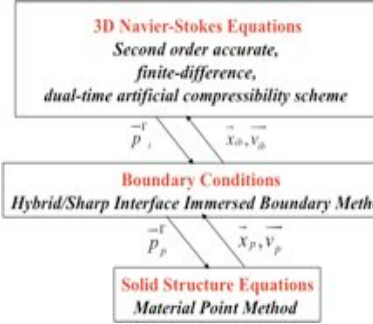
Simulation of Blood Flow-Oxygen Concentrations in Arterial Vessels with Stenosis
 Top: Our Computations Bottom: Results from Moore & Ethier



Simulation of Solid Structure: Deformation of arterial structure under the pulsation of pressure in the form of progressive wave. The pressure is given as

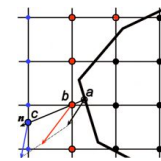
$$\Delta P(s, t) = f(s - c_0 t)$$

FSI Algorithm

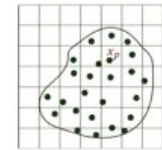


Surface Mass Transfer Rate in Arterial Vessels with Stenosis: Comparison of our Computations (solid) with Moore & Ethier

IBM



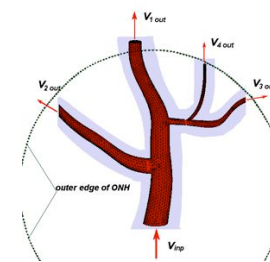
MPM



Background grid for solution of momentum equations

Connections with CyberTools

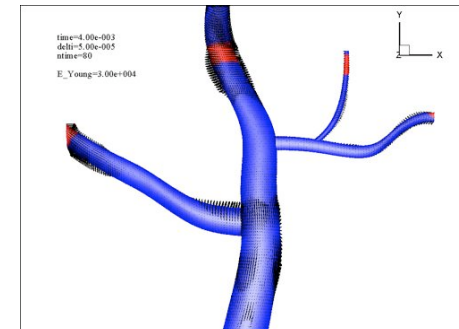
A key goal of the proposed work is to understand the oxygen transport behavior in arterial vessels.



An example of a branched arterial structure is shown in the figure. We will utilize the FSI algorithm developed to solve the problem & understand the essential flow physics. We will use CyberTools and the CFD toolkit to solve highly resolved calculations that include:

- FSI involving tissue deformation;
- diffusional transport and consumption in tissue/walls;
- upscaling of atomistic simulations for transport properties.

WP4 Collaborators: S. Jha, M. Tyagi, E. Schnetter



Acknowledgements

This work is currently supported by the NSF EPSCoR. The simulations were run on LSU's and LONI's HPC resources.

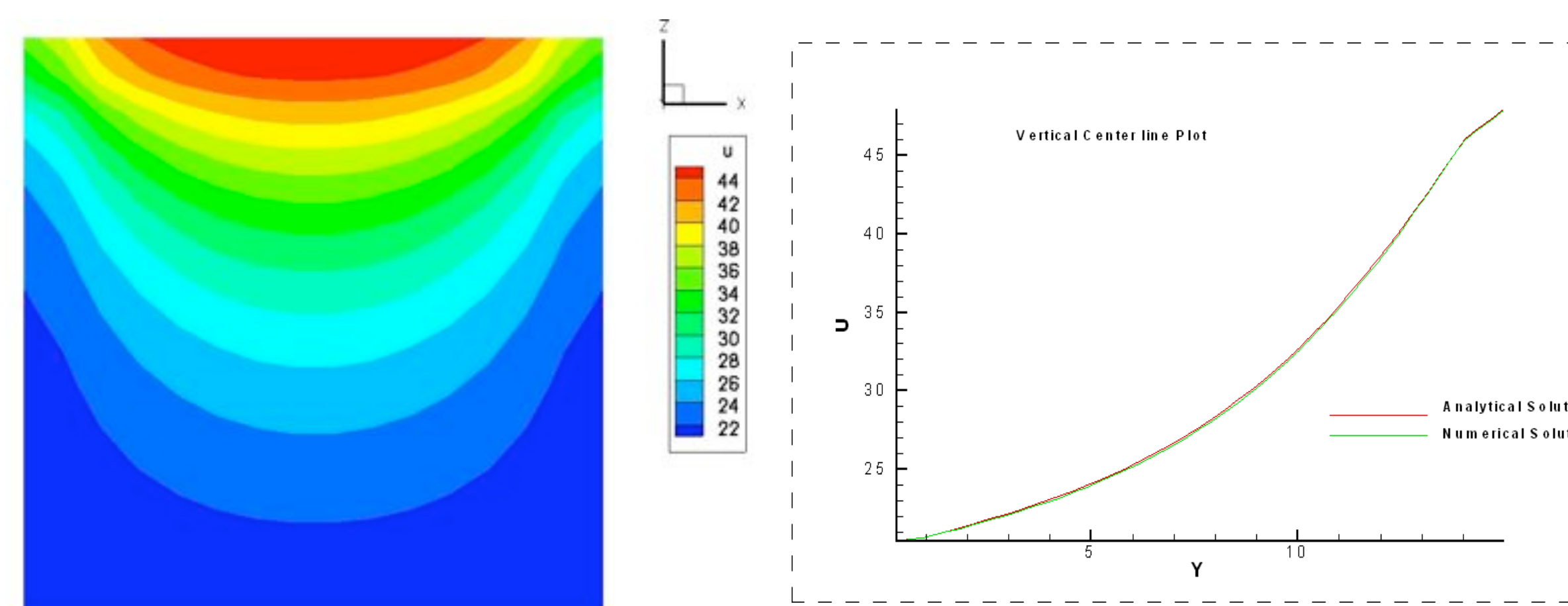


ABSTRACT

Bio-fluid systems of interest are invariably characterized by low Re flows in deformable complex domains such as blood flow in arteries. 3D-simulation of such a flow scenario requires an adept flow solver handling complex domain and low Re flows.

A block structured finite volume code to solve unsteady incompressible Navier-Stokes Equations is being developed with CGNS grid interface. A hybrid Staggered/Non-Staggered formulation is being used and is specifically suitable for implementing the immersed boundary method on curvilinear meshes. This feature is useful for biological systems.

Validation of Diffusion on Multi-block

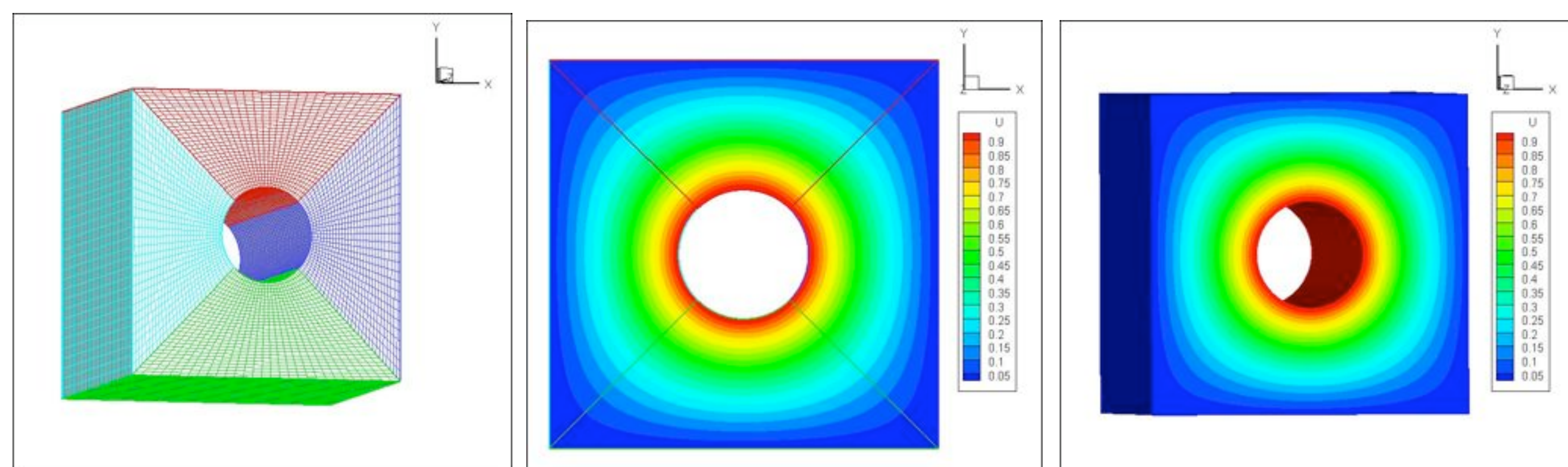


Governing Equations

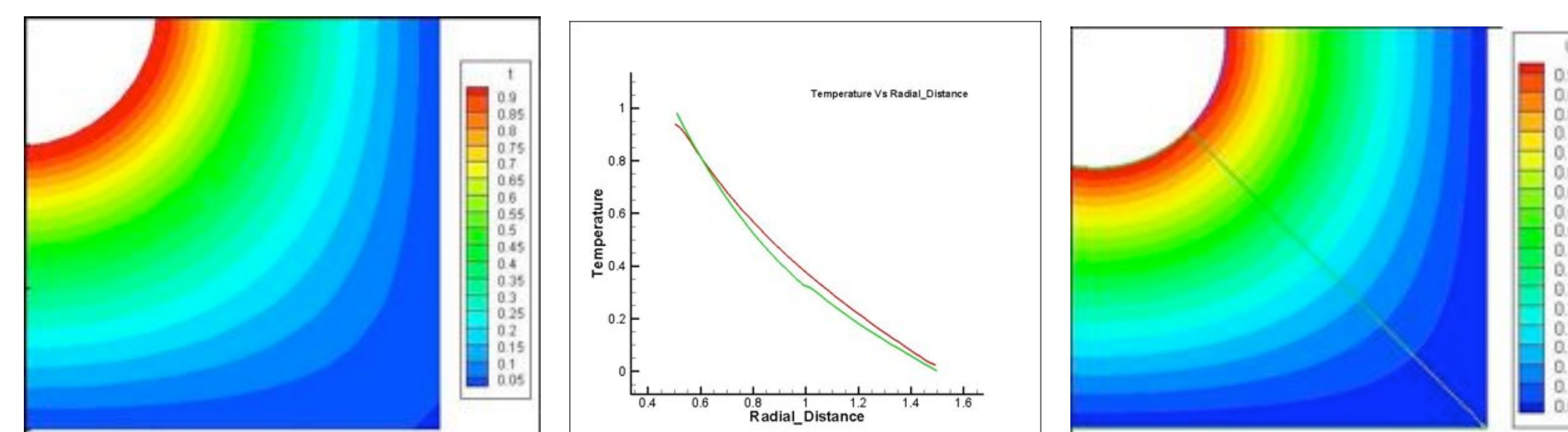
$$\frac{\partial v_i}{\partial x_i} = 0$$

$$\frac{\partial v_i}{\partial t} + \frac{\partial v_i v_j}{\partial x_j} = -\frac{1}{\rho} \frac{\partial p}{\partial x_i} + \frac{\mu}{\rho} \frac{\partial^2 v_i}{\partial x_j \partial x_j}$$

Diffusion in Curvilinear Multi-block Mesh



Comparison With Multi-Patch Simulation in Cactus



Multi Patch Simulation

Comparison of CFD Modules with Multi-Patch

CFD Module Simulation

*Courtesy Dr. Schnetter

Data Structure

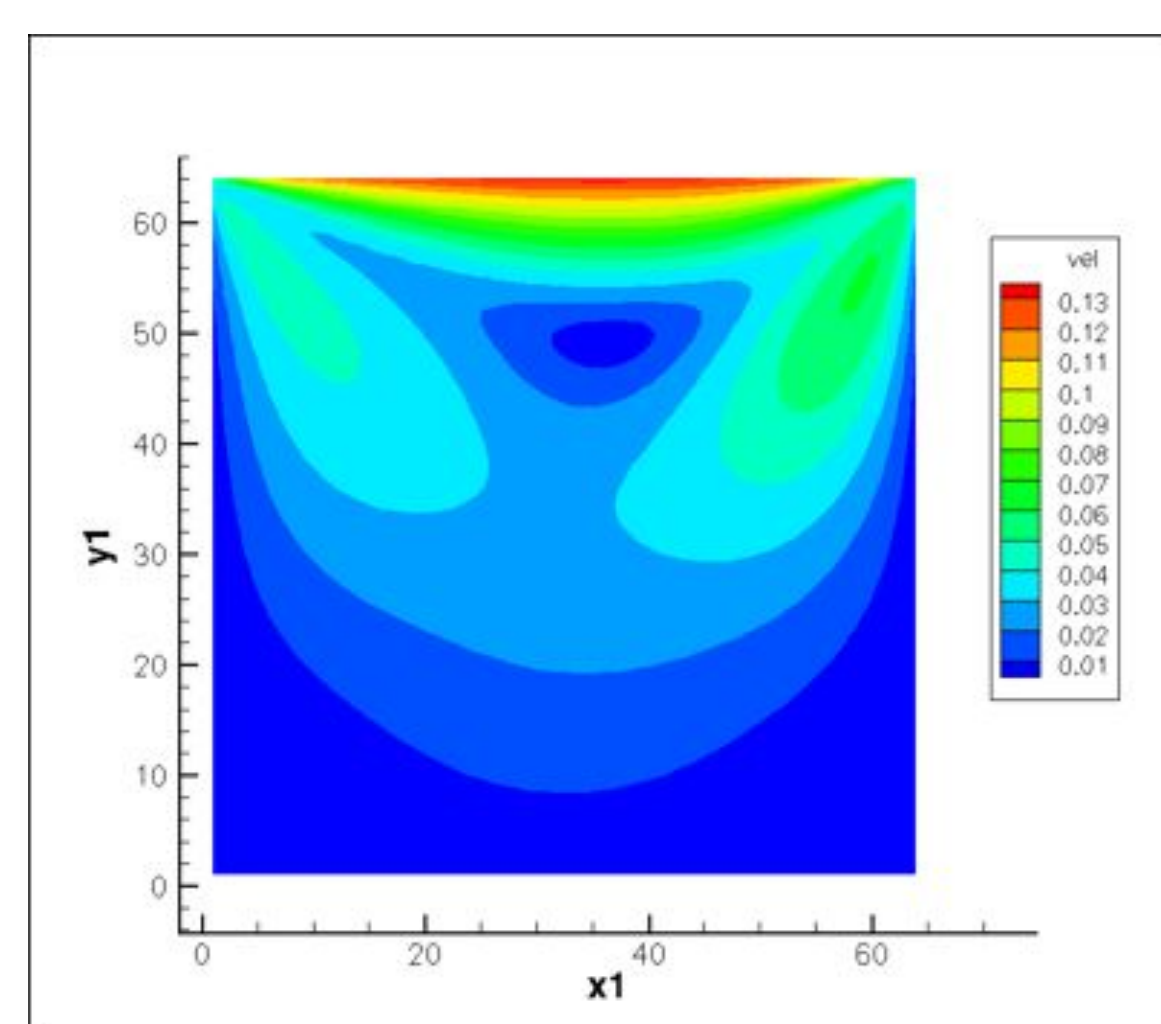
4D array Data Structure
 $U[m][j][k][l]$
 $M \rightarrow$ Block ID (grid Hierarchy)
 $J, k, l \rightarrow$ local grid index

Connections with CyberTools Subroutines To be Ported in Cactus

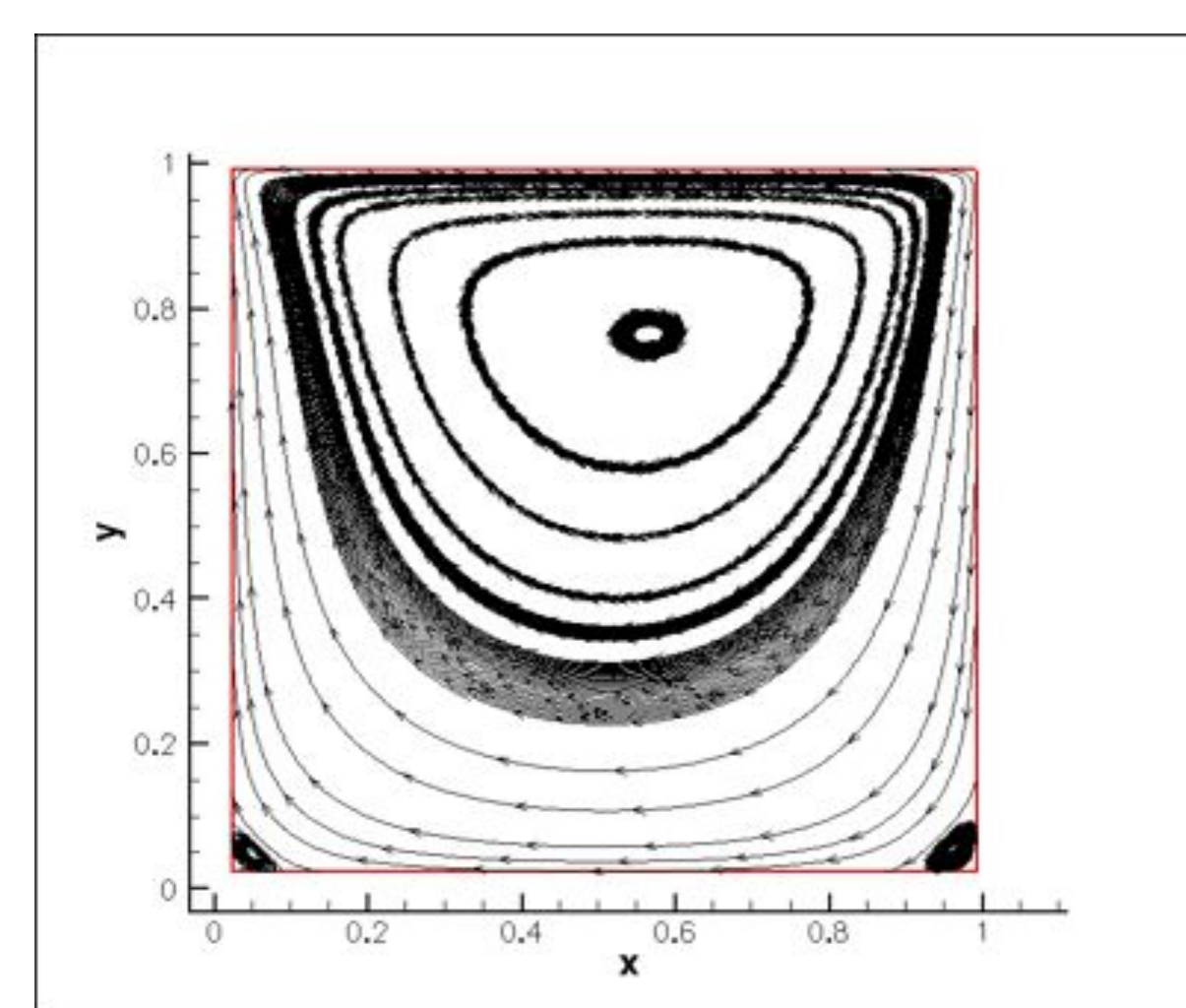
ReadCg_Grid.c
 ReadCg_Bc.c
 Allocate_Mem.c
 Geom.c
 Metric.c
 Set_Ghost_zone.c
 Exchange_Ghost_Zone.c
 Diffusion_Flux.c
 Convective_Flux.c
 PressurePoisson.c
 FractionalStep.c

These Modules will be ported as Cactus thorns

Flow Simulation Results Lid Driven Cavity, Re = 100



Velocity Contours



Stream Lines

Features of Code

- CGNS interface, imports MB grids & BC's from commercial grid generator.
- Staggered/Non-staggered approach on MB curvilinear grid.
- 2nd order accurate FV discretization
(CD for diffusion & QUICK for convection, second order time integration)
- Fractional Step Method for pressure momentum coupling.
- BC's tagged to each boundary cell face to support partial block connectivity.
- Hype solver for efficient parallel calculations of algebraic system of equations.

Acknowledgements

This work is currently supported by the NSF EPSCoR. The simulations were run on LSU's and LONI's HPC resources.

Towards Cyber Infrastructure for Dynamic Storm Surge Predictions

Archit Kulshrestha¹, Harsha Bhagawaty², Gabrielle Allen³, Nathan Brener⁴, S.S.Iyengar⁵

^{1,2,3,5}Center for Computation & Technology, Louisiana State University

^{1,2,3,4,5}Department of Computer Science, Louisiana State University

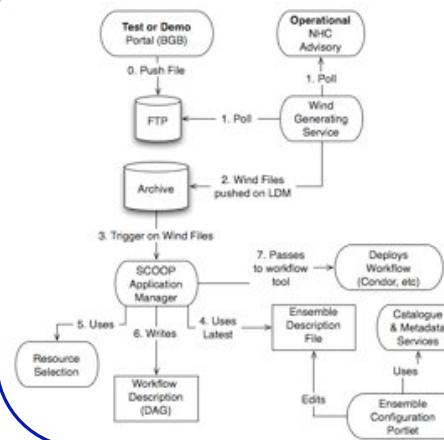


Abstract

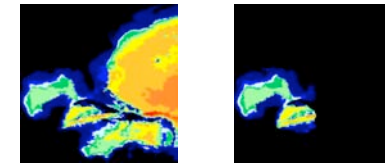
The Louisiana Coastal Area presents an array of rich and urgent scientific problems, such as hurricane forecasting or wetland erosion, that require new computational approaches. Dynamic and adaptive capabilities are crucially important for many of these problems, providing the ability to integrate coupled models with real-time sensor information, or to enable deadline based scenarios and emergency decision control systems.

This poster describes a scenario where new real time data driven algorithms could improve decision support systems for responding to the effects of hurricane and severe storm events. Motivated by the SURA Coastal Ocean Observing and Prediction workflow, we illustrate how dynamic selection of runtime parameters for storm surge models can effect both the accuracy and total runtime of the system. Research on algorithms for dynamic data driven application systems (DDDAS) is important for many science drivers in CyberTools which involve real time data or control systems.

SCOOP Workflow



ADCIRC Grids



Two different grids were used one with 31435 nodes covering a large area and other with 598240 nodes which is a high resolution grid of the New Orleans Lake Pontchartrain area.

Finer grids improve the accuracy of the results but also take longer to run. Scaling issues cause the time taken to generate the results to increase. Depending on the urgency of the impending storm/hurricane, an optimal grid can be chosen so as to predict a path of reasonable accuracy in a short span of time and provide accurate results for emergency planning.

Introduction

Hurricane are a major threat to life and property in Louisiana and other coastal areas. Hurricane Katrina and Hurricane Rita demonstrated that the key to saving lives is timely prediction and ample warning. In order to predict the effect of hurricanes and disseminate the results to the proper authorities it is important that the whole process be automated and the system be capable of making dynamic decisions based on available information. As part of the SCOOP program an end to end system was developed that reacts to coastal events and triggers various wind, surge and wave models. The SCOOP system relies on the SCOOP archive to receive and archive various data products and trigger coastal models upon their arrival. The output from these models is then ingested back into the archive and visualized. In this work we study the use of different grids for storm surge predictions and the effect on the turn around time and accuracy of the models. We propose that a optimal schedule can be established that provides fast turn around times and accurate results dynamically based on the threat level.

Results



Results were obtained by running the storm surge simulation for Katrina storm using ADCIRC on the two grids described in the poster. The results showed that a 7 day forecast ran for 1hr 39mins on 64 processors of the LONI queenbee machine while the smaller grid took less than 10 minutes to run. Larger grids with over 2 million nodes will take more than 6 hours to complete which is too long for emergency response purposes. Future work will focus on making dynamic decisions on which grid to use.

Connections with CyberTools

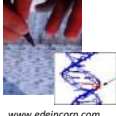
This work is connected to CyberTools WP1 due to its use of the LONI resources. WP3 will provide the visualization services and WP4 will provide the dynamic decision algorithms.

Acknowledgements

We would like to thank the entire SCOOP team, Brett Estrade, LONI support staff, Werner Bengert, Hartmut Kaiser, RakeshYadav.



Introduction



Molecular testing and genotyping is of significant importance in diagnostics/prognostics of disease states or detection and identification of biopathogens. These tests typically require multiple laboratory operations performed by highly trained personnel using a collection of task-specific instruments. For example, genetic testing involves the following complex set of steps: (i) cell lysis; (ii) nucleic acid extraction; (iii) amplification; (iv) sequence variation discrimination; (v) detection of reaction products.

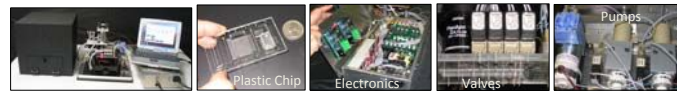


Genotyping

We are developing a universal, portable instrument for automated sample preparation and genetic testing. All of the bioanalytical processing, from sample reception to readout, is done on a disposable, plastic microfluidic chip. The operation of the chip is provided by electronic, optical, and hydraulic controls located off-chip. The sequence of sample processing steps performed on the flow-through plastic biochip includes cell lysis, DNA extraction, polymerase chain reaction (PCR) with or without ligase detection reaction (LDR), and DNA universal array read-out or micro capillary electrophoresis.

The unique feature of the system is that it can be easily reconfigured and used with other test specific chips for a much broader range of applications based on nucleic acid testing such as human identification and pathogen detection. The CyberTools are being used to optimize the design and performance of this system.

System Overview and Operation



- Load sample and reagents
- Insert chip into instrument
- Press "RUN" and wait for results

- Instrument measures 12" x 12" x 8" (electronics, optics)
- Fully integrated (load sample and reagents only operator requirement)
- Fluidic chips are hot-embossed or injection molded (no active components)
- Low cost per integrated chip
- Off-chip active components (reusable)
- Reconfigurable – performs different molecular assays
- Fast assays (< 30 min)
- Computational simulations used for component optimization

System Configurations

Cell Lysis, DNA Immobilization (SPE), PCR, LDR

microarray readout
SEM of microarray chip; Schematic of microarray unit; 1- integrated waveguide; 2- coupling prism; 3- microfluidic channel; 4- coverplate

Cell Lysis, DNA Immobilization, PCR

Due to material requirements, the SPE and PCR functions must be carried out using a polycarbonate (PC) and poly(methyl methacrylate), PMMA, is employed for the electrophoresis and microarray readout.

micro capillary electrophoresis

System integration using Passive Alignment Structures

The final system has fluidic modules that must be interconnected with no leaks to provide the necessary processing steps. Our approach to module integration is based on the implementation of passive assembly technology in molded polymers. Screw theory can be applied to the design of appropriate combinations of kinematic pairs that do not over-constrain the assembly

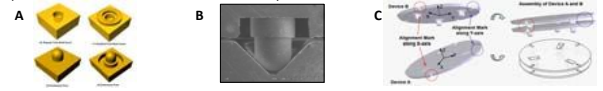
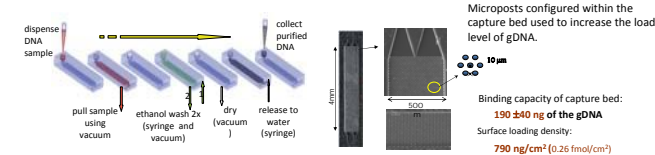


Figure A presents the regular design of a hemisphere tipped recess and the resulting hemispherical pin (a, b) and the modified design of the hemisphere tipped recess with the annular structure (c, d). (B) is a cutaway image of an assembled hot embossed stepped alignment structure, showing the stepped hemisphere-tipped pin in the v-groove. (C) is test bed for evaluating the use of passive alignment structures for the assembly of polymer microfluidic devices.

Developed Methodology and Technologies

Purification of DNA using Solid Phase Extraction (SPE)

Molecular tests require obtaining pure extracts of nucleic acids (i.e., removal of proteases, enzyme inhibitors, salts, dyes and other contaminants). Generally, solid phase extraction includes three steps: (i) selective immobilization of nucleic acids from a crude sample on an activated surface; (ii) removal of contaminants through washing; (iii) release of purified nucleic acids. The extraction bed is created following embossing of the fluidic network using a simple UV activation step of PC.



Continuous Flow - Polymerase Chain Reaction (CF-PCR)

Reactions such as the polymerase chain reaction (PCR) or Ligase Detection Reaction (LDR) rely on subjecting the reaction mixture to predefined thermal cycles. Conventional methods are chamber-type processes in which a stationary reaction mixture is alternately heated and cooled. Continuous flow (CF) thermal cycling is based on flowing the reaction mixture in a microchannel repetitively through different isothermal zones – primary advantage of CF format is FAST cycling.

The cocktail with DNA template is transported to the CFPCR, hosting 30 cycles. The reaction is performed with 3 temperature zones; 10 s for denaturation, 10 s for annealing and 30 s for extension with sample flowing at 0.6 μl/min. Longer extension times are achieved using a deeper (240 μm) channel in that zone.

Polycarbonate (PC)

- Thermal zones ratio: D:A:E = 1:1:4
- Channel width: 80 μm
- Channel length: 1450 mm

Biochemical reactions that are thermally controlled and using active heating/cooling elements must be "isolated" from other processing steps included in the system.

PCR Efficiency

(A-B) A cross-section view of grooves and fins and (B) the temperature distribution of CFPCR reactor obtained via FE simulations with ANSYS. (C) The relative intensity of amplification efficiency at each flow rate compared to the reference –commercial thermal cycler.

On-chip Reagent Mixing

The Reynolds number in microfluidic channels is low, resulting in laminar flow. Therefore, the mixing of binary or multicomponent fluid streams in a microchannel relies mainly on diffusion. Diffusional mixing is fast in the nanoscale, but slow in the micro- and macroscale, owing to the nonlinear dependence of diffusion time with distance ($t \propto 2D$).

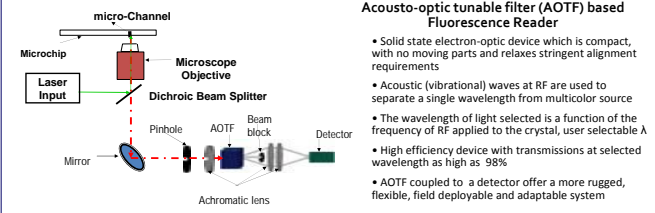
Numerical simulations aid in the design of the most effective mixer for reaction buffers.

Microarray Readout - Pathogen Detection rapid, selective, specific, and simultaneous detection

- Foodborne pathogens (*Escherichia coli* O157:H7 and *Salmonella*)
- important targets for the control of food safety and public health
- approximately 70 million illnesses and 5,000 deaths each year in the US
- food safety testing and healthcare costs total nearly 10 billion dollars

Results of pathogen detection; C1, C2: 20 μM and 10 μM Cy5-(T)₁₀-NH₂ spotting and immobilization control; - negative control; S1- probe targeting *E. coli* O157:H7 *eaeA* gene; S2 - probe targeting *Salmonella sipB/C* gene; +- hybridization positive control.

Laser-Induced Fluorescence Detector for Multi-Color Analysis



Microchip Capillary Gel Electrophoresis

Alu Mobile Element-based Gender Determination

Gel electrophoresis of amplicons of (A) *AluSTXa*: Male (M): 556 and 878 bp, Female (F): 878 bp only and (B) *AluSTYb*: M: 199 and 528 bp, F: 199 bp. Lanes (a-h) are different F:M DNA ratios; (a) 0:10, (b) 1:9, (c) 3:7, (d) 5:5, (e) 7:3, (f) 9:1, (g) 10:0, (h) 0:0.

The PCR cocktail contained both *Alu STXa* and *STYb* primer sets, targeting different loci on the X and Y chromosomes. For the *STXa* a filled site in X chromosome would give an 878 bp product and for an empty site in Y chromosome, a 556 bp product. For *STYb*, a 528 bp and 199 bp products were expected for filled sites in Y chromosome, and an empty site in X chromosome, respectively. For both loci, males are distinguished as having 2 amplicons, while PCR with female DNA gives one.

Experimental results

Numerical Simulations

Numerical simulations of loading and dispensing of sample into cross injectors with different geometries. A The pictures present only the central part of the simulated microchannels. 1-waste, 2-buffer, 3-sample, and 4-separation microchannel. Loading: 1 at 33.4 V, 3 at GND, 2 and 4 float. Dispensing: 1 and 3 float, 2 at GND, 4 at 66.8 V. $E_{flow} = E_{stop} = 167$ V/cm; $v_{flow} = 7.5$ s, $t_{stop} = 11$ s. t_1 corresponds to the start of dispensing; t_1 and t_2 were taken at 1 s increments.

Electropherograms of (A) pUC18 (stained with POPO-3, $E = 200$ V/cm) and (B) amplicons from typing *Alu STXa* for male DNA ($E = 125$ V/cm).

Connections with CyberTools

- Numerical simulations of fluid flow, heat transfer as well as electrical transfer, are currently used as an aid to develop design rules for multi-module biosensors required for constructing systems. Currently, only component level simulations can be carried out, once Fluent and ANSYS are migrated to HPC, system-level optimization simulations will be carried out.
- The use of simulations will minimize the number of test devices/systems that need to be fabricated using lithographic or HPMM processing, significantly reducing cost and time associated with the development of prototype devices.
- Current Experimental results will be used for algorithm and simulation optimization and verification. Once CyberTools are verified, these tools can be used for future system design.
- System modeling and numerical calculations include system assembly, material mismatch and selection, integration, geometrical architectures, thermal management, mixing etc.

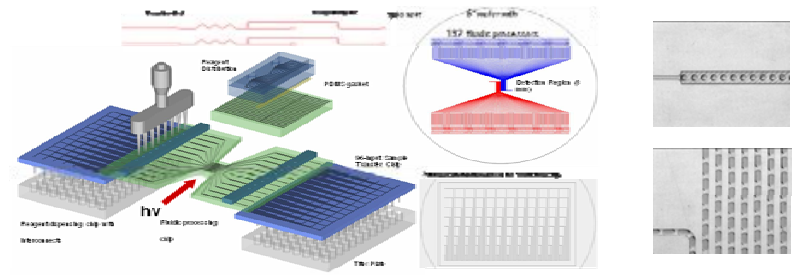
Acknowledgments

This work is generously supported by the National Science Foundation (EPS-0346411) and the State of Louisiana Board of Regents Support Fund.

INTRODUCTION

We are developing a high throughput screening (HTS) modular microfluidic system that will provide high levels of automation and the ability to carry out HTS campaigns in a variety of small laboratory/company settings embarking upon drug discovery projects. The fluidic elements will be fabricated into polymers using replication technologies from masters developed through a variety of processing techniques. The basic fluidic element will consist of: (i) Arrays of capillaries oriented in a footprint to match a conventional 96-well titer plate to feed inhibitor (small molecules) candidates from the titer plate into the fluidic system; (ii) Passive micro-mixer consisting of high aspect ratio microstructures for minimizing mixing time; (iii) Nanoreactors consisting of aqueous fluidic droplets suspended in an immiscible fluid and; (iv) Highly sensitive fluorescence reader to monitor enzymatic activity.

To test and evaluate the performance of the proposed system, we will screen inhibitors, from small molecule combinatorial libraries, of L1-EN. L1 genomic elements are active autonomous human mobile elements making up approximately 17% of the genome. At this point there are approximately 45 diseases caused by L1-driven events. We will use the normal oligonucleotide motif recognized by L1-EN and insert fluorescent labels onto this oligonucleotide. In order to perform a large number of assays, we will investigate and implement a parallelized detection scheme based on a CCD detector. The parallelized measurements will include fluorescence cross-correlation spectroscopy (FCCS). A rendition of this system is shown schematically below.



Integrated fluidic system for performing HTS assays. The system is configured on a 6" wafer and the wafer shown has 192 processors. The wafer consists of a stack of fluidic chips, with one chip used for containing the substrates and buffer reagents required for the HTS, a 96-element transfer chip to move drug candidates to the processor wafer and the HTS processor chip containing passive mixers, 2-phase flow generator and detector elements. The system is operated in a 2-phase flow format with an inert separator liquid to significantly increase processing throughput. The figures to the right show aqueous droplets or plugs suspended in a fluorinated hydrocarbon carrier fluid.

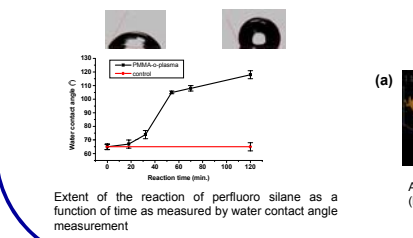
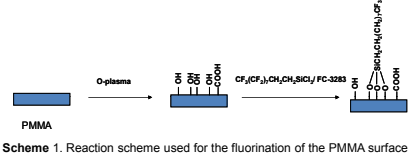
Connections with CyberTools

CyberTools will enable rapid progress and understanding of the scientific and engineering processes used to optimize and rationally guide design, construction and operation of components and eventually, systems comprised of thermal and fluidic components using the HPC platform. In addition, hybrid-codes (continuum/MD codes) will be transitioned to the HPC platform as well for evaluating multi-phase flows in mixed-scale structures. Specifically:

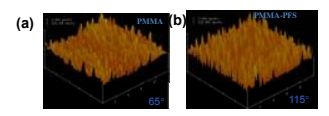
- Source Code Review:** Review of existing open-source CFD and MD software, which will be included in WP4 and modified for LONI use. This will provide us the ability to perform system-level optimizations.
- Microchannel/nanochannel Geometry:** Mixed-scale CFD simulations are being developed to monitor fluid transport in microchannels (continuum formulations) and nanochannel domains (MD formulations).
- Test Case Simulations:** CFD and MD simulation methods to predict experimental observables in sensor test cases operated in mixed-scale domains.
- CFD/MD Integration with CACTUS:** CACTUS-based toolkit used for CFD and MD test case simulations.
- Non-Newtonian Fluidic simulations:** For molding high aspect ratio structures over mixed scales, new codes will be developed to model molding and demolding of fluidic components using flowing polymer melts.
- Toolkit-based Simulations:** Utilization of toolkits for full scale simulations across institutions.

Surface Engineering for Droplet Microfluidics

- In droplet microfluidics, each droplet of approximately 1 nL volume is used as a microreactor. The controlled and rapid mixing of fluids in the droplet reactors results in decreased reaction times. In this format a large number of reactions can be carried out in parallel using small volumes of the reagents.
- In order to carry out the kinetics of the reaction of L1-EN with the library of compounds, droplets of the enzyme, the substrate and the compound libraries should be formed in the immiscible carrier perfluoro liquid (FC-3283) and mixed precisely.
- In PMMA and PC microfluidic devices, the aqueous droplets are stable only for a few minutes. In order to form the stable two-phase flow for longer time, the surface of the microfluidic device should be rendered hydrophobic.
- We modified the surface of the PMMA microfluidic device, by reacting with the perfluoro compounds as shown in Scheme-1.
- The water contact angle measurement showed that the modified PMMA surface is hydrophobic.

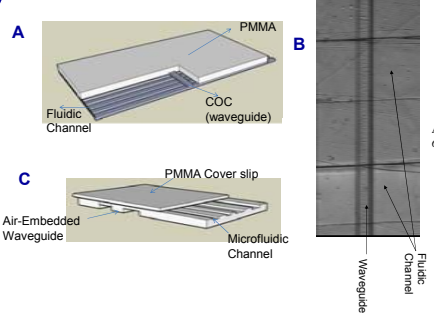


- Water contact angle (WCA) of PMMA ($65 \pm 2^\circ$) was increased ($118 \pm 3^\circ$) upon modification.
- The AFM images show that the reaction does not increase the surface roughness. The RMS surface roughness of these films were for PMMA 14.87 nm and after the reaction 13.17 nm.
- This method is applicable to modify surfaces of other polymer such as polycarbonate (PC).



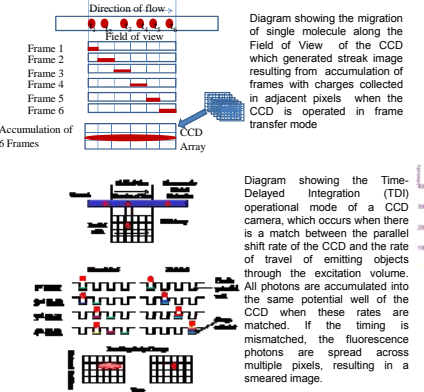
AFM images of (a) cleaned PMMA and (b) perfluoro silane modified PMMA surfaces

Embedded Waveguide

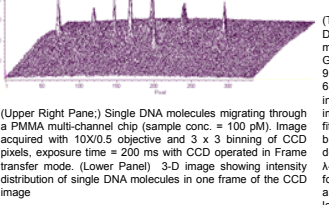
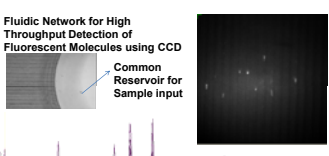


(A). Schematic of COC core embedded waveguide showing the integrated fluidic geometry. (B) Optical image of the fabricated fluidic device with orthogonal air-embedded COC core waveguide. (C) Schematic of air embedded waveguide fabricated on COC wafer.

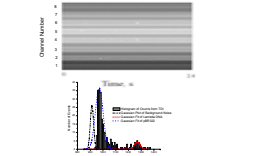
Single Molecule tracking



High Throughput SMD with Frame Transfer CCD



High Throughput SMD with CCD Operated in TDI Mode



(Top Panel) TDI image of λ-DNA and pBR322 DNAs traveling electrokinetically through 8 microfluidic channels with an orthogonally situated Gaussian laser beam (25 mW borate buffer pH 9.1; shift rate 8 ms; E = 125 V/cm; 10 mW; λex = 635 nm). (Bottom Panel) Histograms of the peak intensities versus number of events from TDI images shown in Figure 4a. The histograms were fit to Gaussian functions from which the mean burst amplitude and standard deviations were derived (mean = 1268, standard deviation = 23 for λ-DNA and mean = 974, standard deviation = 17 for pBR322). A Gaussian curve of the noise was also plotted to determine the detection threshold level of 952.

Fluorescence Cross-Correlation Spectroscopy

Crosscorrelation function $G(\tau)$: Mathematically, the normalized cross-correlation function $G(\tau)$ is calculated as time average $\langle \cdot \rangle$ of the product of the fluorescence fluctuations of two fluorescent species i at times t and $t + \tau$, normalized by the product of the time-averaged fluorescent signals of two species i and j .

$$G(\tau) = \frac{\langle \delta F_i(t) \delta F_j(t + \tau) \rangle}{\langle F_i(t) \rangle \langle F_j(t) \rangle}$$

Hardware used for monitoring FCCS responses. This is a dual-color system for exciting the substrate for L1-EN. While a single detector is shown, it will be combined with a CCD.

Design and Fabrication of Small Footprint Continuous Flow PCR Devices for a Multi-Well CFPCR Platform

D. S. Park¹, P.-C. Chen^{1,2}, B. H. You^{1,2}, N. Kim^{1,2}, T. Park^{1,2}, T. Y. Lee^{1,2}, P. Datta³, Y. Desta⁴, S. A. Soper^{1,5}, D. E. Nikitopoulos^{1,2}, M. C. Murphy^{1,2}

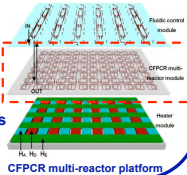
¹Center for Bio-Modular Multi-Scale Systems, ²Department of Mechanical Engineering, ³Center for Advanced Microstructures and Devices (CAMD), ⁴BioFluidica Microtechnologies, ⁵Department of Chemistry, Louisiana State University, Baton Rouge

Abstract

Small footprint (8 mm x 8 mm) continuous flow (CF) PCR devices were designed, fabricated, and used to amplify DNA fragments as part of a multi-well CFPCR platform for high throughput (HT) PCR applications. A variety of spiral CFPCR devices were designed and fabricated by UV-LIGA technique for a nickel large area mold insert (LAMI) and grooves and fins by micro-milling for a brass LAMI. Double-sided micro molding in polycarbonate (PC) with two LAMIs was done using hot embossing. The molded PC chips were sealed in a custom-designed thermal fusion bonding apparatus. Small footprint, 20- and 25-cycle CFPCR devices for a CFPCR multi-reactor chip successfully amplified 99-bp target DNA fragments from a 48k bp λ -DNA template.

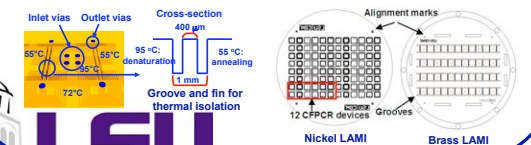
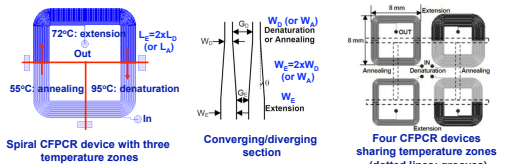
Motivation and Objective

- High demand for a highly parallel, polymerase chain reaction (PCR) multi-reactor platform: exploration of the accumulated genetic information from the Human Genome Project
- Incorporation of CFPCR devices into a polymer, 96-well titer plate format (120 mm x 96 mm) for a HT CFPCR multi-reactor platform
 - CFPCR multi-reactor module
 - Heater module
 - Fluidic control module
- Small footprint, CFPCR devices for a 1st generation, double-sided CFPCR multi-reactor module chip
 - Optimization of the geometry for CFPCR devices
 - Verification of DNA amplification capability

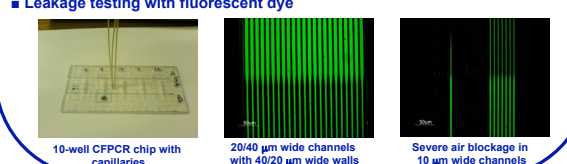
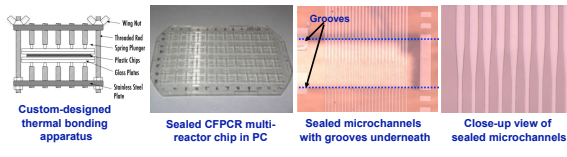
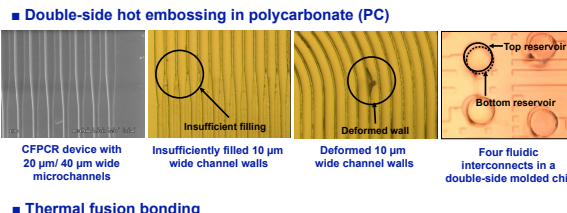
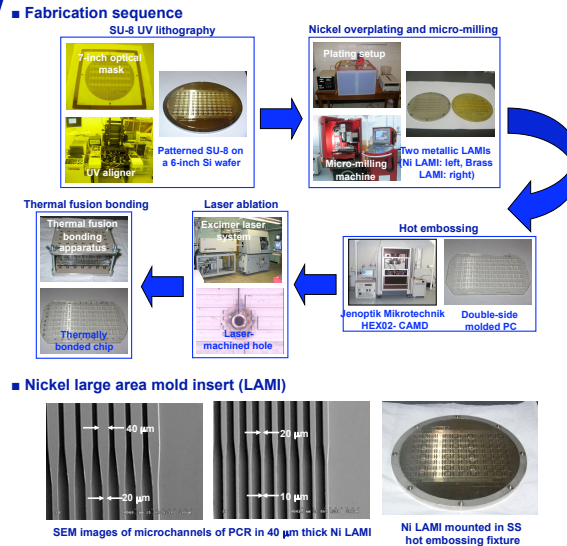


Design

- Effective footprint of each spiral CFPCR device: 8 mm by 8 mm
- Residence time ratio of 1:1:4 for denaturation : annealing : extension
 - Length and width of the microchannels in extension zones doubled compared to those in denaturation or annealing zone
- Various dimensions: microchannel widths of 10-40 μ m, wall widths of 10-55 μ m, microchannel depth of 40 μ m (six types of devices) \rightarrow a group of twelve CFPCR devices for 20- and 25-cycles
- Sharing of temperature zones for adjacent CFPCR devices

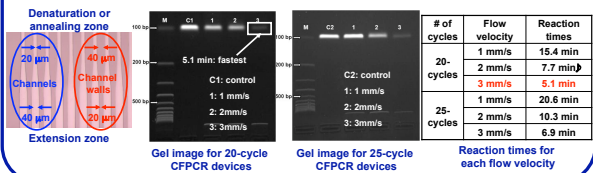


Fabrication



DNA Amplification

- Small footprint, 20- and 25-cycle CFPCR devices with 20 μ m/40 μ m wide microchannel (40 μ m/20 μ m wide channel walls) used
- DNA template: 48k bp λ -DNA c1857Sam7
- Primers to generate 99 bp target DNA fragments
- Thermal cycling with three copper plates, strip heaters, and TCs (94°C for denaturation, 63°C for annealing, and 72°C for extension)
- Different flow velocities: 1 mm/s, 2 mm/s and 3 mm/s corresponding to 0.048 μ l/min, 0.096 μ l/min, and 0.144 μ l/min



Conclusions

- Optimization of the geometry for the 1st generation 96-well CFPCR multi-reactor chip throughout manufacturing processes
 - 20 μ m/40 μ m wide microchannel walls for structural rigidity
 - 40 μ m/20 μ m wide microchannels for smooth fluid control
- Successful demonstration of DNA amplification capability in small footprint CFPCR devices
 - Reaction times as fast as 5.1 min for 20-cycle CFPCR devices at 3 mm/s
- Development of a heater module and a fluidic control module for complete realization of the high throughput CFPCR platform under way

Connections with CyberTools

- Simulation challenges for micro-scale devices in large area format (120 mm x 96 mm)
- Device simulation
 - Temperature distribution over the whole CFPCR multi-reactor module
 - Fluid flow and heat transfer for individual CFPCR devices
 - Tracking plugs through multi-well devices
- Process simulation
 - Filling behavior analysis in molding process
 - Failure analysis in de-molding: thermal stress and local deformation

References

[1] M. Hashimoto, P.-C. Chen, M. W. Mitchell, D. E. Nikitopoulos, S. A. Soper, and M. C. Murphy, 2004, Lab Chip, pp. 638-645
 [2] D. S. Park, P.-C. Chen, B. H. You, N. Kim, T. Park, T. Y. Lee, P. Datta, Y. Desta, S. A. Soper, D. E. Nikitopoulos, and M. C. Murphy, 2008, Hilton Head Workshop 2008, pp. 114-117

Acknowledgements

This work was supported by the National Science Foundation under Grant Number EPS-0346411 and the State of Louisiana Board of Regents Support Fund, Industrial Ties Program through Grant Number LEQSF (2005-08)-RD-B-04. The authors thank the Center for Advanced Microstructures and Devices (CAMD) at Louisiana State University for the microfabrication support.

Abstract

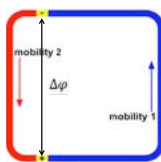
The aim of this work is to design and realize a continuous flow micro-fluidic device for PCR (Polymerase Chain Reaction) or LDR (Ligase Detection Reaction), two cyclic reactions needed in DNA analysis. The device, called an Electrophoretion, combines electroosmotic and electrophoretic effects to induce cyclic motion of buffer, DNA and other reactants in a single-loop micro-channel, with only one constant difference of potential applied.

It should be noted that the following study is conducted assuming PCR conditions (buffer: PCR buffer at pH 8.3, species: DNA) in a Polycarbonate device; however, other applications are possible (e.g. mixing).

Principle^[1]

Channel 2:

- Chemical reversal of the EOF
- EOF and Electrophoresis complementary



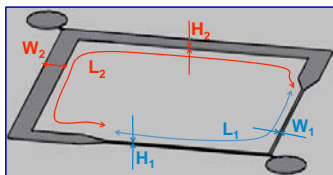
Channel 1:

- No EOF treatment
- EOF and Electrophoresis adverse

Figure 1: Scheme of an Electrophoretion

Theoretical Analysis

Figure 2: Example of a 3D Electrophoretion Design



- Assumptions**
- Electrical Debye Layer infinitely thin
 - Electrodes effects negligible
 - Bends effects negligible
 - DNA Diffusion negligible
 - Geometry transition effects negligible

Solving Electrical potential and Flow gives velocity profiles in channel i:

$$w_i(x, y) = \frac{\Delta\phi}{L_i} \left(\mu_{ef,i} - \frac{\pi^2}{4} F_i(x, y) \left(\frac{\mu_{e01} H_1 W_1 + \mu_{e02} H_2 W_2}{L_1} + \frac{\mu_{e01} H_1 W_1 + \mu_{e02} H_2 W_2}{L_2} \right) \right)$$

$F_i(x, y)$ and g_i are quickly converging series depending on channel i geometry
 μ_{e0i} : electroosmotic mobility of channel i
 $\mu_{ef,i}$: effective mobility of channel i (sum of electroosmotic and electrophoretic)

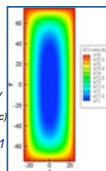


Figure 3: Example of Electroosmotic Velocity Profile in Channel 1 (Configuration from P2)

Optimization

Using theoretical analysis results and Matlab Optimization toolbox, we investigate design variations (α : L_1/L_2 , β : W_2/W_1 , γ : H_2/H_1) to maximize velocity in the center of Channel 1.

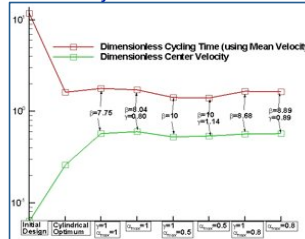


Figure 4: Comparison between different Optimum Configurations

Note:
Function used detects only local maxima => Initial conditions and limits have a huge impact on the optimized solution.

Simulations

Simulations allow to take into account: bends effects and electrodes influence, as well as DNA diffusion. Designs were realized with AutoCAD 2008, and mesh and running were done using Coventorware 2006 (Solver: Fluent). These confirmed cycling (Figure 6) as well as validated theoretical velocity profiles shape (Figures 7 & 8)

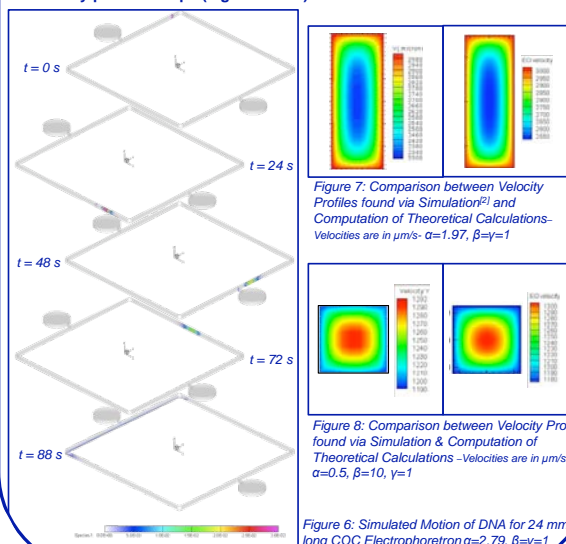


Figure 6: Simulated Motion of DNA for 24 mm long COC Electrophoretion $\alpha=2.79$, $\beta=\gamma=1$

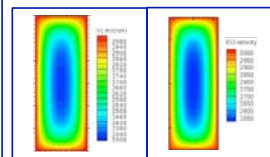


Figure 7: Comparison between Velocity Profiles found via Simulation^[1] and Computation of Theoretical Calculations - Velocities are in $\mu\text{m/s}$ - $\alpha=1.97$, $\beta=\gamma=1$

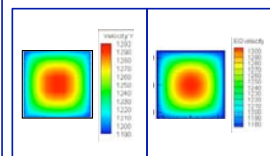


Figure 8: Comparison between Velocity Profiles found via Simulation & Computation of Theoretical Calculations - Velocities are in $\mu\text{m/s}$ - $\alpha=0.5$, $\beta=10$, $\gamma=1$

Main Practical Limitations

- 96 well format: footprint 8x8 mm

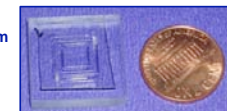


Figure 9: Initial design chip hot embossed in Polycarbonate (PC)

- EOF: large uncertainty & protein (e.g. Polymerase for PCR) influence

Figure 10: Comparison of Different Measurements of Electroosmotic Mobilities inside PC microchannels

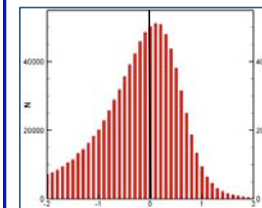
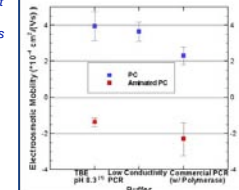


Figure 11: Monte-Carlo Simulations: Mean Velocity Repartition in Channel 1 due to Electroosmotic Mobility Variations and Geometry Variations - $\alpha=2.88$, $\beta=\gamma=1$

- Hydrolysis: out electrodes

- Visualization of EOF only challenging (absolutely neutral dye and/or particles needed)

Connections with CyberTools

Current simulations have been done with commercial software on individual workstations. Obtaining simulation results to support an optimization study of a complex, multi-physics device/process which involves a large number of parameters is untenable through present means. CyberTools (e.g. WP1, WP3, WP4) enables the use of High Performance Computing for the solution of the governing equations and their coupling with optimization algorithms on a user-friendly platform (e.g. CACTUS). This results in faster and more efficient design of devices/systems for the science-driver application (geno-sensor), as well as better understanding of the related physics through visualization.

References

- ^[1] Choi et al., Journal of Chromatography A, 924, 53-58 (2001)
^[2] Elmajdoub, LSU thesis (2006)

Acknowledgements

All CBM² members, especially Murphy's and Soper's groups, Jason Guy and Proyag Datta (Microfab).
 Fundings: NIH-BRP, NSF-EPSCoR



Real-time Information Services for Scientific Applications

Katerina Stamou^{1,2}, Gabrielle Allen^{1,2}, Erik Schnetter^{1,3}

¹Center for Computation and Technology, LSU

²Department of Computer Science, LSU

³Department of Physics and Astronomy, LSU

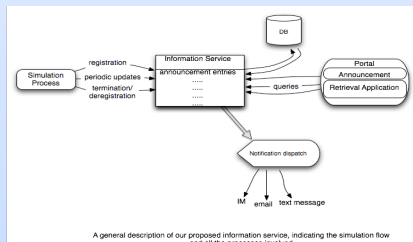


Abstract

Distributed scientific communities can immensely benefit from having a central infrastructure for keeping important information, given the overall collaborative nature of their running simulations, that are usually conducted in different local sites. Such data needs to be structured in a way that can be described and queried with precision and speed, for later retrievals.

Core Scenario/Motivation

A scientist who would like to run her simulation, submits her task to run to a cluster of machines. When the requested resources become available, the task is selected and executed. During initialization phase, the simulation registers with an application information service, and dispatches basic execution details. As information arrives a notification service informs collaborating scientists. While the simulation runs, it periodically updates the current application status and information.

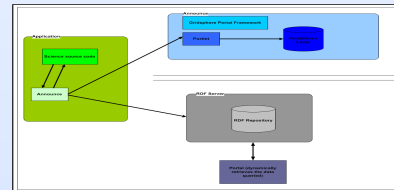


Drawing from this use case, we were motivated into investigating the following:

- Measure the performance, functionality and usability of both Announce and Formaline Cactus thorns by running actual tests on several LONI clusters
- Integrate both technologies within LONI portal through a smooth migration and interoperability process
- Extend the SAGA Advert Service, by incorporating it into the suggested information system

Announce & Formaline in Cactus

Cactus provides a vast array of application-specific scientific functions, through extension libraries, called 'thorns', while taking advantage of modern large scale, parallel computing resources.

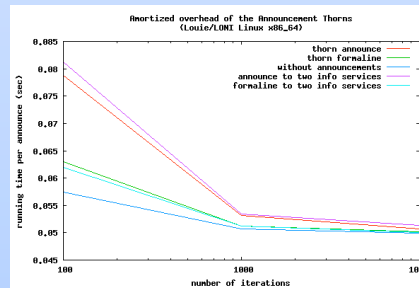


The "Announce" thorn was developed to automatically communicate general information about Cactus simulations to a service viewable from a portal.

A different Cactus thorn, "Formaline" similarly preserves important results and metadata about simulations by announcing them to an information service where they can be kept for prolonged periods of time, for later analysis.

We are conducting tests, in order to measure and compare the efficiency of both the "Announce" and "Formaline" systems:

- net impact of each thorn on the overall simulation time
- amortized overhead of the systems
- user interface responsiveness
- * backend store database scaling, under increasing amounts of announcement entries

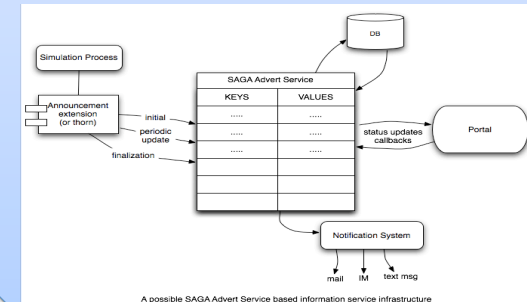


The above diagram represents results on the amortized overhead time of the announcement thorns, in relation to the number of iterations and the simulation time

SAGA-Advert Service

A full-fledged information service, built on top of the SAGA-Advert service, would require:

- From a client-side perspective, an extension library for the simulation application (or a thorn, in the case of Cactus), that would communicate the simulation metadata to the advert service, using the SAGA library interface.
- An information service, build around the Advert Service, which would be able provide means for publishing and retrieving metadata, as well as providing notification services.
- An application for visualizing the stored metadata, giving convenient access through an interface for querying and viewing real-time as well as historic archived simulation information. Preferably, this could be implemented as a web portlet on top of a portal platform, like gridsphere.



Connections with CyberTools

Through this effort, we build on, and extend existing well-established architectures and packages, i.e. the Cactus toolkit, and the SAGA library. This work will lead to a general information service and announcement mechanism which can be easily incorporated into any CyberTools simulation code.

Acknowledgements

We thank Ian Kelley and Thomas Radke, co-authors of Announce and Formaline for their cooperation and assistance in this work. Also, Hartmut Kaiser, SAGA lead architect, for providing us with useful advice on SAGA advert service.

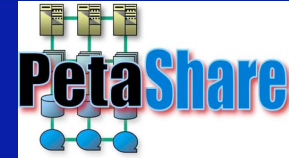
Cybertools is supported by NSF/EPSCoR Award No. EPS-0701491



Distributed Data Management in CyberTools

Ibrahim H Suslu¹, Xinqi Wang¹, Ismail Akturk¹, Tevfik Kosar¹

¹Louisiana State University, Center for Computation and Technology



Abstract

CyberTools will provide services such as information processing, data management, storage, and co-scheduling for the science projects in LONI environment. Data management services help manage large amount of experimental and observational data. The larger data require the better data management tools need to be developed. User friendly and intelligent data management tools will decide what type of remote data access technique to use either remote I/O or staging, client tools can access remote data using three different interfaces: petashell, petafs, and pcommands, and the ontology based metadata search gives logical filenames that match the semantic search criteria, and then, each logical file name has corresponding set of physical file names, for the searched data entity.

Remote I/O and data staging are the most widely used data access methods for large scale distributed applications with non-local data sources. We are developing such a model for the CyberTools data management clients which will choose the most appropriate data access method for applications. We define the parameters that potentially affect the end-to-end performance of the distributed applications which need to use remote and distributed data.

Extendable metadata management is essential in large-scale distributed data management, traditional metadata management is not sufficient to provide interoperability for large-scale, physically and semantically heterogeneous dataset. We present a semantically enabled metadata management framework based on ontology. We seek to address two main issues: data integration for semantically and physically heterogeneous distributed knowledge stores, and semantic reasoning for data verification and inference in such a setting. Our metadata management aims to enable data interoperability among otherwise semantically incompatible data sources, cross-domain query capabilities and multi-source knowledge extraction.

Modeling to Access Remote Data

Preliminary Model

Parameters:

Staging

$$T_s = T_{in} + E + T_{out}$$

Where

$$T_{in} = R_{rin} + N_{sin} + W_{lin} + R_{lin}$$

$$T_{out} = W_{lou} + R_{lou} + N_{sou} + W_{lou}$$

Remote I/O

$$T_r = R_{rin} + N_{rin} + E + N_{rou} + W_{rou}$$

For Remote I/O to be more efficient than staging:

$$R_{rin} + N_{rin} < R_{rin} + N_{sin} + W_{lin} + R_{lin}$$

$$\Rightarrow N_{rin} - N_{sin} < W_{lin} + R_{lin}$$

and

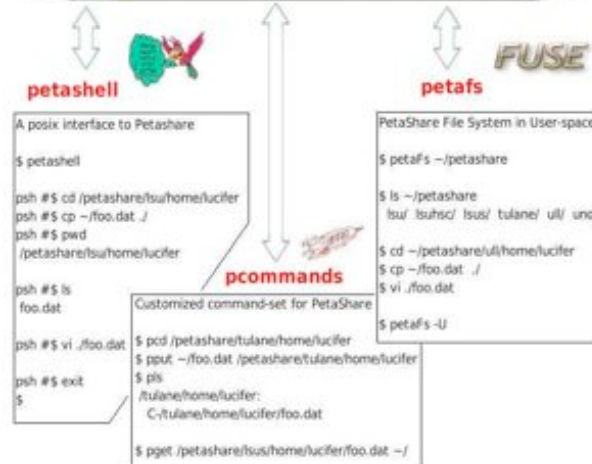
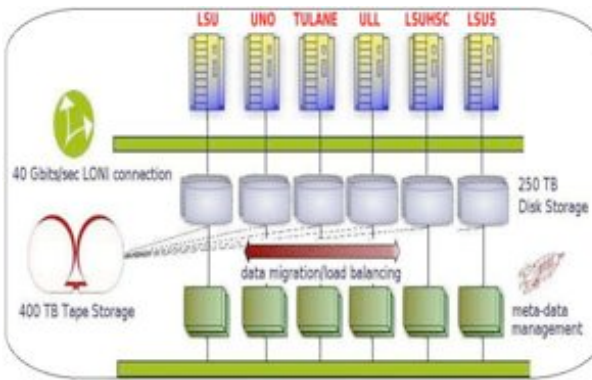
$$N_{rou} + W_{rou} < W_{lou} + R_{lou} + N_{sou} + W_{lou}$$

$$\Rightarrow N_{rou} - N_{sou} < W_{lou} + R_{lou}$$

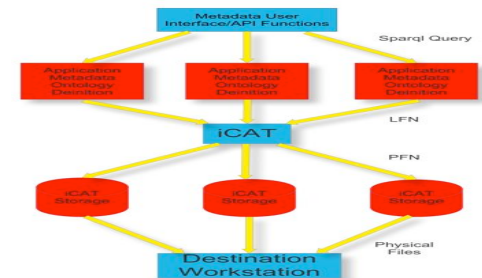
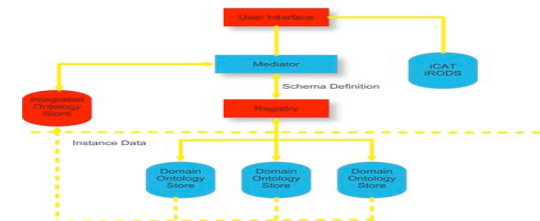
If remote I/O library performs good in data transfer over network, or local disk performance is slow, remote I/O might be advantageous over staging, otherwise, staging method would perform better.

Petashare

CyberTools's distributed data management infrastructure PetaShare provides scientists with access to data widely distributed across multiple geographically far-apart institutions. So far, three PetaShare clients have been developed to provide three distinct access modes to underlying PetaShare infrastructure: PetaFs allows PetaShare infrastructure to be mounted as a folder on any Linux machines; PetaShell provides a regular shell environment for access to PetaShare, user can use regular Unix commands to access PetaShare under both PetaFs and PetaShell; Pcommand, on the other hand, provides a set of PetaShare enabled commands user can use to directly access PetaShare.



Semantically Expanded Data Access



Connections with CyberTools

- ✓ Among CyberTools related projects, Petashare will seek to provide an iRODS based distributed data management infrastructure in which data can be more easily located, understood and retrieved.
- ✓ We seek to address the problem of lack of integration of data produced by different scientific domains through semantic enabled metadata management.
- ✓ Petashare user client interfaces (petafs, petashell, pCommands) allow transparent data management, so that the CyberTools scientists can focus on their own research and the content of the data rather than how to manage it.
- ✓ Staging and Remote I/O model can be applied to most data intensive distributed cyberTools applications to decide the best data access model for those applications.

Acknowledgements

This project is in part sponsored by the National Science Foundation under award numbers CNS-0619843 (PetaShare) and EPS-0701491 (CyberTools), and by the Board of Regents, State of Louisiana, under Contract Number NSF/LEQSF (2007-10)-CyberRI-01.





LIGO Outreach Tangibles: Integration of Tangible Interaction and Visual Computing as Gateways to Science

Cornelius Toole, Jr., Zachary Dever, Alvin Wallace, Jr., and Brygg Ullmer
Louisiana State University
Department of Computer Science and
Center for Computation and Technology

LIGO Outreach Tangibles

The LIGO Outreach Tangible Kiosk is a platform that combines visual computing, tangible interaction, and visual & physical design efforts to deliver engaging educational content on science topics related to the Laser Interferometer Gravitational Observatory project. Longer term, we also seek to provide a path for accessing and engaging with high-end computational resources used for scientific inquiry or their byproducts. Here we describe work in progress in the development of this kiosk platform and a game activity based upon a key LIGO outreach activity. We also describe future iterations for this platform.

Motivation

- To stimulate interests and reinforce science instruction in formal and informal contexts
- To help fill gap, in costs and flexibility, between two types of successful LIGO outreach activities: Exploratorium-developed exhibits(\$10K-50K in costs) and "science snacks"(\$0-50)
- To address tech literacy/usability gaps by using tangible interaction to wield chains of complex, digital actions through simple physical interactions

Connections to Cybertools

- When deployed in places with network connectivity, can be used to provide access to key cyber-infrastructure
- As we extend this tangible interaction kiosk platform to other applications, users will be able to access scientific data repositories, visualization services

Acknowledgments

- This project was supported by the Louisiana Board of Regents, contract #33027 (2008-2009) and the LSU Huel D. Perkins Doctoral Fellowship.
- We would like to thank John Douthat, Ian Wesley-Smith, Srikanth Jandhyala, Rajesh Sakaran and Kexi Liu



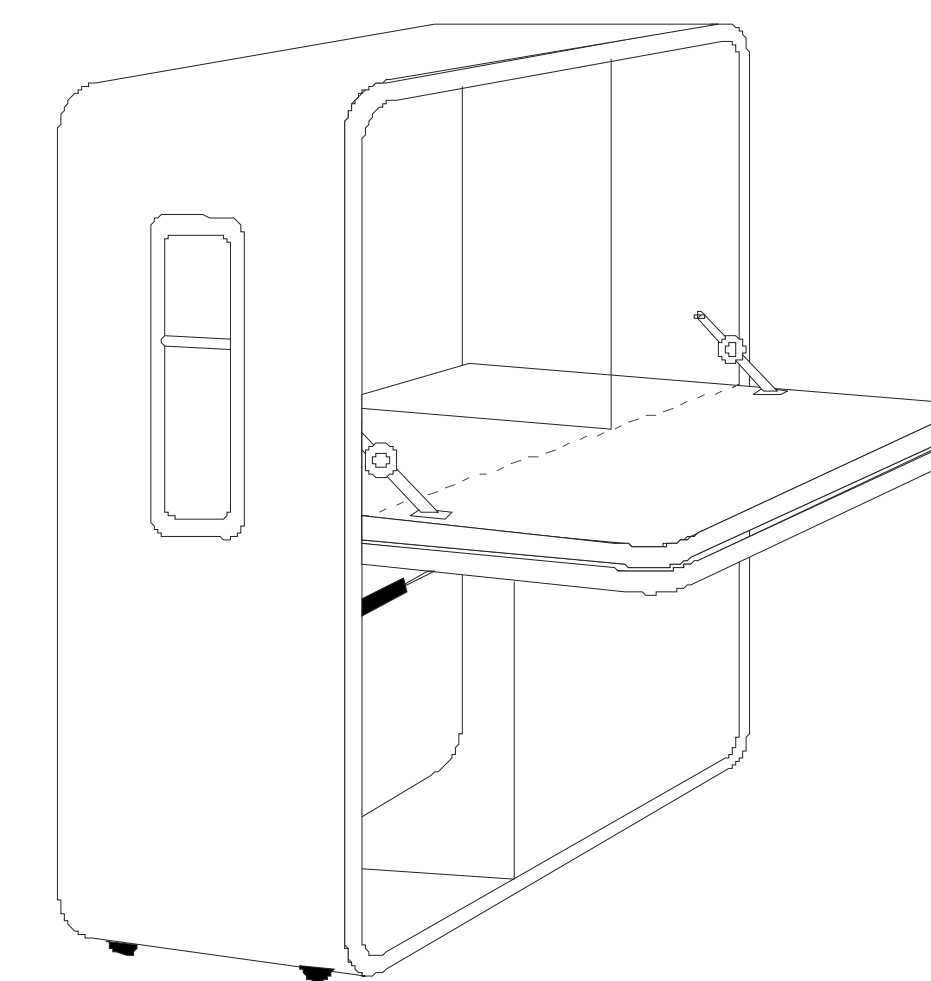
Children driving hurricane visualization(left) and handheld microscope(right) with tangibles



Images from the 1977 Ray and Charles Eames film, "Powers of Ten"



Touchscreen tablet + Powermate® knob enclosure(right) and three-wheeled parameter tray(left)



Design sketches of LIGO Outreach Kiosk for museum settings(left) and for classroom settings(right)

LIGO Kiosk Content and Activities

- A wide range of applications can be delivered through the tangible kiosk platform
- For initial phase of project we chose to develop a game centered around a film, which is pre-screened by most visitors to the LIGO Science Education Center
- We plan to develop information visualization content based upon galaxy catalog data

Powers of Ten Game

- Based upon a Ray and Charles Eames 1977 film that depicts the relative scale of the universe
- Our game pits player against each other as they try to correctly match orders of magnitude with images

Galaxy Catalog Visualization

- Corso et al provide a tool that analyzes LIGO run data along with Compact Binary Coalescence Galaxy catalog data to visualize the sensitivity of LIGO thus showing which galaxies can be observed

Future Work

- Limited deployment at science education centers and middle schools
- More content development with aid of scientist consultant
- Finalize evaluation plan with educational consultant
- Integration of novel tangible interaction devices
- Design a high level communication framework capable of supporting both local and remote interaction for easier integration of other applications
- Longer term development of tangibles kiosks for access to high performance computing applications such as large data visualization, remote collaborative visualization and computational steering.

References

1. Corso, B., Bengler, W., and Gonzalez, G. Visual Representation of Inspiral Group Galaxy List, Technical Report, 2008.
2. Sankaran, R., Ullmer, B., Jandhyala, S., Kallakuri, K., Sun, S. and Laan, C. Blades and Tiles: An Extensible Hardware Architectural Approach for Ubiquitous Interaction Devices. In Proc. of Ubicomp'07, 2007.
3. Ullmer B., Sakaran, R., Jandhyala, S., Tregre, B., Toole, C., Kallakuri, K., Laan, C., Hess, M. Harhad, F., Wiggins, U., and Sun, S. Tangible Menus and Interaction Trays: Core Tangibles for Common Physical/Digital Activities, In Proc. of TEI'08., 2008



Predicting Optimal Level of Parallelism in Wide Area Data Transfers

Esma Yildirim¹, Dengan Yin², Tevfik Kosar³

^{1,2,3}Center for Computation and Technology,
^{1,2,3}Louisiana State University



Abstract

Using multiple parallel streams for wide area data transfers may yield much better performance than using a single stream, but overwhelming the network by opening too many streams may have an inverse effect. The congestion created by excess number of streams may cause a drop down in the throughput achieved. Hence, it is important to decide on the optimal number of streams without congesting the network. Predicting this 'magic' number is not straightforward, since it depends on many parameters specific to each individual transfer. Generic models that try to predict this number either rely too much on historical information or fail to achieve accurate predictions.

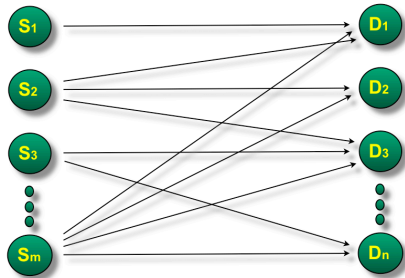
We present a set of new mathematical models which aim to approximate the optimal number of streams to open with least historical information and lowest prediction overhead. An algorithm is also introduced to select the best combination of historical information to do the prediction. We measure the feasibility and accuracy of the proposed prediction models by comparing to actual GridFTP parallel data transfers.

We are able to predict the throughput of any parallelism level accurately by using only little historical information. The decision of the correct parallel stream number will provide us with the optimal data transfer rate without congesting the network. Current data schedulers (e.g. Stork) could use these insights to optimize multiple data transfers and do intelligent decisions without requiring a large amount of historical information about bulk data transfer characteristics.

Data Scheduling Problem

Transfer k files between m sources and n destinations

- Ordering requests (considering priority, file size, etc.)
- Throttling - deciding number of concurrent transfers (considering available target storage space, network capacity, etc.)
- Tuning protocol transfer parameters (considering current network condition)



Models

Mathis Throughput Equation

$$Th \leq \frac{MSS}{RTT} \frac{c}{\sqrt{p}} \quad \text{for } n \text{ streams} \quad \rightarrow \quad Th_n \leq n \frac{MSS}{RTT} \frac{c}{\sqrt{p_n}}$$

Th = Throughput
 MSS = Maximum Segment Size
 c = Constant
 p = Packet Loss Rate

Model Th with a partial order-c equations

Model Th with a full second order equation

Approach 1

$$p'_n = p_n \frac{RTT_n^2}{c^2 MSS^2} = a'n^c + b'$$

$$Th_n = \frac{n}{\sqrt{p'_n}} = \frac{n}{\sqrt{a'n^c + b'}}$$

Approach 2

$$p'_n = p_n \frac{RTT_n^2}{c^2 MSS^2} = a'n^2 + b'n + c'$$

$$Th_n = \frac{n}{\sqrt{p'_n}} = \frac{n}{\sqrt{a'n^2 + b'n + c'}}$$

We only need 3 throughput measurements of different parallelism levels to solve the above equations: Th_{n1} , Th_{n2} and Th_{n3}

$$\frac{n_3^c - n_1^c}{n_2^c - n_1^c} = \frac{Th_{n3}^2 - Th_{n1}^2}{Th_{n2}^2 - Th_{n1}^2}$$

$$a' = \frac{\frac{n_2^2}{Th_{n2}^2} - \frac{n_1^2}{Th_{n1}^2}}{n_2 - n_1}$$

$$b' = \frac{n_1^2}{Th_{n1}^2} - a'n_1^c$$

To be able to solve c' we apply an approximation method called Newton's Method

$$a' = \frac{\frac{n_3^2}{Th_{n3}^2} - \frac{n_1^2}{Th_{n1}^2}}{n_3 - n_1} - \frac{\frac{n_2^2}{Th_{n2}^2} - \frac{n_1^2}{Th_{n1}^2}}{n_2 - n_1}$$

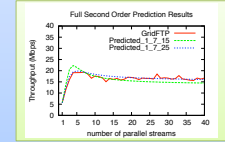
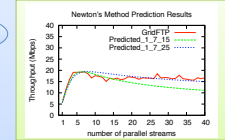
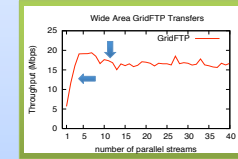
$$b' = \frac{\frac{n_2^2}{Th_{n2}^2} - \frac{n_1^2}{Th_{n1}^2}}{n_2 - n_1} - (n_1 + n_2)a'$$

$$c' = \frac{n_1^2}{Th_{n1}^2} - a'n_1^2 - b'n_1$$

Application

Can we predict this behavior?

Yes!



GridFTP parallel transfers have a characteristics of a **steep increase** first, then a **slow decrease** with a lower bound

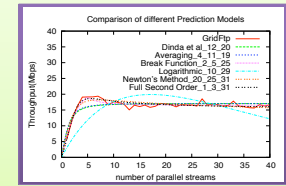
Best Parallelism Data

Algorithm
Input: m throughput values of different parallelism levels

For $i=1$ to $m-2$
For $j=i+1$ to $m-1$
For $k=j+1$ to m

- Calculate a' , b' and c'
- if the coefficients are within certain boundaries
- Calculate **Error Rate**

Find i, j, k that gives minimum **Error**



Connections with CyberTools

The Scheduling and Data Services (Work Package 1) work package of CyberTools aims to support a distributed data archival for all LONI projects and management of reliable and efficient data retrieval for Science Drivers who would like to store and access their data. PetaShare will handle all the low-level data handling issues such as data-aware storage systems and schedulers which support application areas that include coastal and environmental modeling, geospatial analysis, bioinformatics, medical imaging, fluid dynamics, petroleum engineering, numerical relativity and high-energy physics. The Stork data scheduler will further be developed to allow on-demand queuing, scheduling and optimization of data placement jobs. With the optimization of parallel stream number, the maximum throughput can be gained for data placement jobs without congesting the network and in this project we find a methodology to decide optimal stream number via mathematical models.

Acknowledgements

This project is in part sponsored by the National Science Foundation under award numbers CNS-0619843 (PetaShare) and EPS-0701491 (CyberTools), and by the Board of Regents, State of Louisiana, under Contract Number NSF/LEQSF (2007-10)-CyberRII-01. Thank You!



Abstract

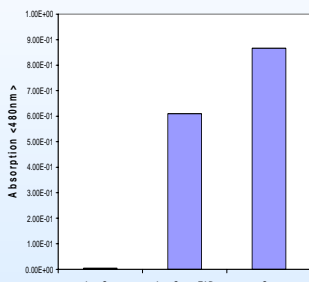
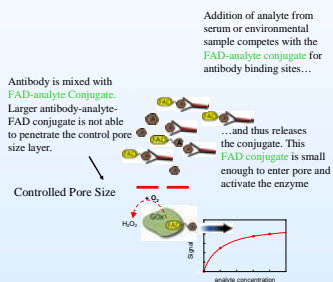
Most currently available immunosensors are designed to detect high molecular weight molecules (primarily proteins and infectious agents); where as low molecular weight chemical agents still remain a challenge to detect. In this project, we proposed to develop a miniaturized immunosensor platform with the versatility to simultaneously detect a large number of low molecular weight agents, including environmental contaminants, serum constituents, and chemical warfare agents. We proposed the development of a micro-mixer for handling fluids and electrochemical detection system for the new sensor format. Initial experiments were performed using electrode made of poly(3,4-ethylenedioxythiophene) poly(styrenesulfonate) (PEDOT-PSS) conducting polymer and carbon nanotubes (CNTs). Different techniques such as electrochemical polymerization, chemical and electrochemical deposition and spin coating were applied for the fabrication of such carbon nanotubes or polymer-based electrodes. A novel omega shaped micro-mixer was fabricated to enhance the mixing of antibody with analyte. The fluid flow and mixing action in microchannels were observed by injecting two test fluids of different colors. From both simulation and experimental results, a laminar flow of specified fluid was observed in the devices with straight channels, whereas a turbulent type of flow was observed in devices with omega channels.

Introduction and Background Work

The enzyme glucose oxidase (GOx) is the key component of many commercially successful biosensors. In order to work as a catalyst, glucose requires a cofactor, Flavin Adenine Dinucleotide (FAD). Figure 1(b) shows the absorption characteristics of apo-Gox, apo-Gox + FAD and GOx in the presence of glucose. Apo-GOX did not give much response indicating the complete removal of FAD from GOx.

Figure 1(a)

Figure 1(b)



Absorption Characteristics of Apo-Gox, Apo-Gox + FAD and Gox in the presence of glucose in UV-vis Spectroscopy.

Immunosensor Fabrication

- Silicon wafer with oxide layer
- Spin coat PR 1813 resist layer
- Pattern PR 1813 resist
- Sputter gold electrodes
- Lift-off PR 1813 resist
- Spin coat polymer layer

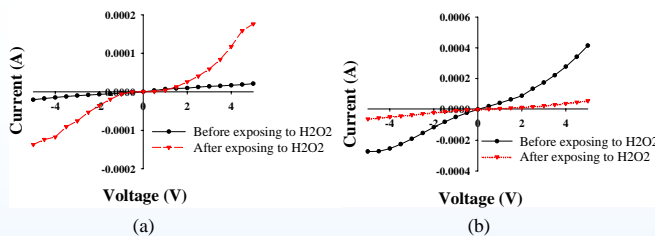


Sensor chip with gold electrode pads and active polymer region for sensing application.

The sensor chips fabricated from the process described above has two sensors and is 4 x 4 mm (length x width) in dimensions.

Immunosensor Results

The electrical characteristics of the PEDOT-PSS and carbon nanotube sensor devices were investigated as a function of time and found that the devices are tending to stabilize after 3-5 days.



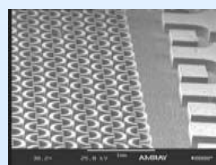
Effect of H₂O₂ on the electrical characteristics of (a) PEDOT-PSS (b) Carbon nanotube film.

Micro-Mixer Fabrication

- Silicon wafer with oxide layer
- Spin coat PR 1813
- Pattern PR 1813
- Etch SiO₂
- Etch PR 1813
- Etch SiO₂
- Bond Top Glass Substrate

Fabrication

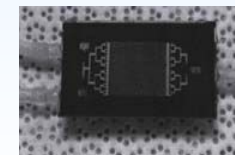
- Lithography
- ICP Etching
- Bonding



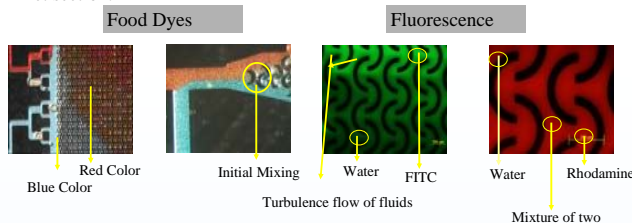
SEM → Omega Channel Micromixer

Micro-Mixer Testing Results

The fluid flow and mixing in microchannels were observed by injecting two sets of different fluorescent dyes along with water respectively (FITC (green) and water, RITC (red) and water).



In the first design the flow is laminar until the fluids reached omega channel and mixing was observed only in middle region of the channel. But in the current omega channel design mixing was observed even in the region that is near to the inlet section.



Summary and Conclusion

- Omega channel design has benefits of better mixing over straight channel.
- PEDOT and Carbon nanotubes may be combined with micro-mixer and immunoassay for the integrated sensor.
- Simulation and modeling may lead to better design of sensor system.

Integration With Cyber Tools

- Dec 13, 2007 → Immunosensor Kickoff Meeting.
- April 28, 2008 → Visit Tulane Group (Dr. Blake).
- May 12, 2008 → Team and Project Leader Meeting.
- May 20, 2008 → Coordinating with CFD/MD Team (Dr. Gaver) (Tulane).
- May 30, 2008 → All Hand Meeting (BoR, EPSCoR)- Modeling Discussions.
- July 23, 2008 → Video Conference with Tulane Group- Simulation Discussions.

Acknowledgments

Acknowledgments are due to the Institute for Micromanufacturing for providing the research facility and to NSF EPSCoR research Infrastructure Improvement (RII) Award.





Coupling Antibody Binding to Enzyme Activation in a Miniaturized Immunosensor

Mehnaaz F. Ali¹, Robert C. Blake II², Thomas C. Bishop³, Amit S. Jain^{3,4}, Henry S. Ashbaugh⁴, Steven W. Rick⁵ and Diane A. Blake¹

¹Department of Biochemistry, Tulane Univ. Hlth. Sci. Ctr. New Orleans LA, 70112

²Division of Basic Pharmaceutical Sciences, Xavier University of Louisiana, New Orleans, LA 70125

³Department of Mathematics and ⁴Chemical/ Biomolecular Engineering, Tulane University, New Orleans LA, 70118

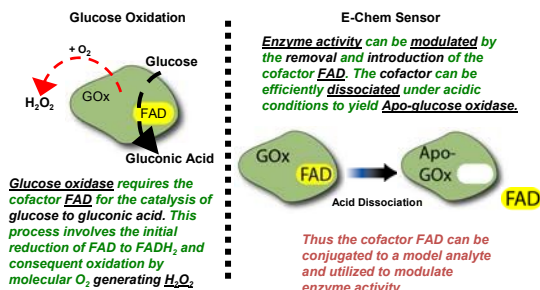
⁵Department of Chemistry, University of New Orleans, New Orleans LA, 70148



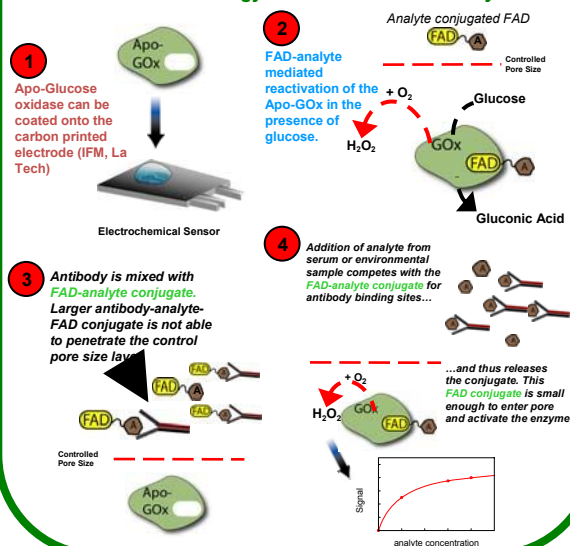
Abstract

The scope of this work is to develop antibody-based sensors for the detection of low molecular weight elements associated with environmental pollution, serum constituents and chemical warfare agents. Specifically, antibody binding will be coupled to the activation of the enzyme glucose oxidase upon the positive detection of the relevant model analyte. An important aspect of the immunosensor is the ability to modulate the activity of the glucose oxidase with the removal and addition of its co-factor flavin adenine dinucleotide (FAD). This aspect of the enzyme can be efficiently harnessed to provide an electrochemical signal transduction system. In order to facilitate the miniaturization and thus efficacy of the proposed 'hand-held' device, it is advantageous to utilize this electrochemical signaling modality in combination with antibody binding events. Another important component of the overall goals of this project involves the close collaborations with theoretical and computational methods groups. This work will facilitate appropriate sensor design and determine physical and chemical limitations to the final project.

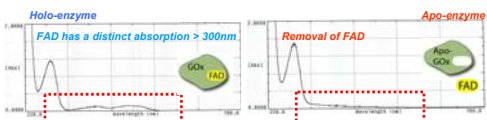
Immunosensor will use GOx Catalyzed glucose oxidation for Signal Transduction



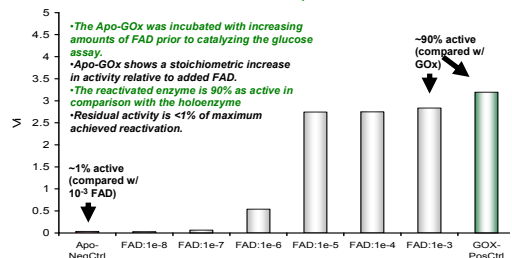
General Strategy for E-chem Immunoassay



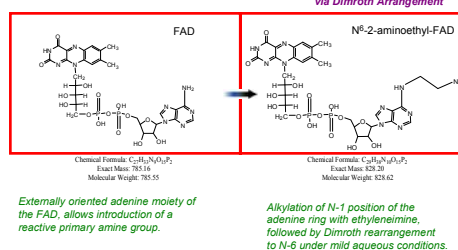
Absorption Spectra of FAD Region



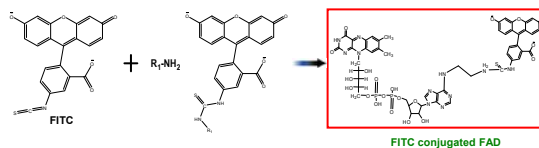
Reactivation of Apo-GOx



Synthesis of N⁶-2-aminoethyl-FAD

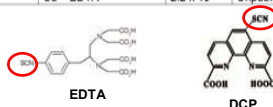


FITC-FAD conjugate via Thiourea Linkage



Antibody - Analyte Selection

Clone Number	Ligand	K _d (M)	Reference
12F6	2,9-dicarboxy-1,10-phenanthroline (DCP)	7.5 x 10 ⁻⁷	Blake et al. (2004) <i>Bioconj. Chem.</i> 15:1125.
12F6	UO ₂ ²⁺ -DCP	9.1 x 10 ⁻¹⁰	Blake et al. (2004) <i>Bioconj. Chem.</i> 15:1125.
4B33	EDTA	1.25 x 10 ⁻⁹	Unpublished data
4B33	Cu ²⁺ -EDTA	2.2 x 10 ⁻⁹	Unpublished data

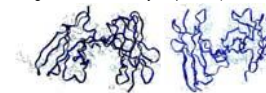


Molecular Dynamics of Antibody Binding Regions

will provide insight into antibody performance and aid in optimization of immunosensor

Simulations of antibody complementarity determining regions

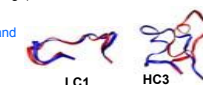
1) Homology modelling based on antibody sequence (Blake, Bishop, Jain)



Different orientations of the antibody 5B2 (both light and heavy chains) modeled on antibody 1NGP
2) *in vacuo*, implicit and explicit solvent simulations of antibody 5B2. LC and HC loops confirm previous identification of metal binding residue Lys⁵⁸ (Blake, Jain, Rick and Ashbaugh)

• Replica Exchange Molecular Dynamic performed of antibody 5B2 in *vacuo* and implicit solvent to generate families of loop structures for minimization to determine robustness of predictions and identify spatial and dynamic correlations between key binding residues (Blake, Jain, Rick and Ashbaugh)

• Initial findings: HC3 loop has more varied and flexible structure than the other five antibody loops



Connections with Cyber Tools

The Molecular Modeling component of this project requires:

- 1) Creation of putative antibody models based on sequence; (Modeler)
- 2) Parameterization of the analytes that bind to the antibodies; (Gaussian)
- 3) Docking analytes in different potential antibody binding loops; (PackMol)
- 4) Optimization of the antibody-analyte interaction by *in silico* point mutations. (Methods under development)

These tasks will require the following Work Packages:

WP 1: Scheduling and Data Services.

The details of integrating our Molecular Modeling packages into WP 1 are being addressed by Drs. Thomas Bishop (Tulane) and Tefvik Kosar (LSU).

WP 2: Information Services and Portals.

Drs. Thomas Bishop and Tefvik Kosar are collaborating to bring Bishop's DNA folding simulations on-line. The Workflow resulting from this effort can be readily modified to investigate the antibody and analyte interactions.

WP 3: Visualization Services.

Work is in progress to create modules that will permit all scientists involved in the project to visualize molecular models and other results via a common user interface without the necessity of transferring data or installing software on local lab computers.

WP 4: Application Services and Toolkits.

Drs. Steven Rick (UNO) and Henry Ashbaugh are developing replica exchange simulation techniques that will enable this group to efficiently identify antibody loop sequences that optimize the antibody-analyte interactions.

Acknowledgement Statement

The authors gratefully acknowledge the National Science Foundation (NSF) for their financial support of this research. This material is based upon work supported by the NSF/EPSCoR under Award No. (EPS-0701491). Any opinions, findings, and conclusions or recommendations expressed in this material are those of the author(s) and do not necessarily reflect the views of the NSF.

ASYMMETRY OF STRUCTURAL CHARACTERISTICS OF LIPID BILAYERS INDUCED BY DIMETHYLSULFOXIDE



Raghava Alapati, Dorel Moldovan, and Ram Devireddy

Department of Mechanical Engineering, Louisiana State University, Baton Rouge, LA -70803

Abstract

Dimethylsulfoxide (DMSO) is one of the most widely used solvents in cell biology and cryopreservation. During a typical cryopreservation protocol the DMSO composition of aqueous buffers inside and outside of the cell is known to differ considerably. To model and understand the structural changes in cell membranes in such a situation we performed molecular dynamics (MD) simulations of an idealized lipid bilayer membrane which separates two aqueous reservoirs with and without DMSO. Zwitterionic dimyritoylphosphatidylcholine (DMPC) lipid bilayers was chosen as model membrane. Various structural and ordering parameters characterizing the DMPC lipid bilayers asymmetrically exposed to water and 3 mol% DMSO solution were evaluated.

Simulation Methodology

➤ MD simulations were performed using GROMACS software¹.

➤ The system consists of two DMPC lipid bilayers (consisting of 96 lipid molecules or 48 DMPC lipids in each leaflet) water placed in between the two bilayers and 3mol% DMSO-water solutions on either side of the lipid bilayers.

➤ The simulation are performed at const pressure (1atm) using semi-isentropic pressure coupling and at constant temperature characterizing liquid crystalline phase of lipid bilayers².

➤ Force field parameters for bonded and non-bonded are taken from Berger et al³.

➤ An energy minimization based on steepest descent algorithm was initially applied to the structure prior to actual run.

Initial System

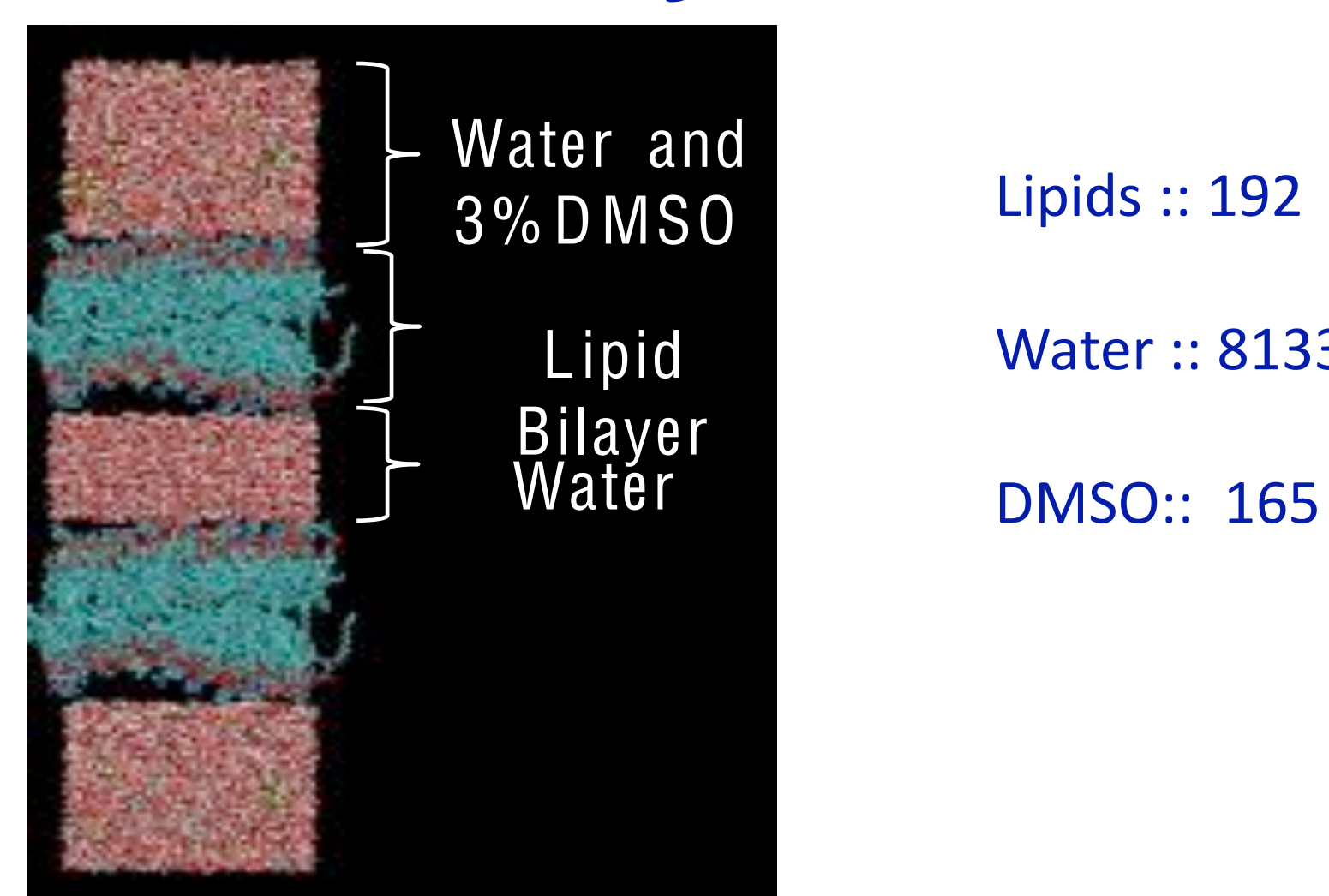


Figure 1. Simulation system showing the initial arrangement of the two lipid bilayers(48 lipids in each leaflet). Each bilayer has one side in contact with water and the other one in contact with 3% DMSO solution.

Simulation Results

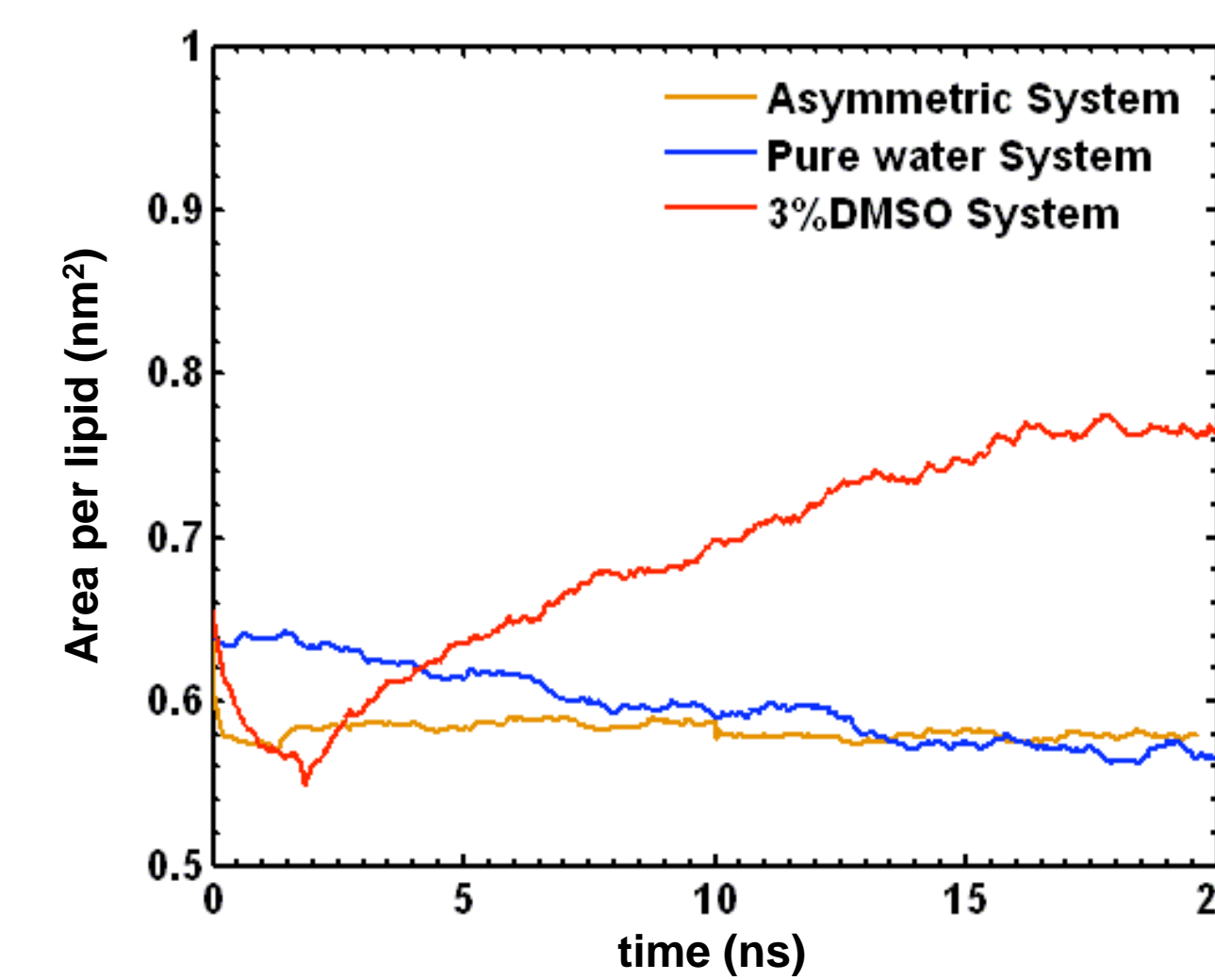


Figure 2. The area per lipid versus simulation for time three membrane systems: i) the DMPC 3 mol% DMSO asymmetric system, ii) the symmetric DMPC membrane embedded in a 3 mol %DMSO solution, and iii) the DMPC membrane in pure water

Single DMPC membrane in DMSO solution

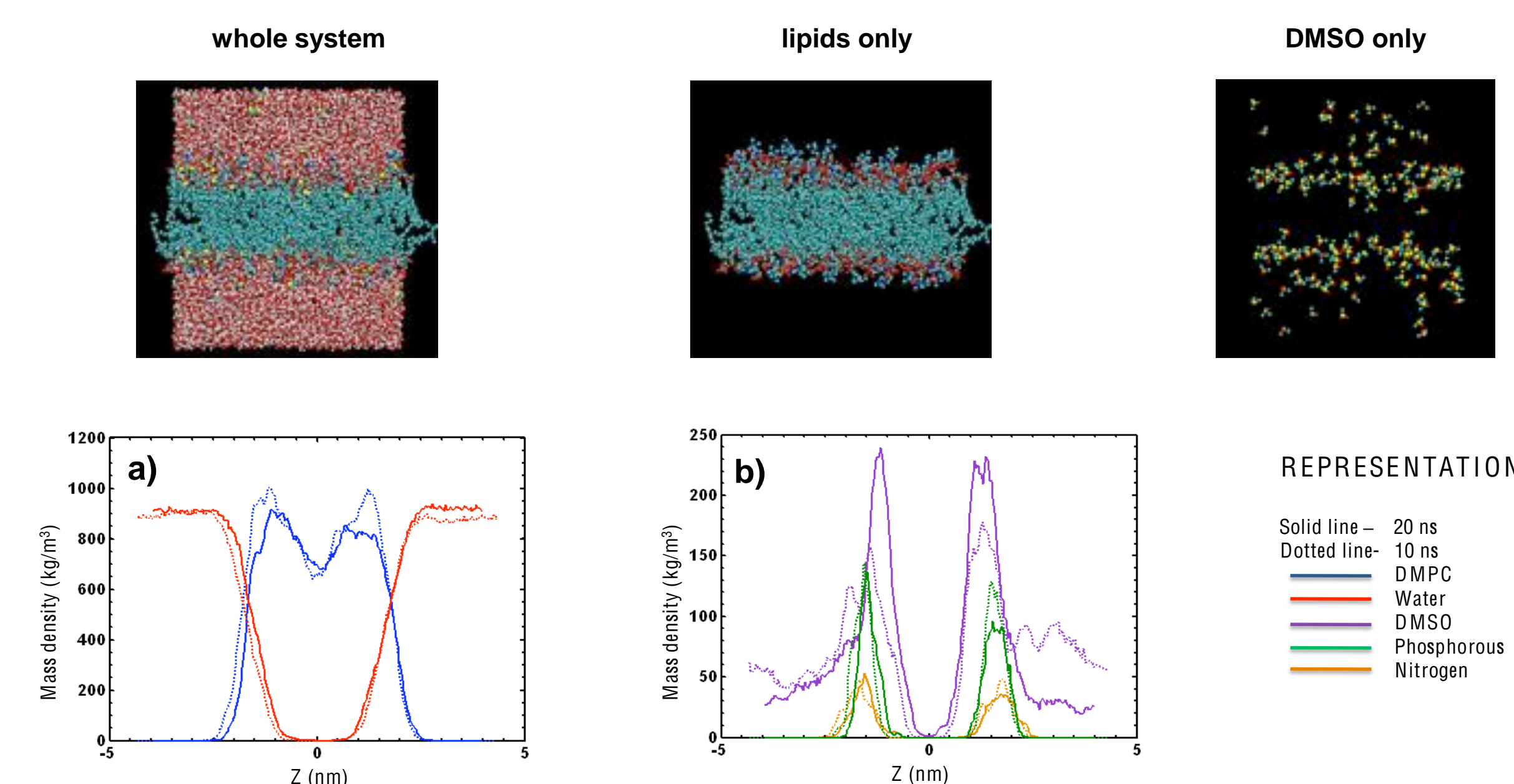


Figure 3: A single DMPC lipid bilayer exposed symmetrically to 3 mol % DMSO solution. Mass density profiles at 10 and 20 ns. a) Mass density profiles of lipids and water b) Mass density profiles of DMSO, phosphorous, and nitrogen.

Asymmetric DMPC system in DMSO solution

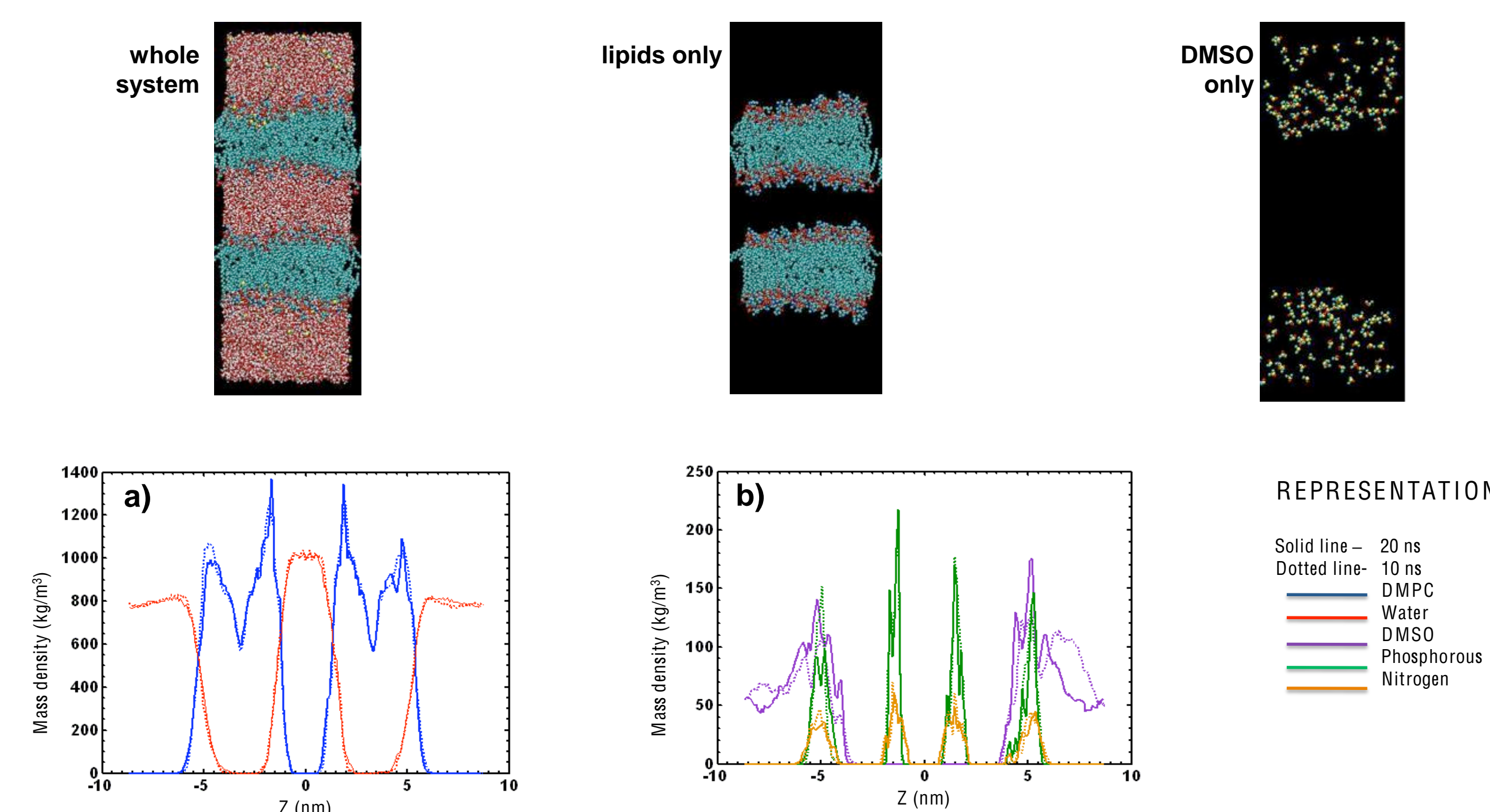


Figure 4: Two DMPC lipid bilayers system exposed asymmetrically to water and to 3 mol % DMSO solution. Mass density profiles at 10 and 20 ns. a) Mass density profiles of lipids and water b) Mass density profiles of DMSO, phosphorous, and nitrogen.

Conclusions

➤ In the asymmetric DMPC bilayer system the average area per lipid remains constant even after 20 ns; similar to the bilayer membrane immersed in pure water.

➤ The DMSO molecules cause large structural rearrangements within the outer lipid leaflets exposed to DMSO-water solution and has a reduced effect on the inner leaflets exposed to pure water.

➤ There is no evidence for DMSO penetration through the lipid bilayer⁴.

References

1. E.,Lindah, et al., J. Molec. Mod., 7,306 (2001).
2. H.J.C., Berendsen, et al., Biophys. J., 81, 3684 (1984).
3. O., Berger, et al., Biophys. J., 72, 2002 (1997).
4. D., Moldovan, et al., App. Phys. Lett., 91, 204104 (2007).

Connections with CyberTools

We are working with CyberTools team to develop a toolkit for job management, data analysis, and visualization. CyberTools (e.g. WP1, WP3, WP4) enables the use of High Performance Computing for the large scale atomistic simulations of lipid membrane systems by enabling the use of a user-friendly interface for submitting and monitoring multiple MD jobs.

Acknowledgements

The authors gratefully acknowledge the National Science Foundation for their financial support through grant NSF-EPSCoR RII Award No. EPS-0701491.

Abstract

This study has made two new contributions to the image fusion area. The new contributions consist of the Adaptive Fidelity Exploratory Algorithm (AFEA) and the Heuristic Optimization Algorithm (HOA). The AFEA and HOA algorithms have been applied on two modalities of images of branching arterial structures. An optimal fusion result has been achieved by giving the visualization of a color image with a complete grayscale image overlay. Control points are detected at the vessel bifurcations using the AFEA algorithm. Shape similarity criteria are used to match the control points that represent same salient features of different images. The HOA algorithm adjusts the initial good-guess of control points at the sub-pixel level in order to maximize the objective function Mutual-Pixel-Count (MPC).

I. Edge Detection

The Canny operator finds edges by looking for local maxima of the gradient of the input image (see Figure 1). It uses two thresholds for detecting strong and weak edges. Canny operator is less likely than the others to be "fooled" by noise, and more likely to detect true weak edges. Therefore, this approach chose Canny Edge Detector to extract the branching arterial structures from the binary images.

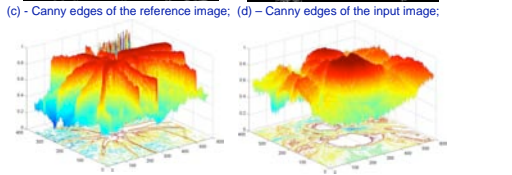
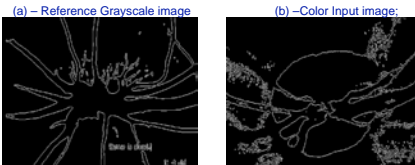
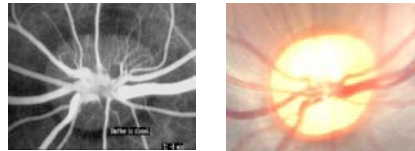


Figure 1 – Reference and input images, Canny edges and 3D surface plots.

II. Control Point Detection

Good-guess of the initial control point ensures fused image generated at an efficient computational time. Bad control point selection will significantly increase the computation cost, or even cause the image fusion to fail. Vessels or other factors may cause images to not necessarily match the arterial structures. Even when structure and function correspond, the mismatch still happens sometimes if inconsistency exists between structural and functional changes. Furthermore, grayscale images usually have higher resolution and are rich in information, whereas color images have lower resolution and are indeed abstract with some details or even missing some small vessels. Practically, those situations are unavoidable and will create difficulties in extracting the control points because the delineation of the vessel boundaries may not be precise. In this study, control points are detected using the AFEA algorithm (see Figure 2 and 3).

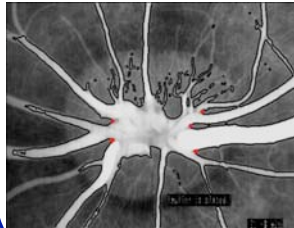


Figure 2 - Grayscale reference image's control points

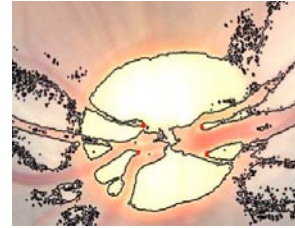
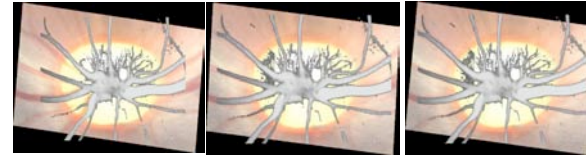


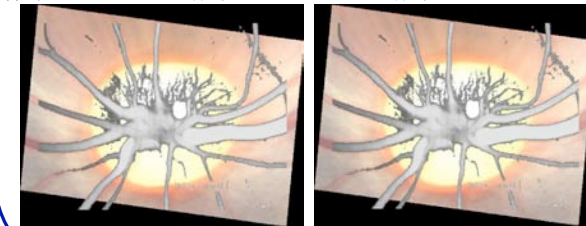
Figure 3 - Color image's control points

III. Heuristic Optimization

An optimization procedure is required to adjust the initial good-guess control points in order to achieve the optimal result. The process can be formulated as a heuristic problem of optimizing an objective function that maximizes the Mutual-Pixel-Count between the reference and input images. The algorithm finds the optimal solution by refining the transformation parameters in an ordered way. By maximizing the objective function, one image's vessels are supposed to be well overlaid onto those of the other image (see Figure 4).



(a) Objective Function MPC = 5144 (b) Objective Function MPC = 7396 (c) Objective Function MPC = 7484



(e) Objective Function MPC = 7681 (f) Objective Function MPC = 7732

Figure 4. Fused image improvement during the iteration.

IV. Objective Function

Mutual-Pixel-Count measures the arterial structure overlap for corresponding pixels in both images. It is assumed that the vessels are represented by 0 (black pixel) and background is represented by 1 (white pixels) in the binary 2D map. When the artery pixel's coordinates on the input image correspond to the artery pixel's coordinates on the reference image, the MPC is incremented by 1. MPC is assumed be maximized when the image pair is perfectly geometrically aligned by the transformation (see Figure 5). After pre-processing, the binary images of the reference and input images are obtained, i.e. I_{ref} and I_{input} . Only black pixels from both images contribute to MPC. The ideal case is that all zero pixels of the input image are mapped onto zero pixels of the reference image. The problem can be mathematically formulated as the maximization of the following objective function:

$$f_{mpc}(x, y, u, v) = \sum_{\substack{u \in ROI \\ \text{and} \\ I_{input}(u, v) = 1}} I_{ref}(T_x(u, v), T_y(u, v))$$

where f_{mpc} denotes the value of the Mutual-Pixel-Count. T_x and T_y are the transformations for u and v coordinates of the input image. The ROI (Region-of-Interest) is the vessel region where the MPC is calculated on.

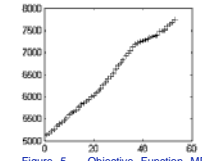


Figure 5 - Objective Function MPC improvement during the iteration.

V. Transformation Model

The 2D affine transformation model is applied to register the input image pixels into those of the reference image. The affine model has the capability to measure the lost information such as skew, translation, rotation, shearing and scaling that maps finite points to finite points and parallel lines to parallel lines.

$$\begin{pmatrix} U \\ V \end{pmatrix} = \begin{pmatrix} a_1 & a_2 & b_1 \\ a_3 & a_4 & b_2 \\ 0 & 0 & 1 \end{pmatrix} \begin{pmatrix} x \\ y \\ 1 \end{pmatrix}$$

VI. Connections with CyberTools

State-of-the-art imaging devices can quickly acquire multi-sensor 2D or 3D images. These images can further be transformed and merged into a single volume and thus combine the information of different modalities. Fusing images captured by different sensors (multimodal analysis) is able to provide the related staff with the complementary information, and thus help them more thoroughly understand both of the functional and structural information.

The application of this novel approach to branching arterial images demonstrates our new data fusion technique. This new algorithm can easily be extended to a number of other types of images.

Acknowledgements

Authors are grateful to Dr. Khoobehi, Dr. Thompson, and Dr. Ning for their support and help during this project. This work is funded in part by the NSF/EPSCOR RII grant.

Data Mining

Asim Shrestha, Dimple Juneja, Nathan E. Brener, S. Sitharama Iyengar,
Louisiana State University

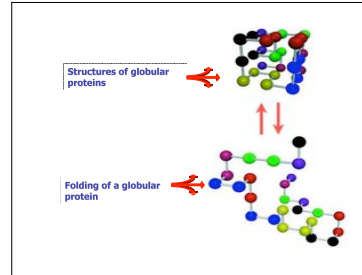
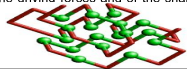


A Robust Data Mining Algorithm for Clustering of Similar Protein Folding Units

The properties of a protein depend on its sequence of amino acids and its 3D structure which consists of multiple folds of the peptide chain. If some of the properties depend primarily on the folding structure, then proteins with certain folding units may exhibit properties specific to those units. In that case, a classification of proteins based on folding units would facilitate the selection of proteins with certain desired properties.

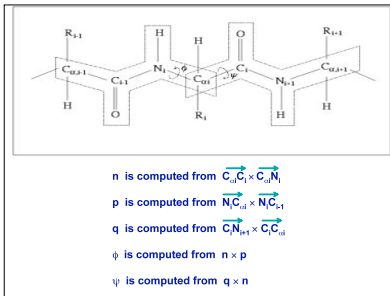
THE PROTEIN FOLDING PROBLEM

- Understanding and predicting the three-dimensional structures of proteins from their sequences of amino acids requires both basic knowledge of molecular forces and sophisticated computer programs that search for the correct configurations
- The Objective: The aim of the efforts in conformational searching is to use only knowledge of Amino acid sequence to predict protein structure. The points of conformance include:
 - Ability to distinguish a successful prediction from a failure
 - Enhanced knowledge of the driving forces and of the shape of the energy landscape
 - Faster Search Strategies



Data Mining Algorithm

- Application of Clustering data mining algorithm to a large medical data sets.
- An example: Protein Folding
- The properties of a protein depend on its sequence of amino acids and its 3D structure which consists of multiple folds of the peptide chain.
- If some of the properties depend primarily on the folding structure, then proteins with certain folding units may exhibit properties specific to those units.
- In that case, a classification of proteins based on folding units would facilitate the selection of proteins with certain desired properties.



GROUPING ALGORITHM

- The peptide chain is decomposed into a series of overlapping fragments of length 8:

Fragment 1: [$(\phi, \psi)_1$ $(\phi, \psi)_2$ $(\phi, \psi)_3$ $(\phi, \psi)_4$ $(\phi, \psi)_5$ $(\phi, \psi)_6$ $(\phi, \psi)_7$ $(\phi, \psi)_8$]

Fragment 2: [$(\phi, \psi)_2$ $(\phi, \psi)_3$ $(\phi, \psi)_4$ $(\phi, \psi)_5$ $(\phi, \psi)_6$ $(\phi, \psi)_7$ $(\phi, \psi)_8$ $(\phi, \psi)_9$]

Fragment 3: [$(\phi, \psi)_3$ $(\phi, \psi)_4$ $(\phi, \psi)_5$ $(\phi, \psi)_6$ $(\phi, \psi)_7$ $(\phi, \psi)_8$ $(\phi, \psi)_9$ $(\phi, \psi)_{10}$]

.....

- We define the distance between two points A_i and A_j , $DIST(A_i, A_j)$, as

$$DIST(A_i, A_j) = \sqrt{(\phi_{i1} - \phi_{j1})^2 + (\psi_{i1} - \psi_{j1})^2 + (\phi_{i2} - \phi_{j2})^2 + (\psi_{i2} - \psi_{j2})^2 + \dots + (\phi_{i8} - \phi_{j8})^2 + (\psi_{i8} - \psi_{j8})^2}$$

where

$$A_i = [(\phi_{i1}, \psi_{i1}), (\phi_{i2}, \psi_{i2}), \dots, (\phi_{i8}, \psi_{i8})]$$

$$A_j = [(\phi_{j1}, \psi_{j1}), (\phi_{j2}, \psi_{j2}), \dots, (\phi_{j8}, \psi_{j8})]$$

- For every $(\psi_{im} - \psi_{jm})$, if $|\psi_{im} - \psi_{jm}| > 180$, then we will use $360 - |\psi_{im} - \psi_{jm}|$, and similarly for $(\phi_{im} - \phi_{jm})$

Let j be the index that labels the groups. We define the center of group j , C_j , as

$$C_j = [(\phi_{j1}, \psi_{j1}), (\phi_{j2}, \psi_{j2}), \dots, (\phi_{j8}, \psi_{j8})]$$

where

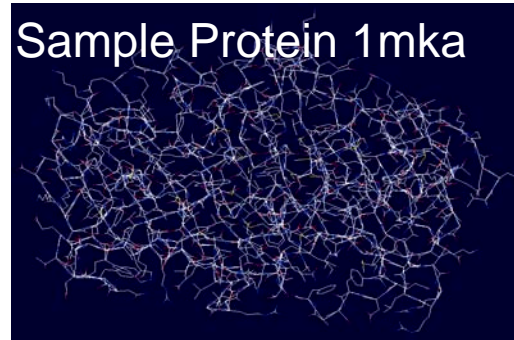
$$\phi_{jm} = \sum \phi_{im} / N_j$$

$$\psi_{jm} = \sum \psi_{im} / N_j$$

$$\{i = 1, 2, \dots, N_j; m = 1, 2, \dots, 8\}$$

N_j is the number of points in the group, and the sum is over i . Such groups are regarded as folding units in our current work.

Sample Protein 1mka



CONCLUSIONS & FUTURE WORK

- This describes a data mining algorithm that can be used to classify proteins according to similar folding units.
- This classification has the potential to facilitate the selection of proteins with specific desired properties.
- The preliminary implementation of the algorithm indicates that it has the capability to discover common folding units in proteins and can be generalized to large sets of proteins.
- This technique will be explored in the context of geno/small molecule sensors (Soper)
- Identification of similar features would enhance the design features of genomic or immuno Sensors.

Common Folding Units Discovered by Data Mining

Proteins

1ash, 1bar, 1caa, 1ccw, 1clm, 1cm, 1fct, 1fb, 1ft, 1fng, 1foe, 1fba, 1fka, 1fmg, 1fnp, 1fud, 1fvg, 1zab, 1zab, 5pb, 3698 fragments

Group 1 - 514 fragments

From 1mka



From 1br



Group 2
188 fragments
From 1br
 β sheet

Group 3
79 fragments
From 1br

Group 4
61 fragments
from 1br

Acknowledgements

This project is funded in part by NSF/EPSCoR RII

Connections with CyberTools

- Connected to WP1
- This technique will be explored in the context of geno/small molecule sensors (Soper)
- Identification of similar features would enhance the design features of genomic or immuno Sensors.

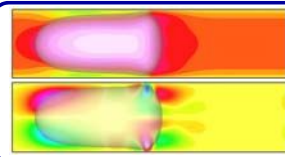
Table 1: A short list of proteins that were randomly selected

PDB Entry	Name of the Protein	Amino Acids Selected	Points Derived
1ash	HEMOGLOBIN (DOMAIN ONE)	1 - 148	138
1bar	RIBONUCLEASE (BOVINE, SEMINAL) (CHAIN A)	1 - 124	115
1caa	CYTOCHROME C PEROXIDASE	4 - 234	222
1ccw	CYSTATIN	9 - 116	99
1clm	CALMODULIN (PARAMEDIUM TETRALRELLA)	4 - 147	136
1cm	CRAMBIN	1 - 48	37
1ctc	CYTIDINE DEAMINASE	4 - 284	285
1fba	RETINOL BINDING PROTEIN COMPLEX WITH N-ETHYL RETINAMIDE 2	2 - 174	164
1fbc	RIBONUCLEASE F1	1 - 107	98
1fng	COE (RAT) (CHAIN B)	2 - 176	166
1foe	ALPHA-AMYLASE INHIBITOR HD457A	1 - 74	65
1fud	HYDROLASE METALLO GEN DEPEPTIDASE	1 - 213	204
1fka	BETA-HYDROXYBIOGENOYL THIOLESTER DEHYDROASE (CHAIN A)	1 - 171	162
1fmg	MANGANESE SUPEROXIDE DISMUTASE (CHAIN A)	1 - 293	194
1fnp	RIBOSOMAL PROTEIN S5	4 - 148	137
1fud	URACIL-DNA GLYCOSYLASE	18 - 244	218
1fvg	UTEROCALCIN (OXIDIZED)	1 - 70	61
1zab	CIBICIA PAPAYA CHYMOTRYPSIN	1 - 218	209
1zab	MHC CLASS II 2K3 HEAVY CHAIN	1 - 274	265
5pb	TRYPSIN INHIBITOR	1 - 58	49



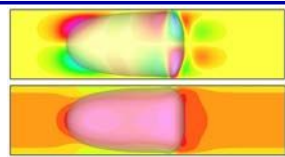
Numerical Simulations of Micro-Scale Segmented Two-Phase Flows for Bio-Analytical Chip Applications

Eamonn D. Walker^{1,2}, Dimitris E. Nikitopoulos^{1,2}, Dorel Moldovan^{1,2}, Mayank Tyagi^{3,4}, Michael C. Murphy^{1,2}, Steven A. Soper^{1,2,5}, Gretar Tryggvason⁶
¹Mechanical Engineering, ²Center for Bio-Modular Multi-scale Systems, ³CCT, ⁴Petroleum Engineering, ⁵Chemistry, LSU, Baton Rouge, LA; ⁶Mechanical Engineering, WPI, Worcester, MA



Abstract

Segmented flows in micro-channels are of great interest to bio-analytical applications. They can reduce reagent volumes and enable high throughput without cross-contamination. A research code is used and being improved to predict such flows accurately & efficiently. This is done in close collaboration with the CyberTools group at CCT. On the scientific level, hierarchical disjoining pressure models and/or local molecular dynamics-based simulations need be implemented to accurately represent surface property effects, nano-scale effects in the thin films, breakup and coalescence.



About the Code

Formulation

- Incompressible, Isothermal Navier-Stokes Equations (each fluid)
- Jump conditions across interfaces (interfacial force balance)
- Boundary conditions specific to problem
 - * Segmented Flow in Micro-channel
 - * No-slip on channel walls
 - * Periodic boundary conditions in stream-wise direction

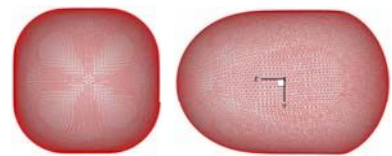
Solution Methods

Eulerian Governing Equations

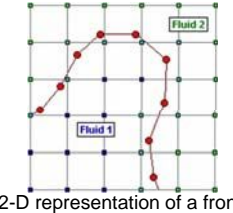
- Solved with a standard two-step projection method
 - * Calculate pseudo-velocities (ignoring pressure effects)
 - * Solve "Poisson" equation for pressure (satisfying continuity)
 - * Correct velocities from pressure with an Euler step
 - * Velocity used to advect the front and update velocity and pressure
- Elliptic "Poisson" solver for the pressure
 - * MUDPACK open source code libraries
 - * Use of Multi-grid method for increased efficiency
 - * Red/black Gauss-Seidel successive over-relaxation (SOR)
 - * Includes OpenMP parallelization capabilities
- Eulerian grid is fixed, regular, Cartesian and staggered (vel. & pres.)

Handling Interfaces – Front Tracking

- Fluid interface approximated as a front
 - * Adaptive, unstructured, triangulated grid on front
 - * Connected marker points (front nodes) advected with front
 - * Marker points added/deleted as needed to maintain grid quality



3-D front obtained from simulation



2-D representation of a front

- Front-to-fixed-grid communication
 - * Front used to assign fluid properties to fixed grid nodes
 - * Surface tension
 - * calculated from front curvature
 - * distributed as a weighted source term to fixed grid nodes
- Fixed-grid-to-front communication
 - * Calculated fixed-grid velocities applied to advect the front points
 - * Grid-front interactions use smoothing to avoid excessive gradients

Objectives

- Accurately predict segmented multi-phase flows
- Validate predictions by comparing to experiment (poster by N. Kim et al.)
- Study segmented flow conditions difficult to realize in the laboratory
- Explain pressure-drop variation trends measured in the experiments
- Predict thin film disintegration for wall contamination assessment
- Examine sensitivity to perturbations in droplet size and pitch

Relevant Physical Parameters

Capillary Number $Ca = \frac{\mu_c J}{\sigma} = \frac{\text{Viscous Forces}}{\text{Capillary Forces}}$ **Density Ratio** $\gamma = \frac{\rho_d}{\rho_c}$
Reynolds Number $Re^* = \frac{\rho_c J w}{\mu_c} = \frac{\text{Inertial Forces}}{\text{Viscous Forces}}$ **Viscosity Ratio** $\kappa = \frac{\mu_d}{\mu_c}$
Weber Number $We = Ca \cdot Re$ **Channel Wall Surface Energy (Wettability)**

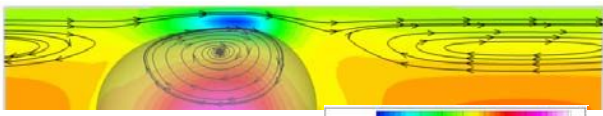
Results at Low Capillary Numbers

Periodic Segmented Liquid-Liquid Micro-channel Flow

$Ca=0.002, We=0.008, Re=4, \kappa=\mu_d/\mu_c=1.4, \gamma=\rho_d/\rho_c=0.55$

Contours of stream-wise velocity relative to that of the droplet and streamlines inside and around one droplet of the segmented flow obtained from 3-D, two-phase (liquid-liquid) simulations in square micro-channel ($w=200\mu m$).

Diagonal Plane



Center Plane



Thin-film physics and wall wettability must be properly introduced

Resolving thin film physics and properly introducing wall wettability into the simulation are critical in accurately predicting pressure drop and wall contamination probability.

Challenges

Scientific

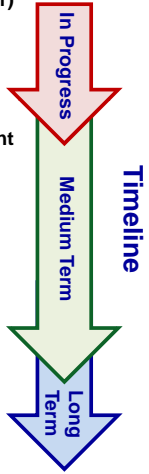
- Introduce thin-film and wall wettability physics
 - * Hierarchical disjoining pressure models (Short-term)
 - * Local Molecular-Dynamics coupled with Continuum (Long-term)
- Physical coalescence/break-up criteria (as above)
- Investigate a large multi-parameter space

Computational

- Improve code efficiency/accuracy/performance
 - * Parallelization
 - * New, elliptic solver algorithm suited to property discontinuities
- Post-processing & visualization of large number of large datasets
 - * Parametric studies
 - * Development of practical correlations from numerical data

Connections with CyberTools

- Multi-Phase flow Simulation Tool (WP4, WP3, WP1)
 - * Parallelization
 - * Implementation of parallelized Multi-Grid solver (WP4)
 - * Distribution of different multi-processor simulations to groups of processors for efficient parametric studies (WP1)
 - * Advanced interactive visualization tools (WP3)
 - * Improvement of Accuracy/Performance
 - * Implement Multi-Grid algorithm designed to handle elliptic "Poisson" equations with discontinuous coefficients (WP4)
 - * Extend code capabilities to handle complex Cartesian geometries
 - * Domain Decomposition (WP4)
 - * Multi-blocking (WP4)
 - * Computational Steering (WP1, WP3, WP4)



Acknowledgements

Special thanks to the NSF EPSCoR RII grant to the State of Louisiana, which has made this research and the collaboration with the CyberTools group possible, and the LA Board of Regents Dean's Fellowship program which is funding Mr. E. D. Walker.



Medical Image Classification Using Weighted Association Rules Based Classifier

Harpreet Singh¹, Sumeet Dua¹, Hilary W. Thompson²

¹Data Mining Research Laboratory, Computer Science Program, Louisiana Tech University, Ruston, LA – 71272

²Department of Biostatistics, School of Public Health, Louisiana State University Health Sciences Center, New Orleans, LA 70112

Contact e-mail: sdua@coes.latech.edu; Phone: 318-257-2830; <http://dmrl.latech.edu>



Abstract

Medical images are widely used by physicians to diagnose various diseases. Advanced in automated image collection routines coupled by our reliance on medical imaging for diagnostic discovery, treatment planning and decision support research has fuelled the demand for automated image mining and classification routines. The high volume of medical images coupled with the difficulty to discover features of interest in them poses an interesting algorithmic development challenge to autonomously interpret them for clinical decision support and early diagnosis. We present a new image representation scheme, a preprocessing method, and a computational framework for the classification of mammograms using Weighted Association Rules (WAR-BC). The framework is demonstrated here for mammogram classification but the classification theory allows extensibility to other domains. In mammogram classification an accuracy of 89% is achieved over ten repetitions, far surpassing the accuracy of other techniques. High Precision (96%) and Recall (91%) values show the strength of the proposed technique. We conclude that Association Rules can be effectively used to uncover the isomorphisms present in images which can be used for the classification of images for content-based image retrieval applications.

METHODOLOGY

The methodology is divided into four parts: Preprocessing, Segmentation and Feature Extraction, Association Rule Generation and Classifier Training, and Classification. During Preprocessing, a mammogram is converted to its binary image, and connected components are found from this image. Then, the image is segmented using these components. The segment boundary is smoothed. Finally, the black background is deleted from the mammogram, and histogram equalization is performed to remove noise.

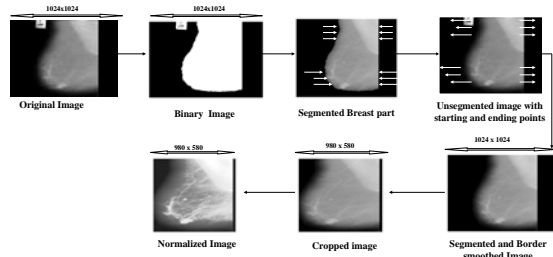


Figure 1. Mammogram Preprocessing for Label and Noise Removal

The preprocessed image is divided into non-overlapping segments of size 20x20 to capture the local relationships present in the image. Once the image has been segmented into blocks, eight texture features are extracted from each segment. Each vector is given a unique Segment ID, which, in our case, is the number of the segment from which the features were extracted, e.g. $TID\ 1\ (f_1, f_2, f_3, \dots, f_8)$ and $TID\ 2\ (f_1, f_2, f_3, \dots, f_8)$. We use eight of the fourteen Haralick[1] coefficients. Since the classification mechanism is a stand alone tool, any set of nonharalick features can be used.

Once the features have been extracted from each segment, the image can be considered a transaction database where one transaction is one row of the database or the features extracted from one segment. The next step is to uncover the isomorphisms present by using association rules. An association rule is of the form $f_1\ (1134), f_2\ (2124) \rightarrow f_8\ (8074)$ with Support = 40% and Confidence = 80%, given by following formulas.

$$\text{Support}(f_1(1134), f_2(2124)) \rightarrow f_8(8074) = \frac{\text{Number of Transactions having } (f_1(1134), f_2(2124), f_8(8074))}{\text{Total Number of Transactions}}$$

$$\text{Confidence}(f_1(1134), f_2(2124)) \rightarrow f_8(8074) = \frac{\text{Number of Transactions having } (f_1(1134), f_2(2124), f_8(8074))}{\text{Number of Transactions having only } (f_1(1134), f_2(2124))}$$

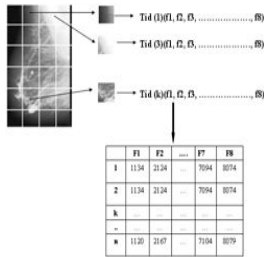


Figure 2. Segmentation and Feature Extraction

Feature Label	Feature	Calculation
f_1 <td>Contrast</td> <td>$\sum_{i,j} I(i,j) - I(i,j+1)$</td>	Contrast	$\sum_{i,j} I(i,j) - I(i,j+1) $
f_2 <td>Local Entropy</td> <td>$-\sum_{i,j} I(i,j) \log_2 I(i,j)$</td>	Local Entropy	$-\sum_{i,j} I(i,j) \log_2 I(i,j)$
f_3 <td>Correlation</td> <td>$\frac{\sum_{i,j} (I(i,j) - \bar{I})(I(i,j+1) - \bar{I}))}{\sqrt{(\sum_{i,j} (I(i,j) - \bar{I})^2)(\sum_{i,j} (I(i,j+1) - \bar{I})^2)}}$</td>	Correlation	$\frac{\sum_{i,j} (I(i,j) - \bar{I})(I(i,j+1) - \bar{I}))}{\sqrt{(\sum_{i,j} (I(i,j) - \bar{I})^2)(\sum_{i,j} (I(i,j+1) - \bar{I})^2)}}$
f_4 <td>Energy</td> <td>$\sum_{i,j} I(i,j)^2$</td>	Energy	$\sum_{i,j} I(i,j)^2$
f_5 <td>Cluster Shade</td> <td>$\sum_{i,j} I(i,j) \log_2 I(i,j)$</td>	Cluster Shade	$\sum_{i,j} I(i,j) \log_2 I(i,j)$
f_6 <td>Maximum variance of Cluster Shade</td> <td>$\max_{i,j} I(i,j) - \bar{I}$</td>	Maximum variance of Cluster Shade	$\max_{i,j} I(i,j) - \bar{I} $
f_7 <td>Maximum variance of Cluster Shade</td> <td>$\max_{i,j} I(i,j) - \bar{I}$</td>	Maximum variance of Cluster Shade	$\max_{i,j} I(i,j) - \bar{I} $
f_8 <td>Maximum variance of Cluster Shade</td> <td>$\max_{i,j} I(i,j) - \bar{I}$</td>	Maximum variance of Cluster Shade	$\max_{i,j} I(i,j) - \bar{I} $

Table 1. Haralick Texture Features for Feature Representation

In our case, we only consider rules which have a minimum support of at least 4% and a confidence of at least 90%. Rules from images in each class are combined to form a separate class-level rule set for each class. Further, the class level rule sets are combined to form a global rule set. Weights are given to global rules according to their presence across images of the same class and across different classes (Horizontal). Class-level rule sets are ranked according to decreasing confidence/support pairs, and the highest ranked rule gets the highest weight (Vertical). For classifying a new image, both Horizontal and Vertical weights are added to find the weight of a matching query rule.

Algorithm: Rule Weighting (RW-Weight) as used to provide Horizontal and Vertical weights to every rule present in the training database
Input: Number of classes C, combined list of training rules for each class R_{ij} ,
Output: Number of rules in each class G_{ij} , Total number of rules R'
Method:
(1) For every rule $R_{ij} \in R_{ij}$ in R_{ij}
(2) $prop_{ij} = \frac{|R_{ij}|}{|G_{ij}|}$ - percentage of images in G_{ij} having R_{ij}
(3) $hor_{ij} = \frac{|R_{ij}|}{|R_{ij}|}$ - percentage of R_{ij} in R_{ij}
(4) End For if Horizontal weighting complete
(5) For every class $j \in C$
(6) Rank hor_{ij} in Desc order according to confidence and then support in each class
(7) Confidence
(8) For every rule $R_{ij} \in R_{ij}$ in G_{ij}
(9) Vertical weight $V_{ij} = \frac{hor_{ij}}{|G_{ij}|}$
(10) End For
(11) Horizontal weight $H_{ij} = \frac{prop_{ij}}{|G_{ij}|}$ - horizontal vertical weights in the image I
(12) End For

Figure 3. Pseudo Code for Rule Weighting

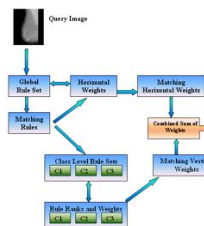


Figure 4. Classification Mechanism

For a query image the whole training procedure, except for rule weighting, is performed. Then, each rule from the query image is matched with the global rule set to find its horizontal weight and with class-level rule sets to find its vertical weight in each class. The horizontal and vertical weight of the rule is added and then multiplied by the number of items present to get a score for the rule. The procedure is repeated for each rule in the query image. Finally, the scores of the matching rules are added on a class-by-class basis and a cumulative sum is calculated for each class. The image is assigned to the class with the highest cumulative sum.

RESULTS

A well known Mammography dataset called MIAS[2] is used for experiments. It consists of a total of 322 mammograms of which 208 are Normal, 63 are Benign, and 51 are Malignant. To make an accurate comparison with other existing techniques, we use the same data for training/testing (90/10).

Our technique (WAR-BC) outperforms others in the 10-fold technique. Class level accuracies are then found to see which class performs worst. We also run experiments with less training/testing data (70/30, 80/20) to check the accuracy.

To check the efficacy of association rules generated by our technique, we provide association rules as input to classifier F-KNN (called in F-KNN2) instead of raw haralick features. The increase in accuracy of F-KNN shows the strength of rules generated. Another set of experiments are carried out using only the Region of Interest (ROI) information for abnormal mammograms. Finally the classification is performed with respect to mammogram density of Fatty, Glandular, and Dense.

	BP NN	JAC	ARC-BC	F-KNN	PNC2	WAR-BC
1st	96.87	69.342	80	59.37	53.13	93.75
2nd	90.62	86.373	93.33	46.87	56.25	90.62
3rd	90.62	77.586	86.67	56.25	62.5	93.75
4th	78.125	72.912	76.67	71.87	62.5	88.27
5th	81.25	78.224	70	53.12	59.37	93.75
6th	84.375	77.065	76.67	75	20	81.25
7th	65.625	77.691	83.33	65.25	68.75	90.62
8th	75	73.752	76.67	56.25	20	90.62
9th	56.25	82.123	76.67	53.12	68.75	87.5
10th	93.75	79.819	83.33	59.37	12.5	90.62
Avg	81.2485	77.4877	80.334	59.647	48.375	89.685

Figure 5. Comparison of Different Techniques Using WAR-BC

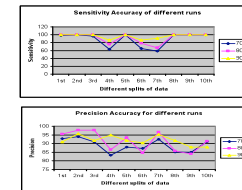


Figure 6. Sensitivity and Precision of WAR-BC over 10 Different Runs

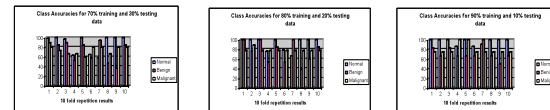


Figure 7. Class Level Accuracies for Different Training/Testing Pair of Data

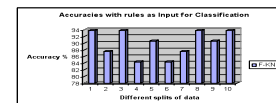


Figure 8. F-KNN2 Showing the Efficacy of Association Rules

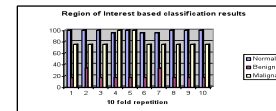


Figure 9. ROI Based Classification Results

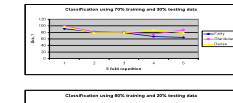


Figure 10. Density Based Classification

CONCLUSION

We have presented a novel framework for the improvement of mammogram classification which includes an improved preprocessing method, a new image representation scheme, and a new rule weighting strategy. Results demonstrate that our technique is superior to existing techniques. For further reference to this research please consult [3].

REFERENCES

- [1] R.M. Haralick, K. Shanmugam, and I. Dinstein, "Textural features for image classification," *IEEE Trans. on SMC*, IEEE SMC Society, Piscataway, NJ, Nov. 1973, pp. 610-621
- [2] MIAS Database, *The PCVC Project*. Benchmarking Vision Systems, <http://peipa.essex.ac.uk/info/mias.htm>.
- [3] S. Dua, H. Singh and H. W. Thompson, "Associative Classification of Mammograms using Weighted Rules based Classification", Elsevier Expert Systems with Applications (submitted).

Connections with Cyber Tools

This work relates to the WP1 (Data Services) aims for the design and development of tools for metadata extraction and data mining services. The work is also connected with the WP2 (Information Services) of Cyber Tools development with regards to information discovery algorithms. The work is a result of collaboration between investigators from Louisiana Tech University and Louisiana State University Health Sciences Center at New Orleans.

Acknowledgements

-NSF/LA-BoREPSCoR program
-NIH/INBRE program

Computational Model of a Microfluidic Mixing Chamber for Miniaturized Immunosensor Devices

Katharine Hamlington¹, Jerina Pillert¹, David Halpern², Donald P. Gaver¹

¹Tulane University
²University of Alabama

Abstract

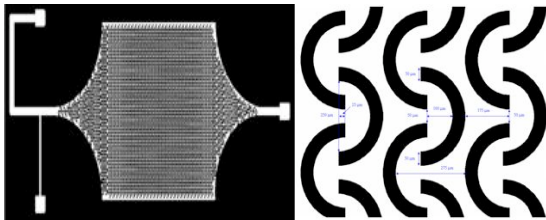
We are using numerical simulations to determine the appropriate geometric configuration of a microfluidic channel network to enhance the mixing and subsequent reactions of biological or chemical species. Convective mixing on the microscale can be difficult with low Reynolds number flows; typically, this requires long length- and time-scales to allow molecular diffusion between laminar streams. Decreasing these mixing scales in a microfluidic network allows for the creation of a portable sensing device that can readily detect harmful biological or chemical agents. The Institute for Micromanufacturing at Louisiana Technological University has developed a microfluidic system consisting of a network of novel omega-shaped channels designed to enhance mixing by introducing circulatory flows. Our goal is to investigate and optimize the design of the "omega channels" for mixing in an immunosensor device. Solvent dynamics in complex geometric domains involving omega-shaped obstructions were computationally determined by solving the equations for Stokes flow using the boundary element method. We analyzed improvement of mixing in the omega channels by examination of convective flow fields.

Miniaturized Immunosensor Devices

- + Detect biological or chemical agents by antigen-antibody binding and subsequent signal detection
- + Useful in disease diagnosis, detection of food toxins, and environmental monitoring for harmful chemical agents
- + Compact size, portability, low cost, and ease of operation would enable widespread use by general public

The Mixing Dilemma

- + Two species must mix and bind to produce signal
- + Fluid flow is purely laminar at microscale (non-turbulent) and mixing occurs only due to diffusion, requiring long length- and time- scales
- + Omega channels developed by LaTech may induce transverse and circulatory flows to promote mixing between two species



GOAL: *Computationally determine the optimal geometric configuration of the omega channel network to enhance mixing of two species.*

Governing Equations

- + Inertial effects negligible at microscale; Reynolds number (Re) $\ll 1$
- + Incompressible flow governed by continuity and Stokes equations

$$\nabla \cdot \mathbf{u} = 0$$

$$\nabla P = \mu \nabla^2 \mathbf{u}$$

Boundary Element Method

- + Used to solve for velocity field and surface stresses
- + Green's theorem is applied to Stokes equations to obtain an integral equation linking the velocity and stress on the boundary surface S

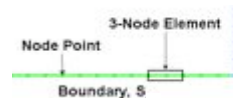
$$\star C_{ij}u_i(\mathbf{x}) + \int_S T_{ik}(\mathbf{x}, \mathbf{y})u_k dS_y = \frac{1}{\mu} \int_S U_{jk}(\mathbf{x}, \mathbf{y})\tau_j dS_y$$

- + U and T are kernels based upon the free-space Green's function

$$U_{ik} = -\frac{1}{4\pi} \left(\delta_{ik} \log|x-y| - \frac{(x_i-y_i)(x_j-y_j)}{|x-y|^2} \right)$$

$$T_{ik} = -\frac{1}{\pi} \left(\frac{(x_i-y_i)(x_j-y_j)(x_k-y_k)}{|x-y|^4} \right)$$

- + Only boundary is discretized into N 3-node quadratic elements



- + Discretized integral equation (\star) expressed as system of linear equations

$$H\mathbf{u} = G\boldsymbol{\tau}$$

Computational Domain

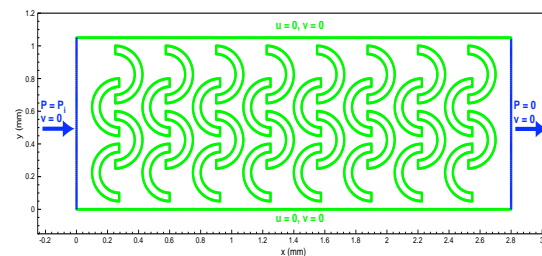


Figure 1: Schematic of computational domain.

- + Omegas modeled with manufactured dimensions
- + Pressure drop imposed over channel length; $P_1 = 3.5$ MPa
- + No slip boundary condition on upper and lower walls and obstructions
- + Fluid viscosity $\mu = 1$ Pa*s

Results

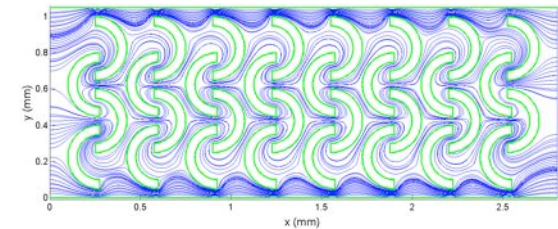


Figure 2: Streamlines of fluid flow in omega channel domain. Flow rate = 1 mL/min, Average velocity = 105 mm/s, Re = 0.03

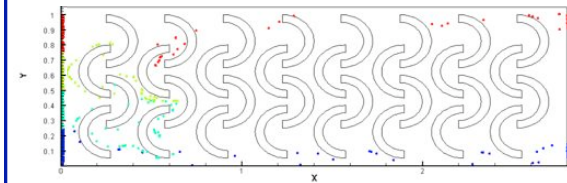


Figure 3: Snapshot of a particle trajectory field. Particles initially positioned along y-axis at $x = 0$ as shown. Path of each particle is traced as it flows through the domain.

Conclusions

- + Closeness of streamlines and particle trajectories indicates that omega channels may enhance mixing by decreasing the diffusion length scale.
- + The lack of obvious vortices suggests that domain modification may be important to improve mixing.
- + We will continue to optimize the geometry for mixing in terms of initial concentrations and overall chamber size by incorporating the convection-diffusion-reaction equations of the species into the calculations.

Connections with CyberTools

- + We have worked closely with Dr. Mayank Tyagi and the WP4 team to parallelize our boundary element code using OpenMP for use in the HPC environment.
- + WP3 is helping us visualize our velocity field using Tecplot.
- + As a long term goal, we are developing a *CyberTool* package to solve Stokes flow equations for use by the scientific community.

Acknowledgements

We thank Mr. John Sullivan who aided in the development of this poster and Dr. Hideki Fujjoka who provided invaluable computational assistance. *This work was funded by NSF EPSCoR.*

Abstract

Multiphase flow is realizing its potential in various lab-on-a-chip devices as a promising candidate for the flow control methods. For the better understanding and application of multiphase flow in microfluidic systems, fundamental physical studies are required. An experimental investigation of multiphase flows in polymer microfluidic channels replicated using hot embossing of poly-methyl-methacrylate (PMMA) and polycarbonate (PC) with micro-milled brass mold inserts was performed. Deionized water and dry air were used for gas-liquid two-phase flow and deionized water and fluorinated hydrocarbon fluid were used for liquid-liquid immiscible flow.

Introduction

Motivation

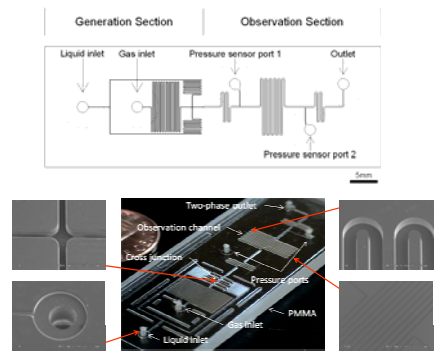
- **Reduced use of reagents** in a microfluidic network
 - Substitution of inert fluid (gas, immiscible liquid) in aqueous reagent instead of filling the entire channel
- **Fast mixing and minimized dispersion** of reagents
 - Two-phase flow: mixing is intensified by internal convective motion in a liquid plug

Objectives

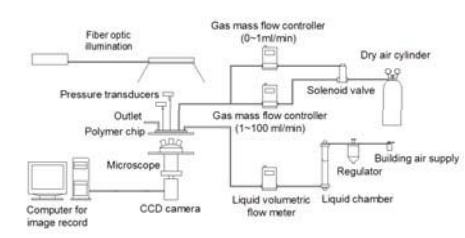
- Experimental Investigation of multi-phase flows
 - Two-phase **flow regimes**
 - **Stability** of gas bubbles and liquid plugs
 - Two-phase **pressure drops**
 - Effect of **surface properties** (Surface energy, roughness)

Gas-liquid two-phase flow

Design for generation and test of two-phase flow



Experimental Apparatus



Two-phase flow patterns

$$\beta_L = \frac{Q_L}{Q_L + Q_G} = 1 - \beta_G$$

Where β_L = liquid volumetric flow ratio
 β_G = gas volumetric flow ratio
 Q_L = liquid volumetric flow rate
 Q_G = gas volumetric flow rate

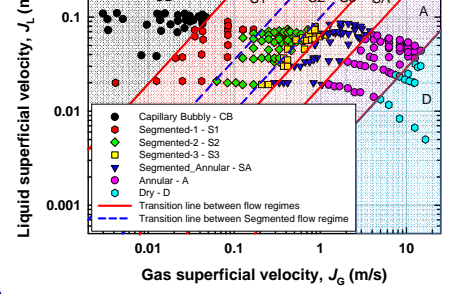
Capillary bubbly flow, $0.66 \leq \beta_L \leq 1$
 $L_b / w < 1$
 - Regular distribution of bubbles
 - No randomly dispersed bubbles
 where L_b = gas bubble length, L_p = liquid plug length and w = observation channel width

Segmented-1, -2, -3, $0.06 \leq \beta_L \leq 0.66$
 Segmented-1: $L_p / L_b < 1$, $L_b / w < 5$
 Segmented-2: $L_p / L_b > 1$, $L_b / w < 5$
 Segmented-3: $L_p / L_b > 1$, $L_b / w > 5$

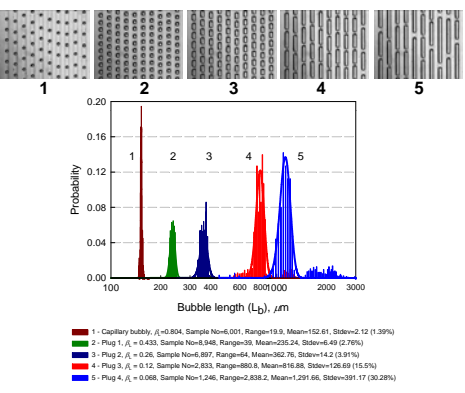
Segmented-annular flow
 $0.018 \leq \beta_L \leq 0.06$
 • Beginning of coalescence of neighboring bubbles with thinning of liquid plug

Annular flow
 $0.0029 \leq \beta_L \leq 0.018$
 • Ring shaped liquid film flow along the channel wall in an irregular pattern

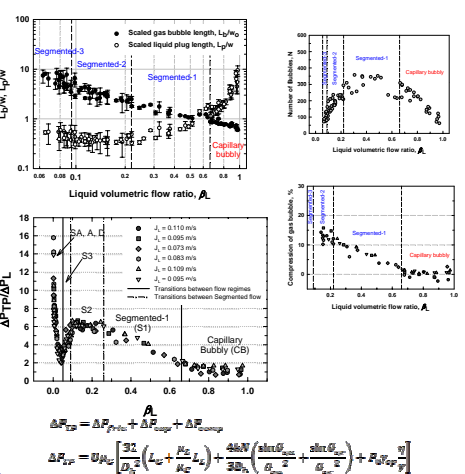
Dry flow
 $0 \leq \beta_L \leq 0.0029$
 • Liquid confined to the corners of the rectangular channel



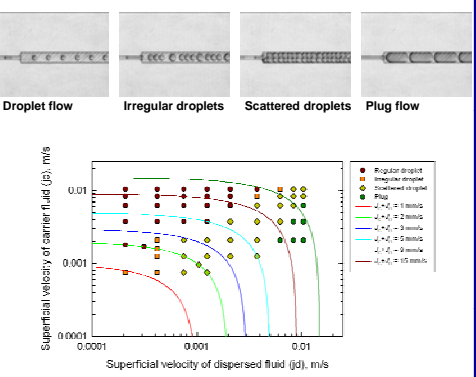
Regularity of flow



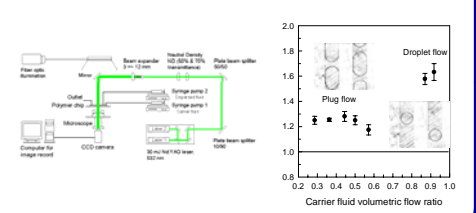
Length of gas bubble and liquid plug & pressure drop



Liquid-liquid Immiscible Flow pattern and map



Droplet and plug velocity measurement

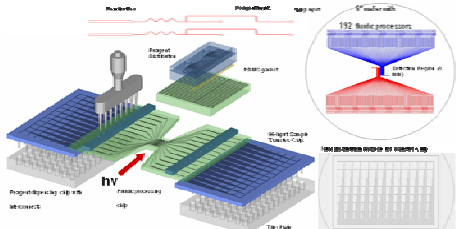


Conclusions

Multi-phase flow patterns, maps, transition between flow regimes, regularity of flows and length of gas bubble and liquid plug were determined for each case. Gas-liquid two-phase flow pressure drops were measured and each flow regime identified on the basis of topological observations is associated with different trends of the pressure drop variation with respect to volumetric flow ratio. While the Lockhart-Martinelli correlation showed good agreement with results at the Capillary bubbly, Segmented-annular, Annular and Dry flow regimes, a new linear model was developed for the segmented regime, which was divided into three more specific flow regimes, segmented 1, 2 and 3.

Liquid-liquid immiscible flow

Small Molecule Sensor: HTS for Drug Discovery - Okagbare et al.



Acknowledgements

This work is supported by the National Science Foundation under grant EPS-034641 and MRI grant NSF-9977576(CTS) as well as the State of Louisiana Board of Regents under grant LEQSF(2005-06)-ENH-TR-20.

Transport of Molecular Clusters Through Nano-Scale Channels

Nancy Lekpeli¹, Dorel Moldovan², and Dimitris Nikitopoulos²

¹Univerite Claude Bernard, Lyon, France

²Department of Mechanical Engineering, Louisiana State University, Baton Rouge, Louisiana 70803

Abstract

We report molecular dynamics (MD) simulation results depicting the behavior of a single molecule in a nanochannel under “gravity” driven Poiseuille flow of a Lennard-Jones liquid. The goal of this research is to further the understanding of the mechanism(s) underlying single molecule translocation through nanochannels. Recent experimental and simulations studies suggest that a similar system involving translocation of DNA molecules through nano-pores could be developed into an ultrafast method of DNA sequencing.

Simulation Methodology

➤The simulation system consists of two walls, a slab of liquid, and a solid molecule (i.e. atomic cluster) embedded in the liquid (Fig. 1). Periodic boundary conditions were applied in the x-direction (the channel axis)

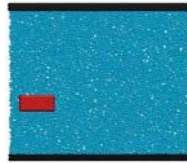


Fig. 1 Schematic representation of the simulation system

➤ MD simulations were performed with the software package LAMMPS

➤The interactions between any pair of atoms are described by the Lennar-Jones potential.

➤The two-dimensional system consists of about 6000 atoms and the molecule has an elongated shape of aspect ratio 2.6

➤The simulations were conducted and analyzed in reduced units

➤The simulations were carried out at temperature $k_B T/\epsilon=1.2$ and density $\rho/\sigma^2=0.81$.

➤The Poiseuille flow was induced by introducing a “gravity” force that is applied parallel to the channel axis to each atom of the liquid and molecule.

Simulation Results

Fig. 2 Simulation snapshots of the molecule moving in a nanochannel in a Poiseuille flow. Time is given in reduced units.

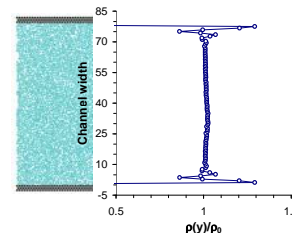
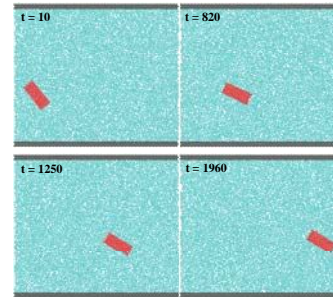


Fig. 3 Normalized atomic density in the liquid phase across the width of the nanochannel. The liquid bulk atomic density is $\rho_0=0.81$.

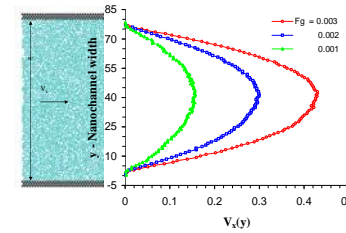


Fig. 4 Velocity profiles obtained from MD simulations of Poiseuille flow. The result are given for three values of the additional constant force, $F_g=0.003$, $F_g=0.002$, and $F_g=0.001$, applied to each “liquid” atom to generate the flow.

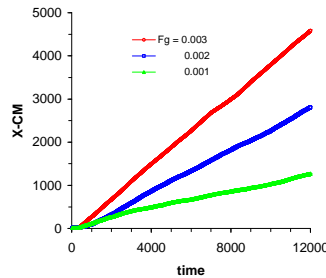


Fig. 5 Variation of the x-component of the position of the molecule center of mass versus time for three flow regimes controlled by gravity forces: $F_g=0.003$, $F_g=0.002$ and $F_g=0.001$

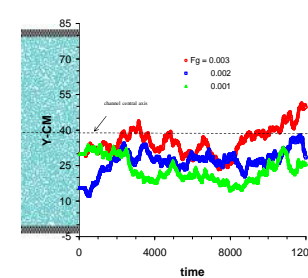


Fig. 6 Variation of the y-component of the position of the molecule center of mass versus time for three regimes controlled by gravity forces: $F_g=0.003$, $F_g=0.002$ and $F_g=0.001$

Conclusions

➤The simulations show that close to the channel walls the liquid is indeed more structured and therefore has significantly different rheological properties compared to the bulk liquid.

➤The velocity profile the of the liquid in Poiseuille flow, indicate that the deviation between continuum and MD prediction is indeed very small.

➤The MD simulations indicate that the presence of a large shear rate in the flowing liquid promotes the motion of the molecule towards the center of the nanochannel.

➤MD simulations can provide detailed atomistic understanding of the mechanism of by which a single biomolecule translocates through long nanometer-narrow channels. In addition by providing dynamical snapshots of the translocation process can they act as computational microscopes therefore having great potential for assisting the design and development of nanochannel-based biosensor systems.

Connections with CyberTools

We are working with CyberTools team to develop a toolkit for job management, data analysis, and visualization. CyberTools (e.g. WP1, WP3, WP4) enables the use of High Performance Computing for the large scale atomistic simulations of single molecule translocation through nanochannels by enabling the use of a user-friendly interface for submitting and monitoring multiple MD jobs.

Acknowledgements

The authors gratefully acknowledge the National Science Foundation for their financial support through grant NSF-EPSCoR RII Award No. EPS-0346411.

Coupling an Einstein and an Euler code via the Cactus framework



Oleg Korobkin^{1,2}, Erik Schnetter^{1,2}

¹ Center for Computation and Technology, Louisiana State University

² Department of Physics and Astronomy, Louisiana State University

Introduction

Cactus is a state-of-the-art high-performance software framework for 3D numerical simulations. The Cactus framework allows to create multiphysics applications, which combine independently developed highly sophisticated codes with various numerical discretization schemes. Here, we demonstrate the coupling between the Einstein evolution code, implemented with high-order finite differences on a non-overlapping multiblock domain (QUILT), and a relativistic hydrodynamical Euler code, implementing a finite volume scheme on overlapping patches (DiFranco). The coupling mechanism is provided by the Einstein toolkit (thorns ADMBase and TmunuBase). Both interacting codes were adjusted to satisfy a few coupling requirements, which now allows us to interface them with other codes used in the numerical relativity community.

Einstein's equations:

$$R_{\mu\nu} - \frac{1}{2}g_{\mu\nu}R = T_{\mu\nu}$$

Constraint equations

$${}^3R - K^{ij}K_{ij} + K^2 = 16\pi\rho$$

$${}^3\nabla_i(K^{ij} - g^{ij}K) = -8\pi J^j$$

Evolution equations

$$\partial_t g_{ab} - (1 + \gamma_1)\beta^k \partial_k g_{ab} = F_{ab}^{(g)}$$

$$\partial_t \Pi_{ab} - \beta^k \partial_k \Pi_{ab} + \alpha g^{ki} \partial_k \Phi_{iab} - \gamma_1 \gamma_2 \beta^k \partial_k g_{ab} = F_{ab}^{(\Pi)}$$

$$\partial_t \Phi_{iab} - \beta^k \partial_k \Phi_{iab} + \alpha \partial_i \Pi_{ab} - \gamma_2 \alpha \partial_i g_{ab} = F_{iab}^{(\Phi)}$$

Matter fields equations:

$$T_{\mu\nu};{}^\nu = 0$$

Fluid evolution equations in conservation form

$$\partial_t Q + \partial_i F^i(P) = S(P)$$

Variables

Formulation-specific: $g_{ab}, \Pi_{ab}, \Phi_{iab}$

ADM: $g_{ij}, K_{ij}, \alpha, \beta^i$

Variables

Stress-energy tensor

Primitive: $\rho, p, u, u_x, u_y, u_z$

Conservative: dD, dQ_x, dQ_y, dQ_z

Elliptic solver

Initial data

Initial data

Initial data

Time step n

Spacetime variables

ADM variables

Stress-energy tensor

Primitive variables

Conserved variables

RHS

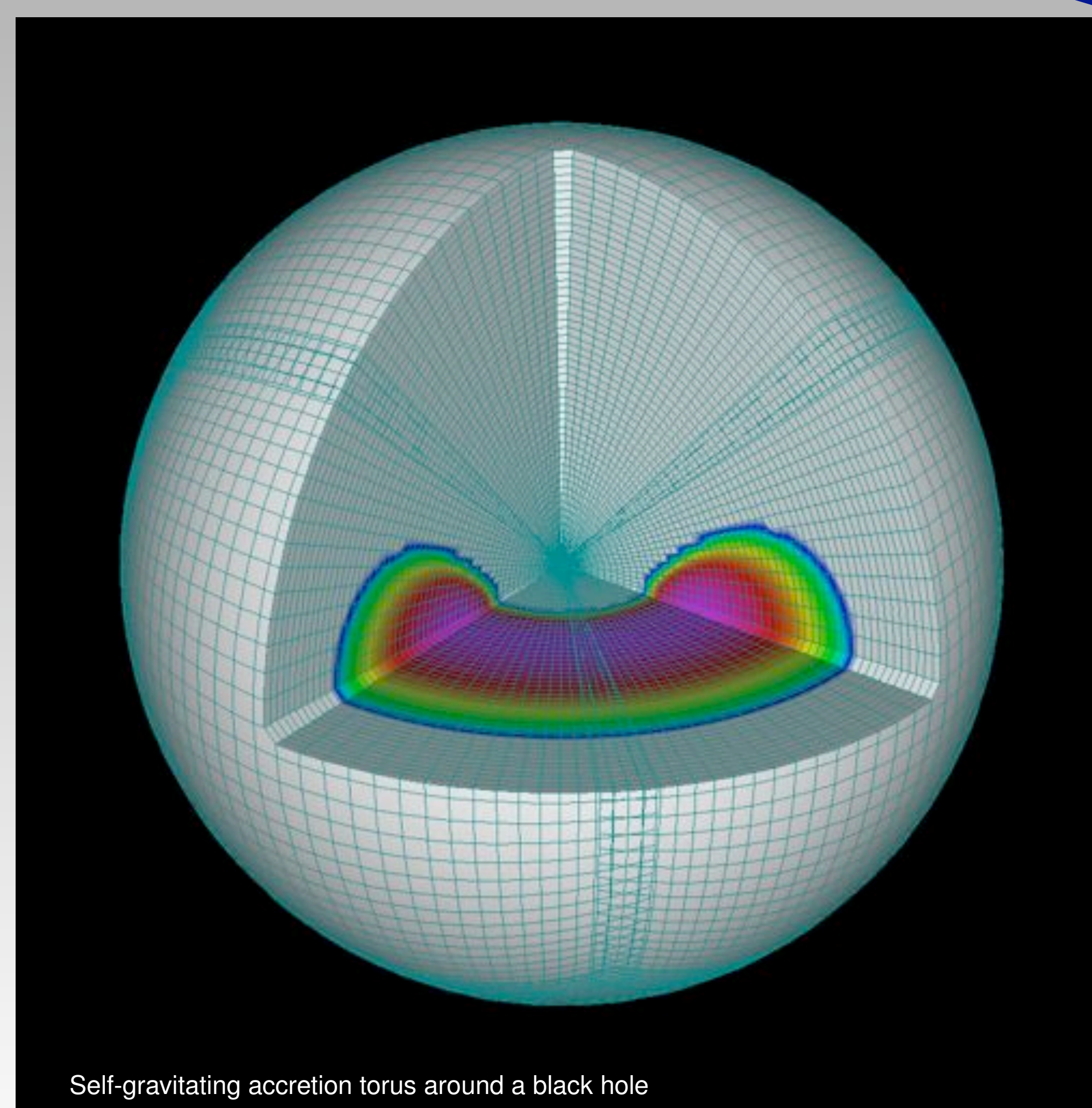
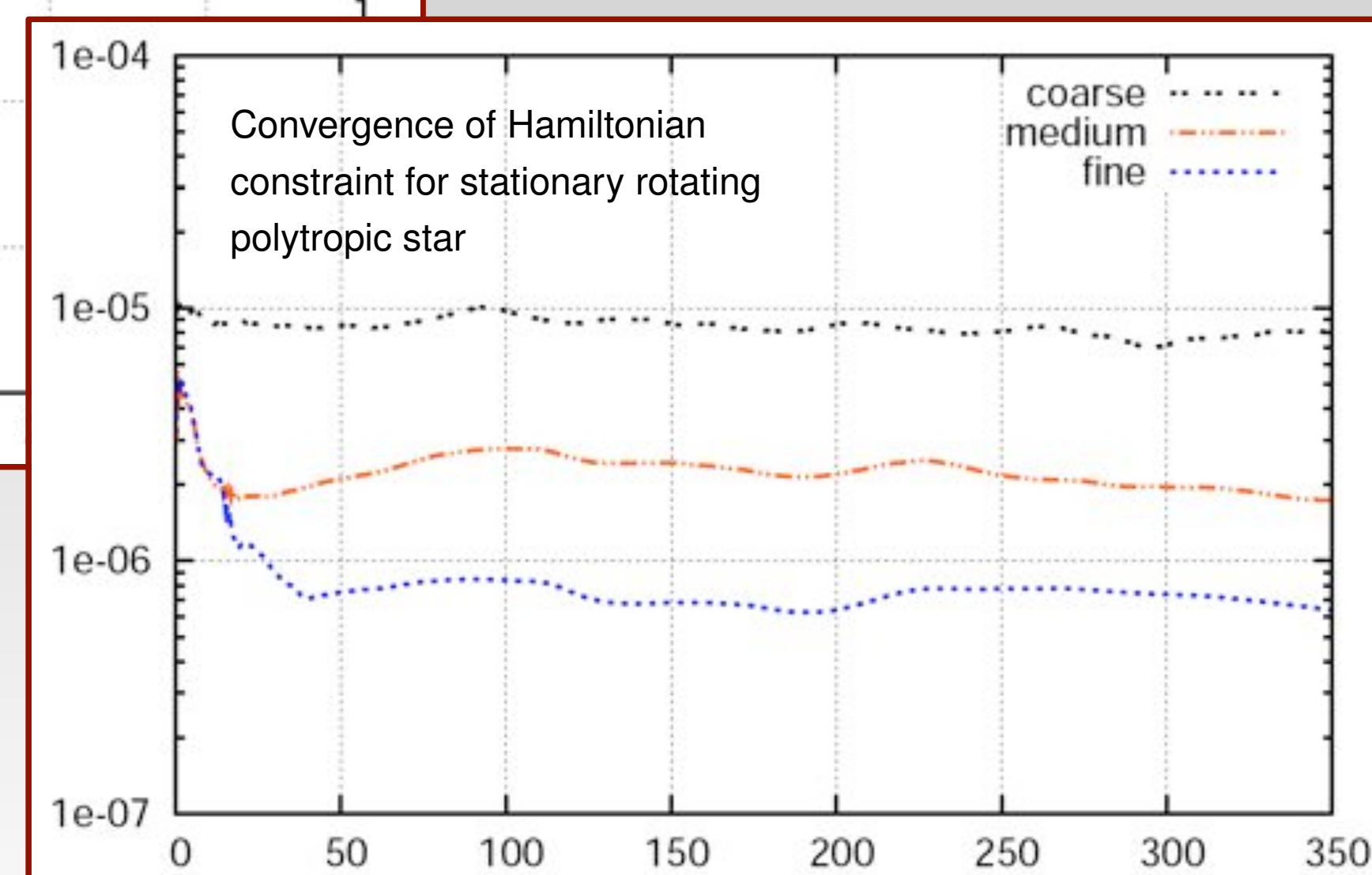
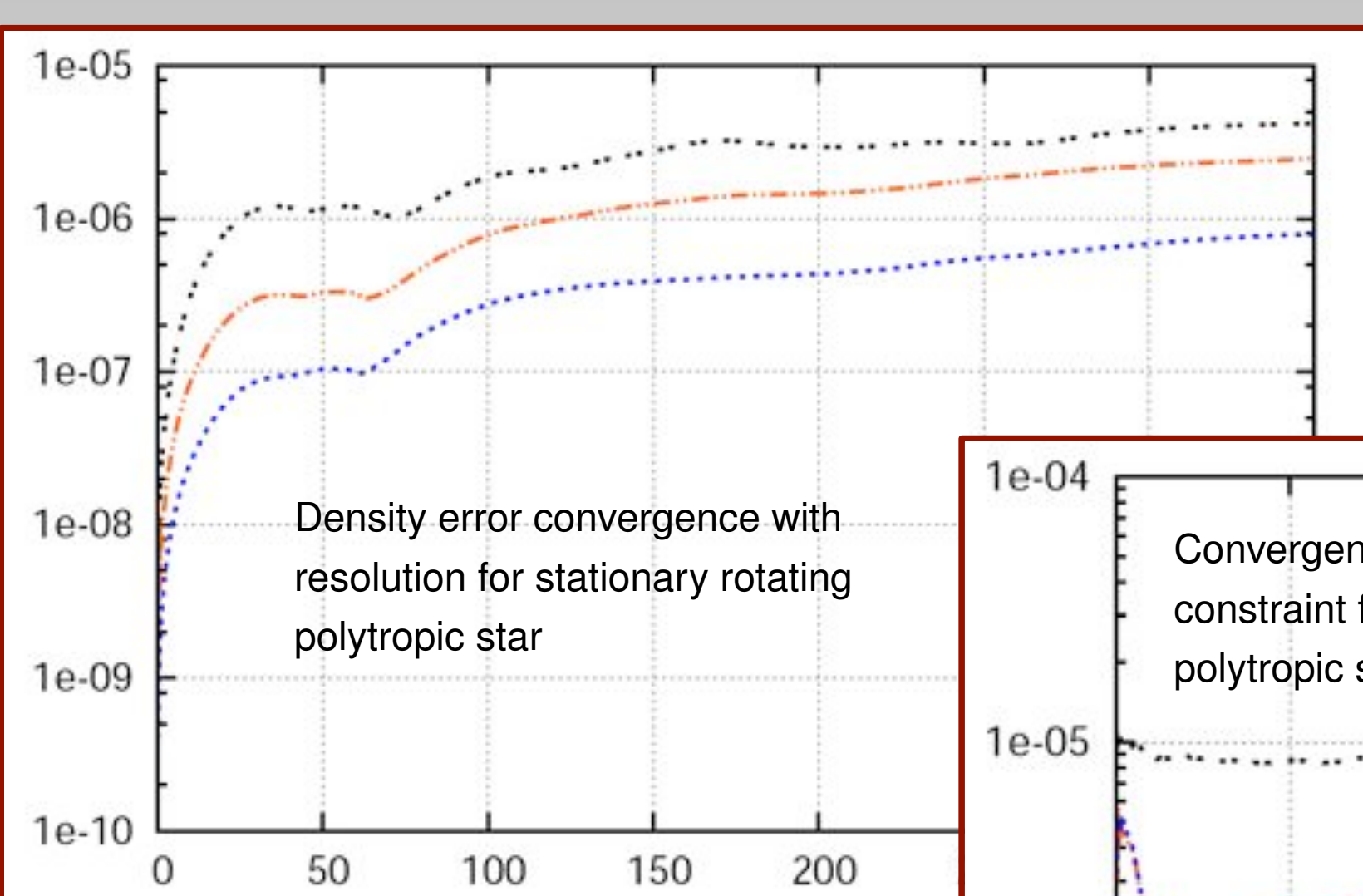
Conserved RHS

Fluxes

Time step n+1

Spacetime variables

Conserved variables

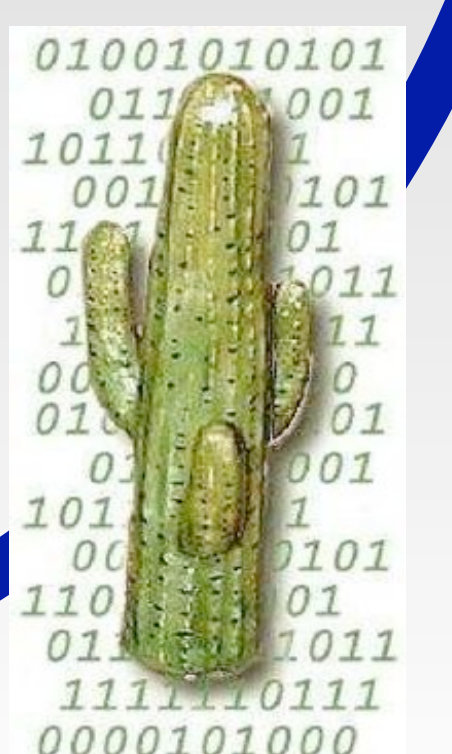


Connections with CyberTools

- WP 1: Scheduling and data services**
Cactus has been used for parallel computation on different architectures and provides tools for parallel data access
- WP 2: Information services and portals**
Cactus connects to portals via thorns Announce and Formaline
- WP 3: Visualization services**
Cactus IO formats are supported by remote visualization tools (such as VisIt)
Cactus has a built-in web-server that can display results interactively.
- WP 4: Application services and toolkits**
- Science Driver: e.g., Biotransport**
Multiblock infrastructure from Cactus can be used to solve problems in biotransport

Acknowledgments

We would like to thank the Cactus Team, Christian D. Ott, Christian Reisswig, Manuel Tiglio, and Burkhard Zink. Simulations were performed on LONI machines. This project is supported by NSF grant 0721915 ("Alpaca")





An Algorithmic Tool for Protein Structure Classification based on Conserved Hydrophobic Residues

Pradeep Chowriappa¹, Sumeet Dua¹, Jinko Kanno², and Hilary Thompson³

¹Data Mining Research Laboratory, Computer Science Program, Louisiana Tech University, Ruston, LA – 71272.

²Mathematics and Statistics Program, Louisiana Tech University, Ruston, LA 71270.

³Department of Biostatistics, School of Public Health, Louisiana State University Health Sciences Center, New Orleans, LA 70112.



Abstract

Motivation: Protein folding is frequently guided by local residue interactions that form clusters in the protein core. The interactions between residue clusters serve as potential nucleation sites in the folding process. Evidence postulates that the residue interactions are governed by the hydrophobic propensities that the residues possess. To this end, an array of hydrophobicity scales have been developed to determine the hydrophobic propensities of residues under different environmental conditions. We hypothesize that proteins of the same homology contain conserved hydrophobic residues that exhibit analogous residue interaction patterns in the folded state.

Product: We developed a graph theory based data mining tool to extract and isolate protein structural features that sustain invariance in evolutionary related proteins, through the integrated analysis of five well-known hydrophobicity scales over the 3-D structure of proteins. The results demonstrate that discriminatory residue interaction patterns shared among proteins of the same family can be employed for both the structural and the functional annotation of a variety of proteins. We obtained an average of 90% accuracy in protein classification with a significantly small feature vector compared to previous results in the area. The tool is usable for a variety of proteins from distinctively different families and classes.

Background

Researchers have investigated the correlation of hydrophobic interactions to similarities in 3-D structural elements, and have exhibited and exploited property conservation at these sites. Although using different approaches, each model suggests a common and unexpected feature of protein packing that proteins significantly rely on based on few members of the set of conserved residues.

- Paiardini et al [1] and Reddy et al, (CKAAPS)[2], using Multiple Sequence Alignment (MSA) techniques show that a significant correlation exists between sequence, structure, and Conserved Hydrophobic Contacts (CHC) that remain invariant during long evolutionary periods.
- Tsai et al [3] propose a method using a scoring function based on the physicochemical properties of hydrophobicity, compactness, solvent accessibility of surface area (ASA), and segmentation to test the validity of fold unit definition based on eigenvector analysis.
- The models proposed by Muppilala et al [4] and Huang et al [5], quantitatively measure the individual contributions of amino acid residues by enumerating contacts between a hydrophobic residue and its surrounding area within a protein structure.

Methodology

We have developed a data mining tool for the integrated analysis of five popular hydrophobicity scales to enhance the detection of structurally conserved regions among homologous proteins, which we believe will also be useful for classification purposes. Incorporating the metric of mutual information to identify compact structural units, we extract frequently occurring patterns using a discriminative weighing function. By doing so, we reduce our feature space and show that the reported conserved hydrophobic residues are sufficient to differentiate between proteins at both the class and fold levels of the Structural Classification of Proteins (SCOP) hierarchy.

Rank	1	2	3	4	5	6	7	8	9	10
Pyle and Doolittle	ARG	LVS	ASP	GLU	ASN	GLN	HIS	PRO	THR	TRP
Huggo Wood	TRP	PHE	THR	ILE	LEU	VAL	MET	CYS	ALA	ASP
Jean et al	LVS	ARG	GLN	GLN	ASP	ASN	TRP	PRO	THR	HIS
Ross et al	LVS	ASP	GLU	ASN	ASN	PRO	ARG	SER	THR	GLY
Eisenberg et al	ARG	LVS	ASP	GLN	ASN	GLU	HIS	SER	THR	PRO

Table 1. Ranks of amino acid based on propensities assigned by the five hydrophobic scales [6], and all the known Amino Acid Indices listed by (<http://www.genome.ad.jp/aaindex/>).

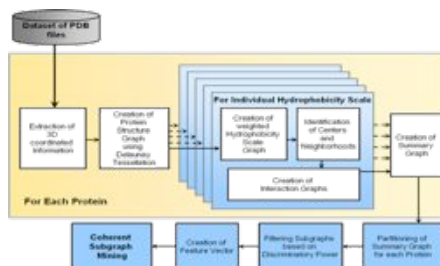
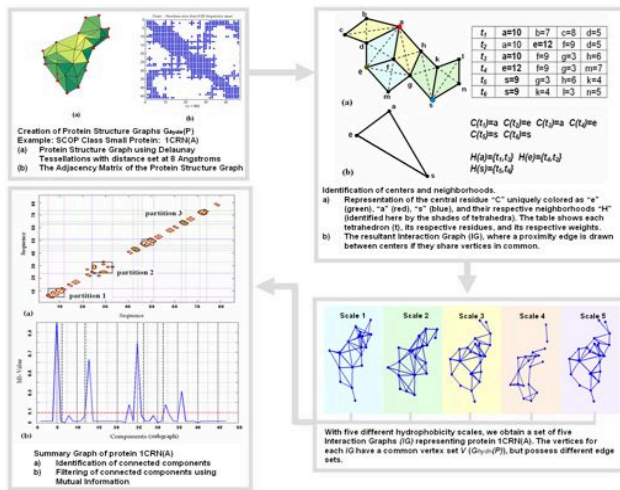


Figure 1. Overview of Methodology

The Process of Feature Extraction



Multi Class Classification:

Constraints: We have selected ten proteins from each class, resulting in a dataset consisting of 30 proteins which satisfy a RMSD of <=3.0 and a Z-score of >=4.5.

The proteins used in our study are located in the fsp-ckaaps-1.2 database

(<http://ftp.sdsc.edu/pub/sdsc/biology/ckaap>)

provided in [2] and belong to three structural protein classes: Coiled Coil, all-Beta, and alpha + beta.

Results reported in Table 3.

The conserved residues reported in sample proteins 1BJ4(A), 1CZQ(A), and 1FE6(A) as shown in Figure 2. Outputs were generated using PDBSUM Astex Viewer.

Conclusion

In conclusion, the proposed tool provides an efficient means to integrate different scales for protein analysis. This study further reinforces, with newer evidence, that the identification of conserved hydrophobic residues is vital to the exposition of the folding of proteins and further aids in the functional annotation of proteins and possible mutational studies.

For further details of the proposed methodology and validations refer [7].

Reference

- [1] A. Paiardini, F. Bossa and S. Pascarella, "Evolutionarily conserved residues and hydrophobic contacts at the super family level: The case of the fold-type I, pyridoxal-5'-phosphate-dependent enzymes," *Protein Sciences*, vol. 13, pp. 2992-3005, 2004.
- [2] B.V.B. Reddy, W.W. Li, I.N. Shindiyatov, and P.E. Bourne, "Conserved Key Amino Acid Positions (CKAAPS) Derived From the Analysis of Common Substructures in Proteins," *PROTEINS: Structure, Function and Genetics*, vol. 42, pp. 148-163, 2001.
- [3] C.-J. Tsai and R. Nussinov, "Hydrophobic folding units derived from dissimilar monomer structures and their interactions," *Protein Science*, vol. 6, no. 1, pp. 24-42, 1997.
- [4] U.K. Muppilala and Z. Li, "A simple approach for protein structure discrimination based on the network pattern of conserved hydrophobic residues," *Protein Engineering, Design & Selection*, vol. 19, no. 6, pp. 265-275, 2006.
- [5] E.S. Huang, S. Subbiah and M. Levitt, "Recognizing Native Folds by the Arrangement of Hydrophobic and Polar Residues," *Journal of Molecular Biology*, vol. 252, pp. 709-720, 1995.
- [6] K.M. Biswas, D.R. DeVido, and J.G. Dorsey, "Evaluation of methods for measuring amino acid Hydrophobicities and interactions," *Journal of Chromatography A*, vol. 1000, no. 1, pp. 637-655, 2003.
- [7] Pradeep Chowriappa, Sumeet Dua, Jinko Kanno, Hilary W. Thompson, "Protein Structure Classification Based on Conserved Hydrophobic Residues," *IEEE/ACM Transactions on Computational Biology and Bioinformatics (to appear)*.

Connections with CyberTools

This work relates to the WP1 (Data Services), especially towards meeting its aims for design and development of tools for metadata extraction and data mining services. The work is also connected to WP2 (Information Services) of CyberTools development with regard to information discovery algorithms. The work is a result of collaboration between investigators from Louisiana Tech University and Louisiana State University Health Sciences Center at New Orleans. While the work has demonstrated evaluation studies on restricted sets of proteins for performance comparison purposes, it is easily extendible to a variety of proteins available from the Protein Data Bank and other databases as they are discovered and made available.

Acknowledgements

- NSF/LA-BoREPSCoR program
- NIH/INBRE program

Validation

Binary Class Classification:

Constraints: Proteins filtered under < 35% pair wise sequence similarity to remove highly homologous proteins, with resolution <=3 and R factor <= 1.0.

(Class Level) Dataset C1:

Consists of proteins from Classes:

All Alpha- Nuclear Receptor Ligand-binding domain proteins (NB 16 proteins), against All Beta-Prokaryotic serine proteases family (PSP, 10 proteins).

(Fold Level) Dataset C2:

Consists of proteins from Folds of Class All-Beta:

Eukaryotic serine proteases family (ESP, 19 proteins) and Prokaryotic serine protease family (PSP, 19 proteins).

Results reported in Table 2.

Dataset	Method	Features	Accuracy (%)
C1	DT	20646	100
	AD	23130-37394	96-100
	LFM-Pro	5282	100
C2	Ours	38	100
	DT	15895	95
	AD	18491-32569	93-95
	LFM-Pro	2180	100
	Ours	29	96.55

Table 2. Comparison of results obtained from Binary Class classification.

Structural Class	Precision (%)
Coiled Coil Proteins (A)	100
All Beta Proteins (B)	90.9
Alpha/Beta Proteins (C)	81.8
Overall Accuracy	90

Table 3. Results obtained from Multiclass Classification using the proteins of CKAAPS database.



Table 1. Ranks of amino acid based on propensities assigned by the five hydrophobic scales [6], and all the known Amino Acid Indices listed by (<http://www.genome.ad.jp/aaindex/>).

Abstract: Molecular Dynamics (MD) is an important step towards understanding the behavior of biological systems. Even though, the state-of-the-art computational resource and techniques have made it feasible to do large-scale MD simulations, MD remains a very compute-intensive job, especially for large realistic systems. Thus there exists interest in developing and understanding the performance of MD code on multiple distributed HPC resources. To realize this goal, we have developed a preliminary parallel and distributed MD code and benchmarked it on the LONI (Louisiana Optical Network Interface) grid, which uses dedicated light-path networks to connect supercomputers across Louisiana. This work is motivated by an attempt to utilize new infrastructure and to devise new programming strategies for MD simulations, with a focus on distributing the workload across various machines while retaining the advantages of parallelization within a single machine. Current practice is to distribute the job amongst various machines only when the resource requirement is more than the capacity of a single machine. In our work, we divided the job into several workloads, even if a single machine was capable of handling it. We tested our developed code on upto three distributed resources of LONI, namely Bluedawg, Zeke and Ducky. These are IBM P5 clusters with 114 nodes per cluster. Based on performance data, we show that without any serious optimization, the performance degradation as defined by total CPU-hrs on multiple machines is about 10-20% of the performance over a single machine, which has useful consequences when time to finish is critical. Based on this analysis, the users of grid resources can pick their choice between two different strategies: (1) optimize the CPU-hours used, and live with the huge wait time involved, (2) or use an extra 10-20% CPU-hours and optimize the overall job throughput. Our analysis has the potential to be extended to parallel codes other than MD. We believe that this study can lead to a better job distribution and resource allocation to optimize throughput.

Molecular Dynamics

- Atoms stretch, vibrate, and rotate about the bonds in response to intermolecular and intra-molecular forces.
- Involves both bonded and non-bonded forces
- Equations to determine velocity and displacement:

$$-(V_i)_{t+1} = (V_i)_t + (F_i/M_i)_t$$

$$-(X_i)_{t+1} = (V_i)_t + (X_i)_t$$

The parallel MD code

- Extended on the existing Mindy code for MD
- Computation of non-bonded forces is the most compute-intensive part, as seen from profiling of the code
- Non-bonded part takes 72-80% of computation time
- Bonded parts (to compute bond-angles, improper and dihedral angles) takes 3-5% of computation time

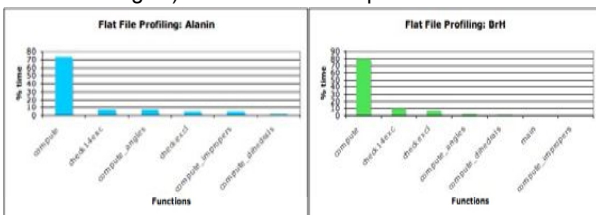


Fig: Flat-file profiling (Alanin)

Fig: Flat-file profiling (BrH)

Test-sets: Proteins

- **Alanin (Alanine)**
 - size 66 atoms
- **BrH (Bacteriorhodopsin)**
 - size 3762 atoms



Source: www.wiki.org



Source: www.pdb.org

Test-bed: LONI (Louisiana Optical Network Initiative)

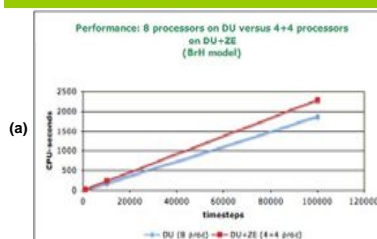
LONI is nation's one of the first network to connect Louisiana's supercomputers with fast light-paths so as to minimize communication delay.

We used LONI because, we wanted to know:

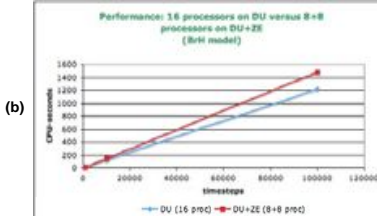
- The behavior of a distributed code, assuming minimum communication delay possible
- Exactly performance degradation a code can have, when run in distributed mode in supercomputers
- We used 3 LONI machines: Bluedawg, Ducky, Zeke
- LONI uses Loadleveler for job scheduling, which implements the backfill algorithm on FIFO scheme.



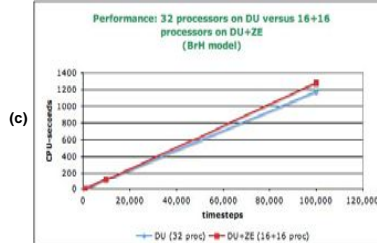
Performance Analysis



timesteps	DU (8 proc)	DU+ZE (4+4 proc)
100	1.5	1.7
1,000	19.5	23.8
10,000	191.5	234.3
100,000	1882.7	2308.1
1,000,000		28132.5

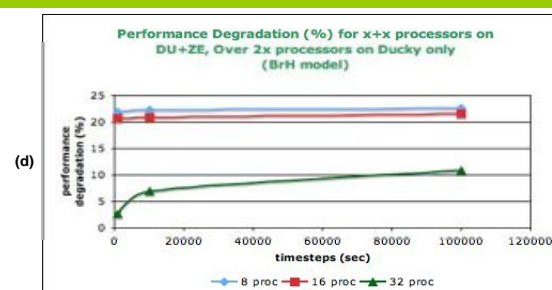


timesteps	DU (16 proc)	DU+ZE (8+8 proc)
100	0.0	0.0
1,000	11.1	13.4
10,000	123.7	149.6
100,000	1219.0	1481.9
1,000,000		57494.3



timesteps	DU (32 proc)	DU+ZE (16+16 proc)
100	0.0	0.0
1,000	3.7	3.8
10,000	116.0	124.0
100,000	1175.5	1282.7
1,000,000	11977.0	13276.9

Fig: Performance degradation when distributed across 2 LONI machines is about 10-20%; (a), (b), (c) shows actual values; (d) shows percentage-comparison; BL, DU, ZE are LONI machines, representing Bluedawg, Ducky, Zeke.



The graphs and tables shown depicts performance for Bacteriorhodopsin protein dataset. Similar performance is seen on Alanine protein dataset - a much smaller size dataset.

Conclusion

- Performance degradation of compute-intensive code like MD is 10-20% of the performance over single machine
- Hence, users can choose any one:
 - optimize CPU-hours used, and try to get maximum resource over a single machine
 - optimize job throughput, because of lesser wait time, by using extra 10-20% CPU-hours

Acknowledgements / Sponsorships

- This research has been supported by:
- Center for Computation and Technology (CCT)
 - Cybertools Project

